TAMPEREEN TEKNILLINEN YLIOPISTO
TAMPERE UNIVERSITY OF TECHNOLOGY

Rajeev K. Dubey

Synthesis and Function of Photoactive Donor–Acceptor Systems of Bay-Functionalized Perylene Diimide Dyes in View of 1,7- and 1,6-Regioisomers

Julkaisu 1127 • Publication 1127

Tampere 2013

Tampereen teknillinen yliopisto. Julkaisu 1127
Tampere University of Technology. Publication 1127

Rajeev K. Dubey

Synthesis and Function of Photoactive Donor−Acceptor Systems of Bay-Functionalized Perylene Diimide Dyes in View of 1,7- and 1,6-Regioisomers

Thesis for the degree of Doctor of Philosophy to be presented with due permission for public examination and criticism in Festia Building, Auditorium Pieni Sali 1, at Tampere University of Technology, on the 24th of May 2013, at 12 noon.

Tampereen teknillinen yliopisto - Tampere University of Technology
Tampere 2013

ISBN 978-952-15-3062-3 (printed)
ISBN 978-952-15-3072-2 (PDF)
ISSN 1459-2045

Abstract

1,7- and 1,6-regioisomers of two important bay-functionalized perylene diimide dyes, namely *N,N′*-dioctyl-di(2,4-di-*tert*-butylphenoxy)perylene diimide and *N,N′*-dioctyl-dipyrrolidinylperylene diimide, have been synthesized, separated, and unambiguously characterized by 300 MHz ^{1}H NMR. A detailed comparative study of their optical and electrochemical properties has been carried out, which revealed virtually the same characteristics of the 1,7- and 1,6-diphenoxy substituted perylene diimides. However, substantial differences have been observed in the properties of the two regioisomers of dipyrrolidinyl substituted PDIs. Subsequently, novel derivatives of dipyrrolidinyl functionalized perylene diimide, with additional substitution sites close to the perylene core, have been prepared by the bay-attachment of 2-(benzyloxymethyl)-pyrrolidine. During this, clear differences have been evidenced in the chemical behavior of the corresponding 1,7- and 1,6-regioisomers. The separated 1,7- and 1,6-derivatives have been utilized to prepare four perylene diimide−fullerene dyads, in which fullerene has been covalently linked to perylene diimide with one or two linkers. The differences in the excited-state dynamics of these 1,7- and 1,6-regioisomers have been studied. In contrast to previously reported perylene diimide−fullerene dyads, all the synthesized dyads have exhibited photoinduced electron transfer from the perylene diimide chromophore to fullerene, not only in a polar but also in a non-polar solvent. The electron transfer was found substantially faster and more efficient in the dyads containing 1,7-regioiosmer.

A new series of donor−acceptor based ensembles, consisting of phenoxy or pyrrolidinyl functionalized perylene diimide covalently linked to Ru(II) polypyridine complex, has been synthesized and studied in detail by steady-state and time-resolved spectroscopy. In all the ensembles, the photoexcitation of either chromophore resulted in a long-lived triplet excited state of PDI (^{3}PDI) as the final excited state, but the photochemical reactions leading to the triplet states were found to be essentially different for the two types of the ensembles. In the case of phenoxy-PDI based ensemble, the excitation of either chromophore leads to the electron transfer from the Ru(II) complex to PDI; whereas for the pyrrolidinyl-PDI based ensembles, the electron transfer is observed in opposite direction and only when the Ru(II) complex is excited. Finally, a dibenzo[*a,c*]phenazine molecule was coupled with fullerene to function as light-harvesting antenna in order to overcome poor absorption strength of fullerene in the visible spectral region. The suitability of the synthesized dibenzo[*a,c*]phenazine−fullerene dyad, for the photovoltaic applications, has been examined by detailed electrochemical and spectroscopic study.

Acknowledgements

It is an honor for me to express my first and foremost gratitude to my supervisor, Prof. Helge Lemmetyinen, for giving me the opportunity to conduct research under his guidance and keeping faith in my caliber throughout the Ph.D. work. I will always be indebted to him for giving me enough freedom and all the possible support for carrying out this work. Without his constant support and motivation, this dissertation would have never been possible. As words are unable to convey even a fraction of feelings, I have to admit that I can never thank him enough for all he did. Next, I would like to thank my co-supervisor Dr. Alexander Efimov for his unforgettable support and help in carrying out the synthesis. My sincere thanks go to him also for his valuable inputs and enriching suggestions, which considerably improved the overall presentation of the articles and the thesis. I also appreciate him for being patient during the hard times.

I am very grateful to Prof. Nikolai Tkachenko for his immense help and guidance to understand the photochemistry of all the molecules included in the thesis. His enthusiasm and dedication for the photochemistry will always be a source of inspiration and motivation for me. I express my gratefulness to Dr. Marja Niemi, Mr. Tatu Kumpulainen, and Ms. Kati Stranius for conducting the ultrafast spectroscopic measurements. Especially, I am thankful to Dr. Marja Niemi for analyzing the pump-probe data of PDI−C_{60} and PDI−Ru(II) dyads and also for writing the transient absorption part in the **IV** article. I appreciate Dr. Vladimir Chukharev who made available his help in a number of ways, especially during the spectroscopic and electrochemical measurements. I also want to thank Dr. Kimmo Kaunisto for his help during the flash-photolysis measurements. The measurements would never been so successful without his help and guidance. I sincerely thank Dr. Terttu Hukka, Dr. Mika Niskanen, and Ms. Tuuva Kastinen for their help to understand the structure and energetics of the PDI−Ru(II) ensembles.

I convey my sincere regards to Dr. Riikka Lahtinen, Dr. Elina Vuorimaa-Laukkanen, Mrs. Marja Asp-Lehtinen, and Mrs. Raija Mikkonen for refreshing and illuminating conversations in the coffee lounge and corridors. I convey my heartiest *kiitos* to Dr. Anne Kotiaho and Dr. Juha Heiskanen, and a big *grazie* to Dr. Paola Vivo for being so friendly, social, and helpful not only at work but also outside. My gratitude goes also to both the secretaries, Mrs. Anna-Kaarina Rantaviita-Tiainen and Mrs. Tea Tanhuanpää, for their help in the academic matters and to Mrs. Anne-Maarit Tikkanen for her help in the laboratory.

My great appreciation goes to my synthetic lab mates Dr. Kalle Lintinen, Dr. Somnath Dey, Ms. Jenni Ranta, and Mrs. Essi Sariola-Leikas for being very kind and cooperative lab mates. It is really

hard to imagine that we managed very peacefully and smoothly even during the times when all of us were working at the same time. My special thanks to Somnath for his memorable help and support not only as a colleague, but also as a friend during the long period of five years. I also thank to Ms. Juuli Wacker, Mrs. Hanna Metsberg, and Dr. Navaneetha Krishnan for their "guest appearances" in the adjacent student lab. The small talks, we had, helped a lot to reduce the stress of the failed reactions. My gratitude cannot be completed without mentioning all my lunch-mates (Dr. Somnath Dey, Dr. Antti Tolkki, Ms. Venla Manninen, Ms. Hannele Kivistö, Ms. Kirsi Huttunen, Ms. Tuuva Kastinen, Ms. Elina Lehtonen, Mr. Tero-Petri Ruoko, and Ms. Minna Ervasti) for creating highly social and humorous environment during the lunch breaks. I am very grateful to Dr. Alexey Veselov and Ms. Tiia-Maaria Ketola for being very friendly and helpful. I am also grateful to my colleagues Ms. Hanna Saarenpää, Dr. Yu Wang, Dr. Noora Kuuloja, and Mr. Ali Al-Subi for helping me in a way or other. I personally feel highly honored and privileged to be a member of the Supramolecular Photochemistry Research Group, and consequently grateful to each and every member of the group.

All my friends in Tampere, especially Dr. Nikhil and Kriti, Alessandro and Alessandra, and Karan Menon, deserve my sincere gratefulness for making my life very easy and pleasant. My special thanks go to my very special little friends, Paarth and Veydant, for accommodating me as a friend and for allowing me to play with their toys.

It would be highly unfair if I don't acknowledge the people who have had an immense contribution in my upbringing. In this regard, I would like to express my deepest gratitude to my beloved and respected parents for their priceless love, care, dedication, sacrifice, encouragement, and efforts. It is my privilege to convey my sincere thanks to my beloved sisters, Mrs. Rashmi Udenia and Ms. Dipti Dubey, my brother in law, Dr. Ashok Udenia, and my adorable nephew, Vinamra, for being very caring, responsible, and supportive through thick and thin. I would never be able to accomplish this work without their support. Finally, I would also like to thank my close and long-term friends, Mr. Ashutosh Sharma, Mr. Ashish Dwivedi, Dr. Rakesh Jaiswal, Dr. Atul P. Singh, and Dr. Kamalakanta Behera for their invaluable companionship.

The research work reported in this thesis was carried out at the Department of Chemistry and Bioengineering, Tampere University of Technology starting from September 2007 to June 2012. The financial support from Academy of Finland is gratefully acknowledged.

Tampere, 21st February 2013

Rajeev K. Dubey

Table of Contents

List of Publications

The thesis is based on the work contained in the following publications, which are hereafter referred by their Roman numerals:

I. **Close Proximity Dibenzo[*a*,*c*]phenazine−Fullerene Dyad: Synthesis and Photoinduced Singlet Energy Transfer**
Rajeev K. Dubey, Tatu Kumpulainen, Alexander Efimov, Nikolai V. Tkachenko, and Helge Lemmetyinen
Eur. J. Org. Chem. **2010**, 3428−3436.

II. **1,7- And 1,6-Regioisomers of Diphenoxy and Dipyrrolidinyl Substituted Perylene Diimides: Synthesis, Separation, Characterization, and Comparison of Electrochemical and Optical Properties**
Rajeev K. Dubey, Alexander Efimov, and Helge Lemmetyinen
Chem. Mater. **2011**, *23*, 778−788.

III. **Direct Evidence of Significantly Different Chemical Behavior and Excited-State Dynamics of 1,7- and 1,6-Regioisomers of Pyrrolidinyl-Substituted Perylene Diimide**
Rajeev K. Dubey, Marja Niemi, Kimmo Kaunisto, Alexander Efimov, Nikolai V. Tkachenko, and Helge Lemmetyinen
Chem. Eur. J. DOI: 10.1002/chem.201203387.

IV. **Excited State Interaction of Red and Green Perylene Diimides with Luminescent Ru(II) Polypyridine Complex**
Rajeev K. Dubey, Marja Niemi, Kimmo Kaunisto, Kati Stranius, Alexander Efimov, Nikolai V. Tkachenko, and Helge Lemmetyinen
Inorg. Chem. (Submitted).

Abbreviations and Symbols

A	acceptor
a.u.	arbitrary unit
bpy	bipyridine
C_{60}	fullerene[60]
COSY	correlated spectroscopy
CR	charge-recombination
CS	charge-separation, charge-separated
CT	charge-transfer
D	donor
D-A	donor−acceptor
DB	double-bridged
DBPz	dibenzo[*a*,*c*]phenazine
DCM	dichloromethane
dppz	dipyrido[*a*,*c*]phenazine
ET	electron-transfer
Fc	ferrocene
F-p	flash-photolysis
HOMO	highest occupied molecular orbital
IR	infrared
ISC	intersystem crossing
LUMO	lowest unoccupied molecular orbital
MS	mass spectrometry
MLCT	metal-to-ligand charge-transfer
NIR	near infrared
nm	nanometer
NMP	*N*-methyl-2-pyrrolidinone
NMR	nuclear magnetic resonance
ns	nanosecond
Pcs	phthalocyanines
PDI	perylene-3,4,9,10-tetracarboxy diimide
PDI−C_{60}	perylene diimide−fullerene dyad

Ph	phenoxy
PhCN	benzonitrile
p-p	pump-probe
ps	picosecond
PTCDA	perylene-3,4,9,10-tetracarboxylic dianhydride
Py	pyrrolidinyl
SB	single-bridged
S_0	ground-state
S_1	the first excited singlet-state
S_2	the second excited singlet-state
$TBABF_4$	tetrabutylammonium tetrafluoroborate
$TBAPF_6$	tetrabutylammonium hexafluorophosphate
TCSPC	time-correlated single photon counting
THF	tetrahydrofuran
UV	ultraviolet
UV	ultraviolet
Vis	visible
Å	angstrom
A	absorbance
ΔA	absorption change
hv	energy of photon
I	fluorescence intensity
k	rate-constant
ε	molar extinction coefficient
Φ_f	fluorescence quantum yield
μs	microsecond
τ	time-constant
λ	wavelength
λ_{ex}	excitation wavelength

1 Introduction

Many intensive efforts have been carried out over the past few decades to construct photosynthetic models, which can mimic natural photosynthesis involving photoinduced electron and energy transfer as fundamental processes.[1−10] Considering the structural complexity of the natural photosynthetic systems, much of the scientific efforts have been devoted toward the preparation and study of the structurally simpler systems, with the aim of reproducing the fundamental processes occurring in the natural photosynthesis. In this context, the research focus has been directed to the design and synthesis of discrete photoactive components that give rise to electron donor−acceptor interactions. For the sake of organization, such photo- and electro-active building blocks must be connected to each other, for which a wide range of well-defined molecular spacers have been considered.[11−14] Important variables are the nature of the donor and acceptor components, their relative distance, mutual orientation, and electronic coupling, as well as aggregation induced by π−π stacking. Common to all of these variables is that they affect yields and kinetics of the charge-transfer reactions in one way or other.[4,15−21]

A better knowledge of the electronic interactions between the donor and acceptor moieties is highly essential not only to enhance our understanding of the natural systems, but also for the development of new molecular photovoltaic and optoelectronic devices. During the past three decades, several photoactive units have been tested as integrative building blocks for the construction of the donor−acceptor based systems with various properties. Among those, the perylene diimide (PDI) dyes stand out as unique components because of their diverse and fascinating properties. One such a unique and crucial characteristic is the possibility to fine-tune their electronic and optical properties by chemical modification, according to the requirements of particular applications. Furthermore, the PDI dyes also exhibit other favorable physical and chemical properties, such as easy functionalization, excellent electron-acceptor ability, high molar extinction coefficient in the visible region, high fluorescence quantum yields, and excellent photochemical stability.[22,23] Owing to these peculiar characteristics, the last two decades have witnessed their extensive and successful utilization in the donor−acceptor based systems and also in numerous high-tech applications..[7,14,22,24] The PDI dyes can also be considered as potential chromophores for many new applications in light of their diverse and fascinating characteristics.

This thesis mainly focuses on the chemistry of bay-functionalized bis-substituted perylene diimide dyes. The work had been planned and implemented keeping following three important aspects in mind:

1. **Regioisomeric contamination:** The synthetic procedure for the preparation of the 1,7-bay-functionalized PDIs, produces the corresponding 1,6-bay-functionalized derivative (so-called 1,6-regioisomer) in 25−30 % quantity as a side product. There are two important aspects associated with this issue. Firstly, the removal, as well as the characterization, of the 1,6-regioisomer is very difficult. Consequently, the properties of the 1,6-regioisomers are not well-known. Secondly, majority of research groups, which are involved only in the application based work, are not well aware about this problem as the contamination originates from the synthesis. Therefore, this contamination has been ignored (knowingly/unknowingly) by the majority of research groups around the world.

2. **Synthesis of the new PDI derivatives with extra functionality:** The PDI molecules usually have two derivatization sites, namely the imide- and the bay-positions, where the attachment of other chromophores can be executed. However, the bay-positions are often utilized for the tuning of the optical and electrochemical properties of the dye. Therefore, only the imide-positions are usually available for coupling with other photoactive molecules. Within this framework, we have synthesized new PDI derivatives with bay-substituents, which offer additional site/sites for the attachment other chromophores.

3. **Synthesis and study of the new electron/energy donor−acceptor dyads:** The synthesized PDI derivatives were utilized to construct donor−acceptor dyads, which can be used in the photovoltaic and optoelectronic applications. Therefore, the strategy of the close-proximity, between the donor and acceptor moieties, was employed in all the synthesized molecular dyads to ensure fast and efficient electron or energy transfer. A detailed study of the photophysical properties of all the prepared dyads was carried out by means of steady-state and time-resolved spectroscopic measurements.

2 Background

The perylene-3,4,9,10-tetracarboxylic acid diimide derivatives (commonly known as perylene diimides and abbreviated as PDIs) represent a classical example of an inherently robust and outstandingly versatile family of organic compounds that have been utilized for a wide range of technological applications. The PDIs were first discovered by Kardos in 1913 and were initially used, exclusively, as industrial colorants, both as dyes and pigments, because of their excellent chemical, thermal, photo, and weather stability.[25,26] Nowadays also, several PDI derivatives are used in fiber applications, particularly in carpet fibers, and in high-grade industrial paints in the automobile industry.[26] In the beginning, for several decades, the utility of PDIs was limited to industrial pigments due to their intrinsic poor solubility in organic solvents. For the same reason, their other excellent properties such as high fluorescence quantum yield and photostability could not be discovered until 1959.[27] However, the subsequent synthetic advancements in the field of PDI chemistry have resulted in the compounds with sufficiently good solubility, and various interesting properties. Consequently, during the last two decades, the PDIs have found many other important applications in the burgeoning field of organic electronics and photovoltaics.

This chapter accumulates a brief description of the chemistry of the PDI dyes in terms of basic synthetic methodologies, their optical and electrochemical properties, and their utilization in donor−acceptor based systems and other applications.

2.1 Preparation of the PDI Derivatives

The development of the synthetic PDI chemistry can be considered in three stages. In the beginning, PDI derivatives have been prepared mainly by the variations of the imide groups, which can primarily change only the solubility and the solid-state color of the PDIs.[28] Therefore, the versatility of this approach is very limited with respect to the modification of either optical or electronic property. In the second stage the chemists have focused their efforts on the functionalization of the bay-positions (1, 6, 7, and 12 positions of the perylene core; Figure 2.1); which enabled them not only to increase their solubility, but also to tune their optical and electronic properties at the same time. The third and the latest stage involves the functionalization of the ortho-positions of the perylene core (2, 5, 8, and 11 positions; Figure 2.1), which mainly helped in retaining the planarity of the PDI core upon chemical modification.[29,30] This approach came in the picture very recently and consequently still in the phase of development. Only the first two synthetic routes, namely the imidization and the bay-functionalization,

are discussed in the following elaboration as the thesis is exclusively based on the bay-functionalized PDIs.

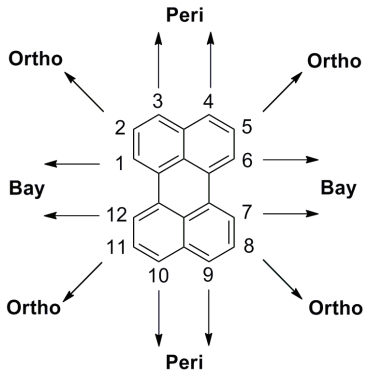

Figure 2.1. The chemical structure of the perylene along with the numbering of the various positions.

2.1.1 Imidization

Imidization involves the condensation reaction between perylene-3,4,9,10-tetracarboxylic dianhydride (abbreviated as PTCDA; Figure 2.2) and an aliphatic or aromatic amine, which results in the formation of the appropriate PDI derivatives, usually in high yields with an easy purification.[26] The solubility of the resulting PDIs varies greatly as a function of the imido-substituents. Small and linear alkyl chains lead to the PDIs quite insoluble in organic solvents. The industrial-scale syntheses of most insoluble PDI pigments, such as Pigment Red 179, Pigment Red 149 and so forth, are carried out following this method.[26,28,31]

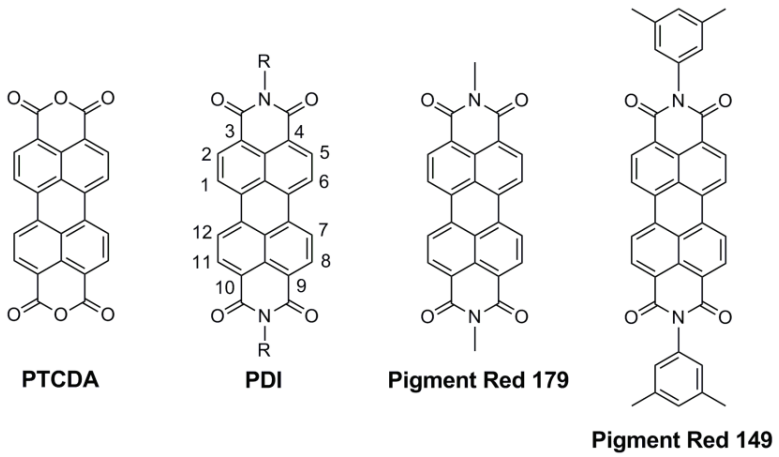

Figure 2.2. The chemical structures of PTCDA and imide-substituted PDIs, also showing the numbering of the positions of the PDI-core.

However, the current applications of PDIs in the field of organic electronics and photovoltaics generally require PDIs with reasonable solubility in common organic solvents. In this regard, Langhals and coworkers introduced their "swallow tails" as early as 1995.[32,33] These bulky imido-substituents are forced out of the plane of the PDI chromophore, thereby reducing the face-to-face π–π stacking of the PDIs.

2.1.2 Bay-functionalization

The chemical modification at the imide positions does not significantly affect the optical and electronic properties of the PDI because the HOMO and LUMO orbitals of these compounds have nodes at the imide nitrogen atoms (Figure 2.3).[22,23,28] However, these properties are drastically changed upon functionalization of the bay-positions with either electron-donor or electron-acceptor groups.

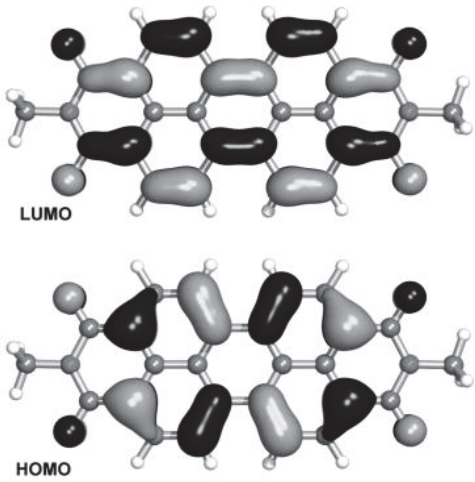

Figure 2.3. Frontier orbitals of *N,N'*-dimethyl-PDI according to DFT calculations.

Therefore, the discovery of Böhm et al. (1997) that PTCDA can be selectively dibrominated to yield regioisomerically pure 1,7-dibromo-PTCDA and subsequently, after imidization, bromine atoms can be exchanged by phenoxy and alkynyl groups, has established a landmark in the field of PDI compounds.[34] This synthetic work not only helped to improve the solubility of PDI based systems, but also opened up an efficient way to tune their electrochemical, optical, and electronic properties through functionalization of the perylene core with either electron-donor or electron-acceptor groups. Moreover, the bay-substitution also provided extra sites, in addition to the imido-positions, for the attachment of other chromophores, which is essential for the construction of the complex systems. The nucleophilic substitution of the bromo bay-substituents is straightforward, and generally the products can be isolated

in high yields. Consequently, as depicted in Scheme 2.1, fluoride-,[35] cyanide-,[36,37] phenoxy-,[34,38] and alkylamino-based nucleophiles[39] have been coupled to dibromo-PDIs, leading to bay-functionalized PDIs with a variety of interesting properties. Moreover, dibromo-PDIs have also been used in transition metal catalyzed C−C coupling reactions, such as Suzuki, Stille, and Sonogashira reactions, to obtain various aryl-, heteroaryl-, and alkynyl-functionalized PDIs.[40−47]

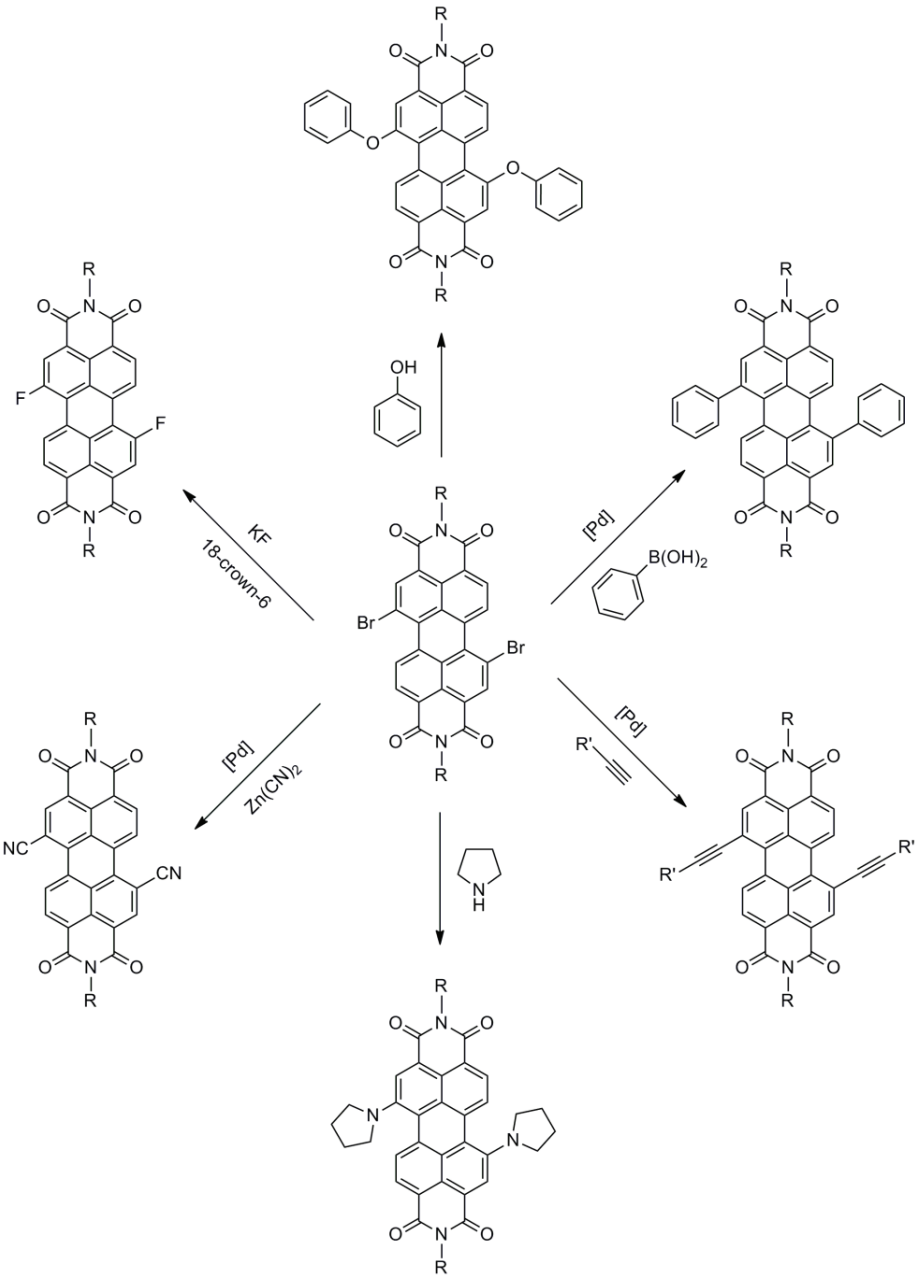

Scheme 2.1. Preparation of some important bay-functionalized PDIs from the dibromo-PDI.

A comprehensive study was carried out by Würthner et al., in the year 2004, on the procedure used by Böhm et al. for the dibromination of PTCDA and subsequent imidization.[48] This study clearly revealed that the dibromination reaction is not regioselective, rather, yields a regioisomeric mixture of 1,7- and 1,6-dibromoperylene dianhydride. Consequently, the subsequent imidization with cyclohexyl amine also yields regioisomeric mixture of 1,7- and 1,6-dibromoperylene diimides, which can be observed only by high-field (> 400 MHz) ^{1}H NMR spectroscopy. Würthner et al. had successfully separated, and also unequivocally characterized, regioisomerically pure *N,N′*-dicyclohexyl-1,7-dibromoperylene diimide from the regioisomeric mixture using repetitive recrystalization method. Until date, it remains the only existing method to obtain regioisomerically pure 1,7-dibromoperylene diimide.

The method is cumbersome and simultaneously has some limitations. Firstly, it is not possible to obtain 1,6-dibromoperylene diimide in pure form. As a consequence, regioisomerically pure 1,6-difunctionalized PDIs could not be prepared. Secondly, the method is very sensitive to the substituents at the imide-positions, and therefore does not work efficiently when the cyclohexyl groups are replaced with other groups. On the basis of their study, Würthner et al. have also suggested that the previously reported 1,7-difunctionalized PDIs were contaminated with 1,6-regioisomer. Scrutiny of the literature shows that even after this unambiguous disclosure, a mixed response has been shown by the research groups on this issue. Some of them took this issue into consideration, whereas others continuously ignored the presence of 1,6-regioisomer.

Recently, it was discovered that PDIs can be directly dibrominated using bromine at room temperature in solvents such as dichloromethane; although mono-brominated derivative is obtained as the main product along with the 1,7- and 1,6-dibromo derivatives.[49] This method has been used in preparing monobromo-PDIs in high yields. More aggravated bromination conditions, such as heating to ca. 50 ˚C, can give the regioisomeric mixture of dibromo-PDIs as the dominant products in very good yields. However, the yield of the dibromo-derivative is found to be significantly dependent on the imide-substituents. It was observed that the PDIs with bulkier imide-substituents underwent bromination more smoothly relative to those with small ones. Accordingly, the bromination of *N,N′*-bis-(dimethylpentyl)-PDI was found very facile at room temperature, but the corresponding *N,N′*-dicyclohexyl-PDI could not be brominated at ambient temperatures. This trend supports the notion that the reactivity of PDIs depends on the extent of aggregation, which in turn influences the solubility properties.

2.2 Physical Properties of PDIs

2.2.1 Optical properties

The extended conjugation in the PDI core results in a strong absorption in the visible part of the solar spectrum. The typical *N,N′*-dialkyl- or *N,N′*-diaryl-PDIs, without substitution on any of the perylene positions, are characterized by an intense absorption showing well-defined vibronic structure; with a maximum at around 525 nm and molar extinction coefficient as high as 10^5 $M^{-1}cm^{-1}$ (Table 2.1).[23] For these PDIs, the fluorescence spectrum is almost a mirror image of the corresponding absorption spectrum, and it exhibits only a small Stokes shift (approximately 10 nm).[23] The fluorescence quantum yields are almost quantitative, and the singlet excited-state lifetimes are ca. 4 ns in common organic solvents.[23,50–53] Due to their intense fluorescence, these dyes have been used as laser dyes.[54] Figure 2.4 depicts the absorption and fluorescence spectrum of *N,N′*-dioctyl-PDI in DCM.

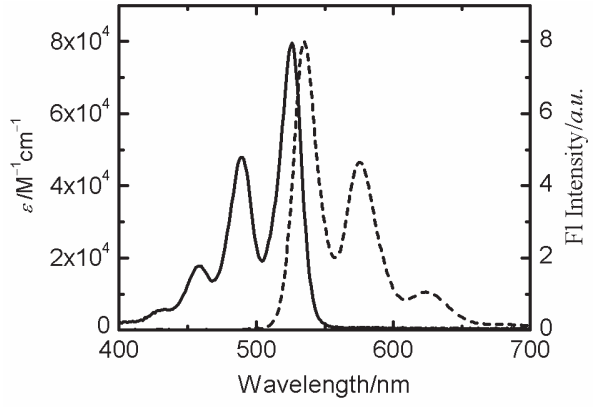

Figure 2.4. Steady-state absorption (solid line) and emission (dashed line) spectra of *N,N′*-dioctyl-PDI in DCM.

As it was mentioned previously, the imide-substitution does not have any major influence on the optical properties of the dye. The absorption and emission maxima generally vary only by ca. 5 nm with the variation of *N,N′*-alkyl or aryl substituents (Table 2.1). Resultantly, the imide-substitution is mostly advantageous to prevent aggregation, and in turn to increase the solubility.

In contrast, the bay-substitution has pronounced effect on the absorption and emission properties of the PDIs. For example, the absorption spectrum shifts to longer wavelength by about 20 nm compared to the corresponding non-bay-substituted PDI, when two phenoxy groups are attached at 1- and 7-positions.[34,55] The shift reaches by almost 50 nm when four phenoxy groups are linked at the PDI bay-region (Table 2.1).[56,57] Accordingly, the color of the fluorescence changes from yellow or yellow green to orange and red. The biggest importance of these phenoxy-substituted PDIs lies in the fact that they

exhibit far better solubility compared to their unsubstituted analogues, while retaining all the favorable properties, namely high fluorescence quantum yield, small solvatochromism and high photostability.

Table 2.1. Optical properties of selected perylene diimides.[a]

Compound	Solvent	λ_{abs}/nm	ε/M^{-1}cm^{-1}	λ_{em}/nm	Φ_f	τ_f/ns
	$CHCl_3$	526	88000	533	1.00	4.0
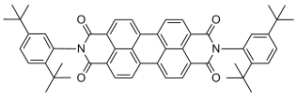	$CHCl_3$	526	95000	537	1.00	3.7
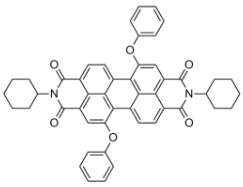	$CHCl_3$	549	55000	578	*ca*. 1.00	4.5
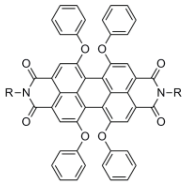	$CHCl_3$	573	45300	608	0.96	7.4
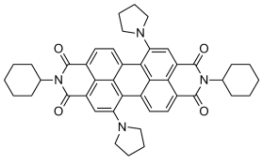	toluene	686	46000	721	0.35	4.5
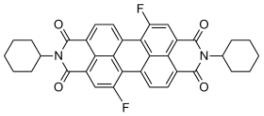	DCM	508	88000	513	0.98	3.6
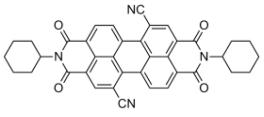	toluene	530	47000	545	1.00	–

[a] The values for the bis-bay-functionalized PDIs might have been determined from a mixture of 1,7- and 1,6-regioisomers.

The introduction of stronger electron-donors, such as *N*-pyrrolidinyl and *N*-piperidinyl groups, lead to even more pronounced shifts.[39,55,58] Accordingly, the substitution of amino groups at 1,7-bay-positions results in a bathochromic shift of ca. 150 nm in the absorption spectrum relative to the corresponding unsubstituted PDIs, and shifts the emission in near infrared region. Resultantly, these PDIs appear dark

green in the solution as well as in the solid-state. In these green dyes, the optical transition acquires significant amino-to-PDI charge-transfer character, and consequently pronounced solvatochromism is exhibited by them and their fluorescence quantum yield is significantly reduced. In contrast to electron-donating groups, the PDIs exhibit smaller spectral changes when electron-withdrawing substituents (*e.g.* fluoro, bromo, and cyano) are attached at the bay-positions.[23,36,59,]

2.2.2 Electrochemical properties

Basically, the PDI dyes have inherently high electron affinity, and consequently they are easy to reduce and rather difficult to oxidize. The electrochemical data of some of the representative PDI derivatives are summarized in Table 2.2. For simple *N,N′*-dialkyl- or *N,N′*-diaryl-PDIs with no core-substitution, two reversible reduction waves and one reversible oxidation wave are observed.[60] Similar to the optical properties, the nature of the *N,N′*-substituents has very little effect on the redox potentials. Even replacing *N,N′*-diphenyl substituents by electron-withdrawing *N,N′*-di(pentafluorophenyl) groups increases the electron-accepting capability of the PDI by only 0.11 V.[61] It also can be related to the location of the imide nitrogen atoms on a nodal plane in the frontier orbitals due to which the imide substituents modify the orbital energies only by inductive effects. In contrary, the bay-substituents can exert significant effects on the redox characteristics of the PDIs. The first reduction potential of non-bay-substituted PDIs is almost comparable to that of Buckminster fullerene.[62] The substitution of strong electron-withdrawing cyano groups leads to PDIs, which are even more easily reduced than fullerene.[36] The di- and tetrafluoro bay-substituents render only a nominal effect on the reduction potential. However, the tetrafluorinated PDIs are found somewhat easier to reduce than the corresponding difluorinated derivatives.[59]

On the other hand, the presence of electron-donating substituents at the bay-positions decreases the electron-accepting capability of PDIs. The substitution of strong electron-donating alkylamino substituents (e.g. pyrrolidinyl, piperidinyl etc.) makes the dye sufficiently electron rich, so that these green PDIs exhibit even two oxidation states at moderate potentials.[39,58] At the same time, the reductions require higher potential. For example, the derivative with two pyrrolidinyl substituents at the bay-positions is ca. 0.3 V less readily reduced and ca. 1.0 V more readily oxidized than analogues PDIs without bay substituents (Table 2.2). Accordingly, these green dyes are the only ones which cannot be considered as electron-deficient. In the presence of moderate electron-donating phenoxy substituents at the bay-positions, the oxidation occurs at relatively lower potential in comparison to the parent unsubstituted PDI. However, the phenoxy groups almost preserve the excellent electron-acceptor

character of the dye. Even in the presence of four phenoxy groups, the reduction peak moves to higher potentials only by ca. 0.1 V.[63] At the same time, these groups significantly improve the solubility of the dye by reducing the π–π aggregation. Resultantly, various phenoxy substitents with bulky substituents have been incorporated at the bay-positions to ensure high solubility and good electron accepting capability of PDIs.[63,64]

Table 2.2. Redox potentials (V vs Ferrocenium/Ferrocene) of some representative perylene diimides.[a]

Compound	Solvent	E_{1red}	E_{2red}	E_{1ox}	E_{2ox}
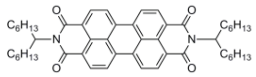	CH_3CN	−0.98	−1.21	+1.21	–
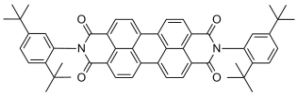	CH_3CN	−0.93	−1.15	+1.25	–
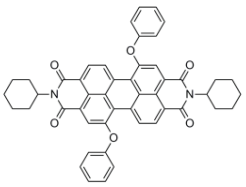	DCM	−1.11	−1.29	+1.05	–
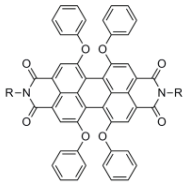	DCM	−1.09	−1.25	+0.88	–
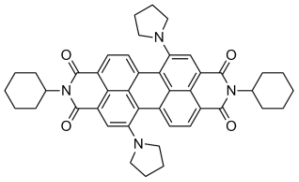	PrCN	−1.28	−1.46	+0.16	+0.23
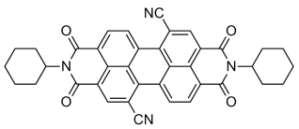	PrCN	−0.59	−0.92	–	–

[a] The values for the bis-bay-functionalized PDIs might have been determined from a mixture of 1,7- and 1,6-regioisomers.

2.3 Different Roles of PDIs in Donor−Acceptor Based Systems

A wide range of donor−acceptor based dyads and more complex systems that absorb visible light and undergo energy and/or electron transfer have been prepared and studied in detail owing to their potential applications in photovoltaic and optoelectronic devices.[9,14,65] In this context, many photoactive molecules (e.g. phthalocyanines, porphyrins, metal complexes, and fullerenes) have been explored as building blocks to construct various donor−acceptor based systems. Most of these molecular components, however, possess certain specific properties, which enable them to play only a particular role in the D−A systems, efficiently. For example, phthalocyanines and porphyrins are most suitable candidates only as efficient electron-donors, whereas fullerenes are used as efficient acceptors.[6,9,10,14] Moreover, for most of the chromophores, it is very difficult to tune their properties significantly by molecular tailoring. In this sense, the PDIs are proved to be very versatile owing to the convenient tunability of their optical and electrochemical properties. Consequently, these versatile chromophores have been employed in the D−A based systems not only as an electron-acceptor, but also as an electron-donor. In addition, these dyes have also been employed successfully as light-harvesting antenna due to their strong absorption the visible region. These aforementioned roles of PDI dyes are discussed below in brief.

2.3.1 PDIs as light-harvesting antenna

An antenna or light-harvesting molecule is the one, which increases the absorption cross-section of solar light without undergoing charge-separation itself. Following the photoexcitation, a series of one or more energy transfer steps occurs, which funnels the excitation energy to a site at which the charge-separation occurs. Resultantly, the robust nature and efficient light-harvesting capability make the PDI chromophores appealing candidates for the development of integrated light-harvesting and charge-separation systems for artificial photosynthesis. As an example, a large molecule (Py-PDI−PDI_4, Figure 2.5), having four diphenoxy-substituted PDIs (designated as PDIs) attached to a central dipyrrolidinyl-substituted PDI (designated as Py-PDI) has been prepared, which self-assembles into stacked dimers $(\text{Py-PDI}-\text{PDI}_4)_2$ in the toluene solution driven by $\pi-\pi$ interactions of the PDIs.[66] In this molecule, the peripheral PDIs act as a light-harvesting antenna. Therefore, the photoexcitation of the dimer results in energy transfer from the PDI molecules to the Py-PDIs in 21 ps, followed by quantitative charge-separation between the two Py-PDI molecules in 7 ps to form $\text{Py-PDI}^{\bullet+}-\text{Py-PDI}^{\bullet-}$ radical ion pair. The ion pair recombines with lifetime of τ_{CR} = 420 ps.

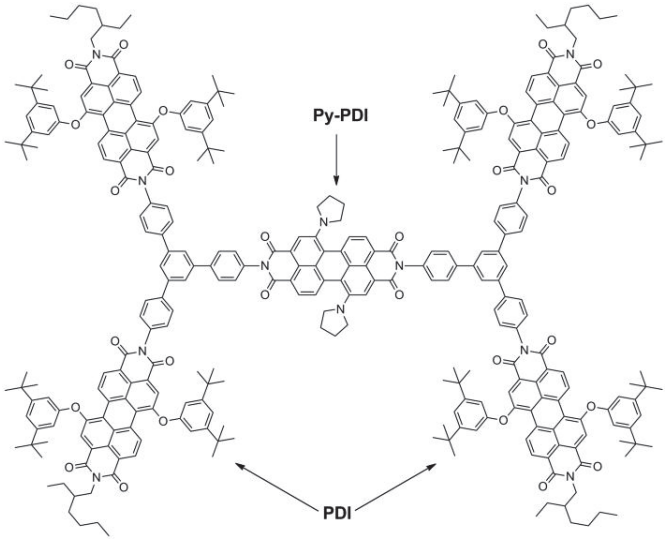

Figure 2.5. The structure of the compound Py-PDI−PDI_4.

Würthner et al. have synthesized calix[4]arene-based light harvesting arrays consisting of orange, red, and green PDIs ordered in a cofacial arrangement.[67] In the system, efficient sequential energy transfer could be observed from the initially excited orange PDI to the red, and finally from the red PDI to the green. Consequently, upon the excitation of the inner orange PDI at λ_{ex} = 490 nm, fluorescence emission of the outer green PDI at 744 nm was observed.

PDIs have also been employed as light-harvesting antenna to enhance the absorption strength of the fullerene and its derivatives, which is discussed in more detail in the section 2.5.

2.3.2 PDIs as electron-acceptors

Taking advantage of strong absorption and high electron-accepting properties of PDIs, the dyes have been extensively applied as electron-acceptors in donor−acceptor based systems to study photoinduced electron transfer. Both intermolecular electron transfer between PDI-based acceptors and various electron donors (*e.g.* polythiophenes), and intramolecular electron transfer within covalently linked donor−PDI molecules have been largely studied using transient absorption spectroscopy.[51,68−77]

The radical anion and the dianion formed by the reduction of PDIs produce easily recognizable absorptions, enabling one to follow the dynamics of the electron transfer processes. The optical spectra of these species have been well characterized due to their reasonable stability and the ease with which they can be generated. The absorption spectra of a neutral PDI and its chemically generated anion and dianion are shown in Figure 2.6. The peak molar absorption coefficient for the PDI radical anion at 713 nm is ca. 1.0×10^5 $M^{-1}cm^{-1}$, while the dianion shows an absorption coefficient of ca. 1.0×10^5 $M^{-1}cm^{-1}$ at 546 nm.[78] As with neutral PDIs, the imide substituents have limited impact on position and strength

of the anion absorption spectra, while the substituents at the bay-positions cause considerable change in the band shapes and peak positions.

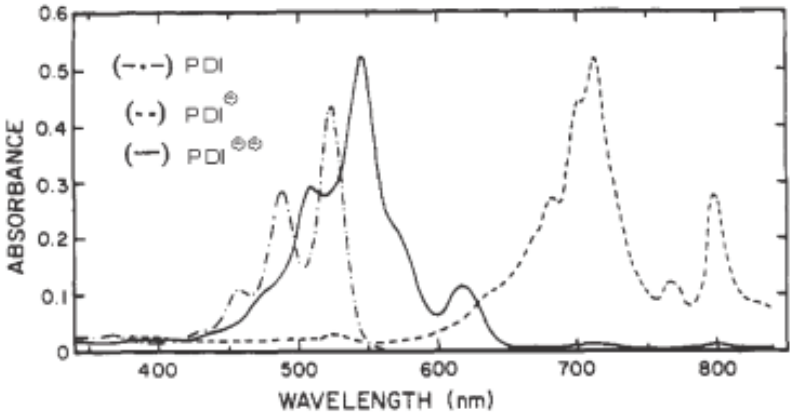

Figure 2.6. The absorption of *N,N′*-di(2,5-di-*tert*-butylphenyl)-PDI, and of its anion and dianion in ethanol (reference 78).

In the quest to prepare highly efficient donor−PDI based systems, both covalently and supramolecularly assembled architectures, consisting of either porphyrins or phthalocyanines (Pcs) as electron-donors, have been extensively synthesized and studied during the last two decades.[69−77] Earlier, the attachment of the donors to the PDIs had been carried out exclusively through the imide positions. However, during the recent years, the electron-donors are linked to the PDIs through the bay-positions using the conjugated linkers thus forming strongly coupled systems. As far as covalently linked systems are concerned, these tightly coupled ensembles have generally shown better electron transfer properties, such as longer-lived CS states. Some of the representative systems/examples are gathered in Figures 2.7 and 2.8.

The results obtained from above studies helped to understand the electron-transfer process in the systems. For example, a D−A−D triad **B1** composed of a PDI and two porphyrin moieties was reported in 1992.[73] In the triad, the photoexcitation of the porphyrin moieties at 585 nm results in the formation of $D^{+}-A^{-}-D$ charge-separated (CS) state with a time constant of 9 ps and the subsequent charge-recombination occurs with a time constant of 120 ps. The further excitation of the triad with much higher intensity irradiation at 585 nm results in formation of a $D^{+}-A^{2-}-D^{+}$ doubly CS state as demonstrated by the observation of the PDI dianion absorption at ca. 546 nm. However, the time constants for both charge-separation (178 ps) and charge-recombination (4.5 ns) were found significantly higher than for the single CS state. In a recently reported porphyrin−PDI−porphyrin triad **B2**, the two moieties were linked through the PDI bay-positions via ethynylene-linker to achieve stronger D−A interactions.[74] In this triad, the lifetime of the CS state (ca. 290 ps) was found to be

longer than that of triad **B1**. In an exactly similar tightly coupled triad **B3**, but with two phthalocyanines connected to the PDI, the excitation of phthalocyanine produces a nanosecond lived charge-separated state.[75]

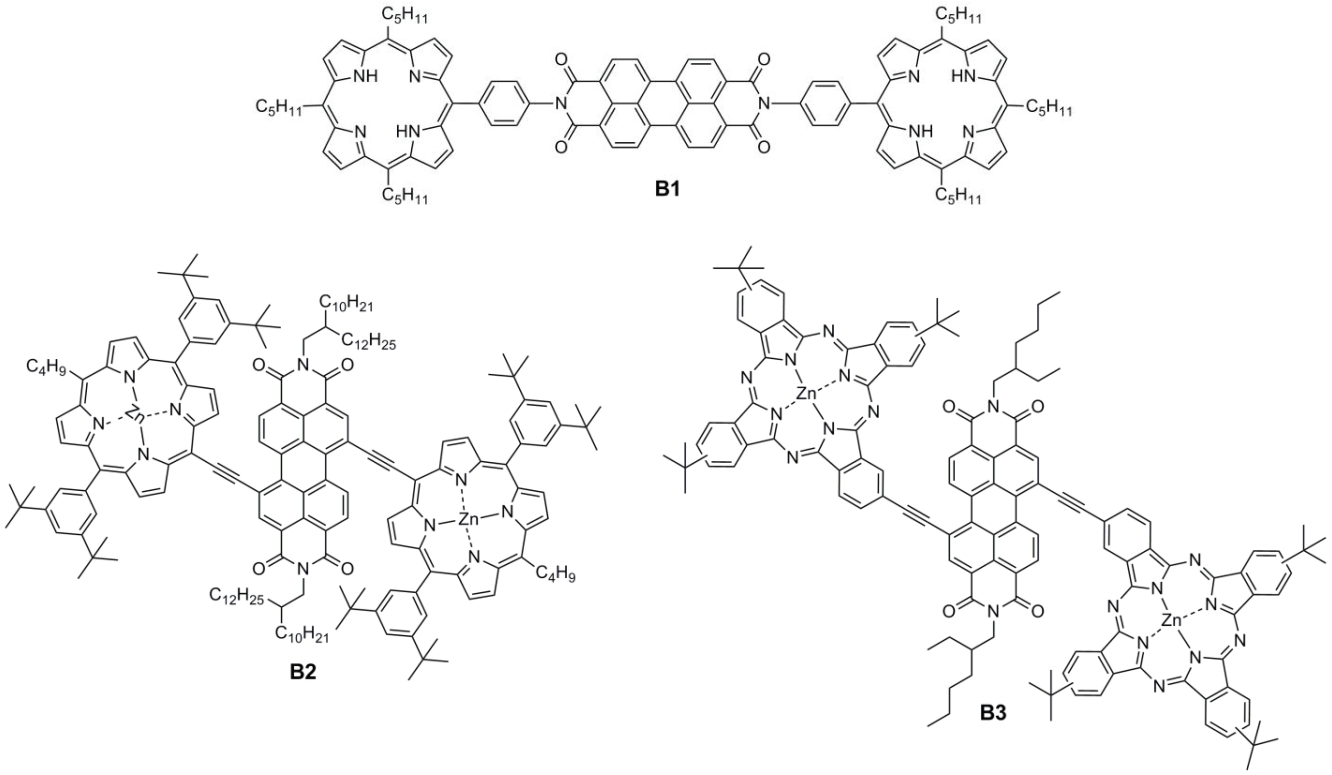

Figure 2.7. The structures of some covalently linked porphyrin−PDI−porphyrin and Pc−PDI−Pc triads studied earlier**.**

Supramolecular electron donor−acceptor assemblies (**B4** and **B5**) have also been prepared through axial coordination of a PDI entity, bearing two 4-pyridyl substituents at the imido-positions, to the Ru(II) metal centers of either two porphyrins or two phthalocyanines fragments.[76,77] Interestingly, the photophysical behavior of the two ensembles has been found to be very different in spite of the exactly similar design. In the Pc−PDI−Pc assembly, photoexcitation of either chromophore resulted in a long-lived charge-separated state with a lifetime of ca. 115 ns. In contrast, in the case of porphyrin−PDI−porphyrin ensemble, electron transfer from the porphyrin to the PDI (τ_{cs} = 5.6 ps and τ_{cr} = 270 ps) was observed only after the excitation of PDI moiety; whereas photoexcitation of the porphyrin moieties resulted in triplet energy transfer.

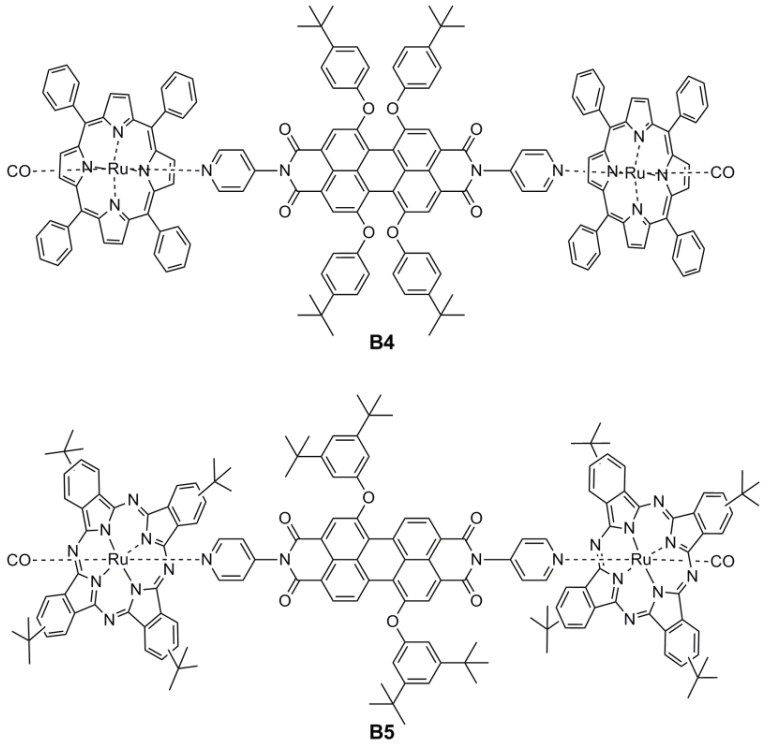

Figure 2.8. The structures of supramolecular porphyrin−PDI−porphyrin and Pc−PDI−Pc ensembles studied earlier**.**

2.3.3 PDIs as electron-donors

As mentioned previously, the substitution of the strong electron-donating groups at the bay-region produces PDIs with a good electron-donating ability.[39] In particular, the dipyrrolidinyl substituted PDI (commonly known as the "green" PDI) exhibits sufficiently low oxidation potential, which makes this derivative a potential candidate for the use as electron-donor in the donor−acceptor based systems. At the same time, this derivative has a broad and strong absorption in the near infrared region.[58] Therefore, it offers a better light-harvesting capability in comparison to most of the other commonly used electron-donors, such as porphyrins. Moreover, similar to the PDI radical anion, the radical cation of the green PDI is easily recognizable by its characteristic absorption (Figure 2.9).[58]

Regardless of the favorable properties, however, the electron-donating ability of this green-PDI has not been fully explored in the D−A systems. The first observation of the use of the green PDI as electron-donor appeared in 2002, when Wasielewski et al. prepared electron donor−acceptor dyads by linking the green PDI to electron-acceptors such as pyromellitimide and naphthalene diimide through the imide positions.[58] In these dyads, the photoexcitation of the green PDI successfully resulted in a formation of the CS state in both polar and non-polar media as evidenced by the femtosecond transient absorption measurements. After this, no further attempts were carried out for a few years.

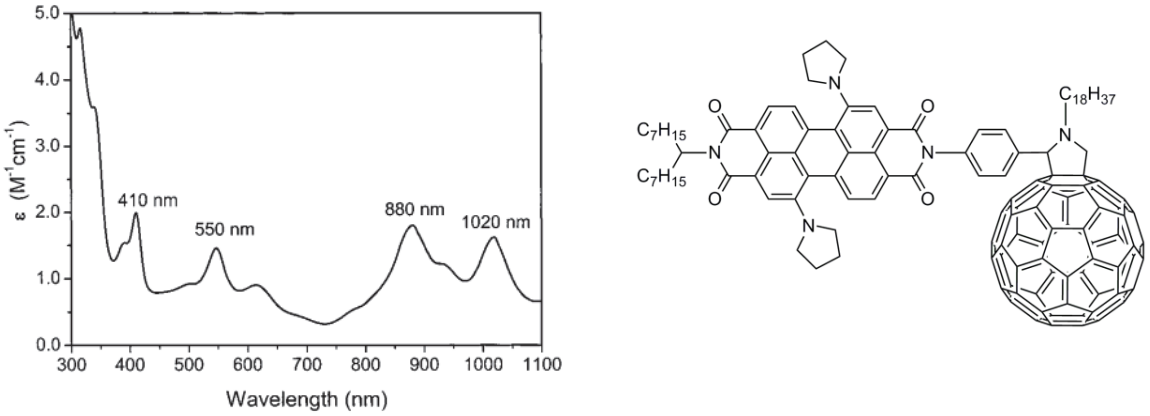

Figure 2.9. The absorption of radical cation of dipyrrolidinyl-PDI in DCM (left) and the structure of PDI−C_{60} dyad reported in 2006 (right).

Eventually, in the year 2006, a dyad has been synthesized by linking dipyrrolidinyl-PDI with fullerene, through the imide position (Figure 2.9).[79] The elaborated study of the photophysical properties of this dyad revealed that the green PDI has large reorganization energy in electron transfer.[80] Consequently, in the dyad, the electron-transfer from the green PDI to fullerene occurs only in polar solvents; whereas in non-polar solvents, the singlet energy transfer governed the excited-state deactivation. This report has hampered the employment of the green PDI as electron-donor, and resultantly no studies were carried out further.

2.4 PDIs in Other Applications

During the last two decades, the PDIs have also gained considerable amount of interest in many other burgeoning fields of applications. In this regard, they have been intensively utilized in organic field effect transistors (OFETs),[35,37,40,61,81] organic light-emitting diodes (OLEDs),[82,83] logic gates,[84] molecular sensors,[85] molecular wires[86], electro-photographic devices[87], and so forth.

Among all the *n*-type organic semiconductors, the PDIs are the most promising compounds. In terms of the absorption profile, stability, and charge carrier mobility; the PDI dyes clearly outperform fullerenes. In addition, the electron affinities of both the chromophores are in a similar range. These facts have tempted the material chemists to employ perylene diimides in photovoltaic applications.[88,89] Resultantly, the PDIs have been extensively utilized in the hetero-junction solar cells mostly as electron acceptors. In addition, they have also been copolymerized with electron rich units to achieve materials functioning as donor−acceptor materials for single system devices.[88] In the beginning, imide substituted PDIs had been employed in the solar cells; but fast intermolecular charge recombination had always been a problem with them, presumably as a result of the strong aggregation of PDIs. Later on, bay-

functionalized PDIs (e.g. diphenoxy substituted) have been used as acceptors. The presence of bay-substituents effectively suppressed the aggregation and consequently the intermolecular charge recombination could be minimized.[90] However, despite a good power conversion efficiency of 3.17 %, the hetero-junction solar cells based on bay-functionalized PDIs are still not able to compete with the solar cells based on other materials.[90] The PDIs have also been applied as sensitizers in dye-sensitized solar cells since they can be easily functionalized with carboxylic acid or anhydride groups, which serve as anchors for the attachment onto inorganic semiconductor surfaces.[88,89]

2.5 Photosensitization of Fullerene (C_{60})

Since their discovery some 25 years ago, fullerenes have generated enormous interest in the field of photochemistry and molecular photovoltaics, due to their high electron affinity,[91] excellent electron accumulation ability,[62] easy functionalization,[92] and high electron mobility.[93] Owing to these properties, fullerene is a widely used electron-acceptor material in organic solar cells. In particular, its derivative [6,6]-phenyl-C_{61}-butyric acid methyl ester (PCBM) has become a key component for the development of highly efficient bulk heterojunction solar cells.[94–97] This approach consists of generating an interpenetrating network by blending the *p*-type electron-donating conjugated polymer and PCBM as an *n*-type material. However, a severe drawback of PCBM is its poor absorption strength in the visible spectral region. Therefore, the C_{60} derivatives are often coupled with dye molecules in order to extend the solar spectrum coverage to achieve better absorption efficiencies.

A literature survey shows that a large number of "fullerene−donor" systems have been reported, in which photoinduced energy and electron transfer processes either compete with each other or take place selectively depending on the polarity of the media.[98−102] Whereas, there are few examples, which exhibit exclusively the transfer of energy from the light-harvesting antenna to the fullerene unit in both polar and non-polar environment.[103−107] In this regard, PDI chromophores have also been chosen as antennas aiming to utilize their excellent light-harvesting properties.[106,107] The structures of some representative PDI−C_{60} dyads are gathered in Figure 2.10. An efficient and fast intramolecular energy transfer from the PDI to the fullerene was evidenced in these dyads. It makes them suitable for the use in bulk heterojunction solar cells considering that PDI will act as a light-harvesting antenna, while an electron transfer will occur selectively from *p*-type polymer to fullerene. However, the practical problem towards the use of these dyads in solar cells lies in the fact that the PDIs have almost comparable electron-accepting capability to that of fullerene. Consequently, in the photoactive layer, the PDI moiety would also act as an electron-acceptor instead of acting exclusively as an antenna.

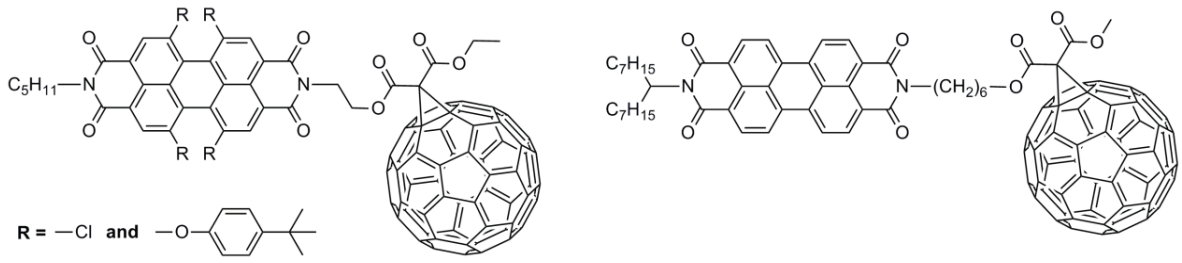

Figure 2.10. The structures of some PDI−C_{60} dyads in which PDI is employed as light-harvesting antenna.

Therefore, in order to perform the specific role of harvesting and transferring the light energy to fullerene, the light-harvesting molecule must have high enough oxidation potential to prevent any electron transfer to fullerene. At the same time, it is also important that the molecule has first reduction potential higher than fullerene. In that case only the fullerene moiety could act as unambiguous electron acceptor, when the system is incorporated in a bulk heterojunction device with the electron-donor material.

3 Materials and Methods

The experimental aspects of the work, especially regarding the characterization, electrochemical, and spectroscopic studies, are described in this section.

3.1 Characterization

All the synthesized compounds were characterized by NMR spectroscopy and/or mass spectrometry. The ^{1}H, ^{13}C, and $^{1}H-^{1}H$ COSY NMR spectra were recorded with Varian Mercury 300 MHz spectrometer in $CDCl_3$ at room temperature. All the chemical shifts are quoted relative to TMS ($\delta = 0.0$ ppm); δ values are given in ppm and J values in Hz. The NMR spectroscopy proved to be a very powerful tool in characterization of the 1,7- and 1,6-regioisomers of bay-functionalized PDIs. The ^{1}H NMR spectra were utilized not only to estimate the relative proportion of the 1,7- and 1,6-regioisomers in the mixture, but also to monitor the separation process of the two. Moreover, the ^{1}H NMR spectra also allowed the unequivocal assignment of the signals to the 1,7- and 1,6-regioisomers. As far as donor−acceptor dyads are concern, the comparison of the ^{1}H NMR spectra of the individual chromophores with those of dyads helped to prove the close-proximity of the donor and acceptor moieties in the dyads. High-resolution mass spectra were measured with Waters LCT Premier XE ESI-TOF benchtop mass spectrometer. To obtain accurate mass value, we simultaneously infused the solution of the reference compound (leucine enkephaline) with analyte, and processed the experimental spectra according to the routine of accurate mass measurements (peak centering and lock-mass TOF correction).

3.2 Opto-electrochemical Studies and Instrumentation

3.2.1 Differential pulse voltammetry

The differential pulse voltammetric studies were performed to compare the redox characteristics of the individual entities and those of the dyads to obtain a better understanding of the ground-state interaction between the two closely linked donor and acceptor moieties. The obtained redox potentials were also used to estimate the energies of the charge-separated states of the dyads [$E_{CS} = E_{1ox}(D) - E_{1red}(A)$].

The differential pulse voltammograms were obtained using potentiostat (Iviumstat compactstat IEC 61326 Standard) controlled by PC with the software Iviumsoft (Version 1.752) in a three-electrode single-compartment cell consisting of a platinum-in-glass as working electrode, Ag/AgCl as reference electrode, and a graphite rod as counter electrode. During the measurements, the values of pulse height,

pulse width, and step voltage were set to 20 mV, 20 ms, and 2.5 mV, respectively. Benzonitrile containing 0.1 M tetrabutylammonium tetrafluoroborate was used as solvent. The concentrations of the samples were ca. 0.5 mM. The measurements were done under continuous flow of nitrogen. A Fc/Fc^+ redox couple was used as an internal standard, which exhibited oxidation at +0.48 V. The measurements were carried out in both directions: toward the positive and negative potential. The oxidation and reduction potentials were calculated as an average of the two scans.

3.2.2 Steady-state absorption and emission spectroscopy

The absorption spectra of the solutions were measured with Shimadzu 3600 UV-Vis absorption spectrophotometer in the range 350−850 nm. In the case of donor−acceptor dyads, the absorption spectra were used to know the absorption regions of the individual chromophores and to select the best possible excitation wavelength for the steady-state emission and time-resolved absorption measurements. The comparison of the absorption spectra of individual chromophores with those of dyads helped to reveal the presence of the ground-state interaction between the two acting moieties.

The examination of the fluorescence emission characteristics of all the donor−acceptor dyads and also of the relevant individual chromophores was performed to have preliminary estimations of the efficiency of photoinduced electron and/or energy transfer processes taking place between the donor and acceptor moieties. The fluorescence quantum yields of the phenoxy-substituted PDIs (the red PDIs) and their derivatives were determined relative to fluorescein (Φ_f = 0.92 in 0.1 N NaOH aqueous solution); whereas cresyl violet (Φ_f = 0.54 in methanol) was used as a reference dye for the compounds based on pyrrolidinyl-substituted PDIs (the green PDIs).[55,108] The quantum yield of dibenzo[*a,c*]phenazine molecule was determined relative to anthracene (Φ_f = 0.27 in ethanol).[109] The given quantum yields are averaged from values measured at three different excitation wavelengths. For these measurements, the optical densities at the excitation wavelengths were maintained at around 0.1 to avoid reabsorption.

3.2.2 Time-resolved absorption and emission spectroscopy

The flash-photolysis method was used to conduct time-resolved absorption measurements in nano to microsecond time scale with 10 ns laser pulses. The optical scheme of the flash-photolysis instrument is shown in Figure 3.1. In this method, the sample is photoexcited by a strong light pulse (known as the pump pulse). The pump pulse is used to excite the sample molecules to the higher energy. Reduced population of the ground-state molecules results in the decreased ground-state absorption (so-called bleaching) at the corresponding wavelengths. The transient states formed upon the excitation have their

individual absorption characteristics, which give rise to the increased absorption at the respective wavelengths. In this way, the sample undergoes negative and positive absorption changes due to the population disturbance caused by the photoexcitation. The absorption changes are monitored by the continuous light called the probe, as a function of time at the given wavelength.

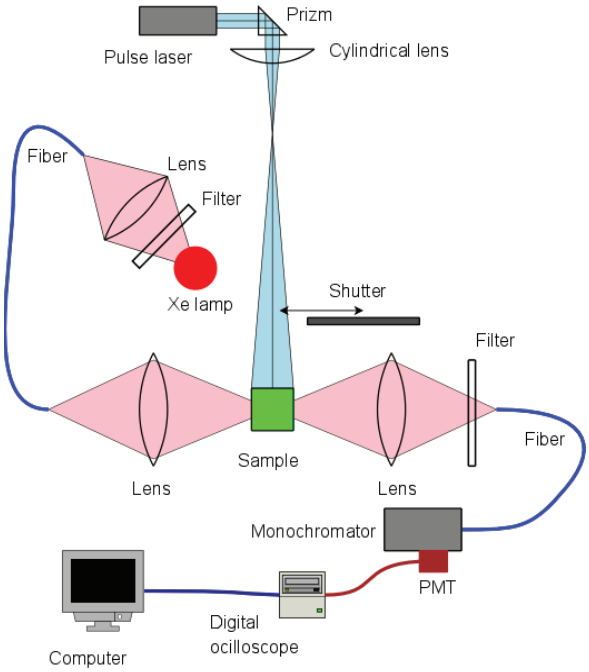

Figure 3.1. The simplified scheme of the flash-photolysis instrument.

In the present study, the pump pulses, either directly from the second harmonic of Nd:YAG laser (λ_{ex} = 532 nm) or from a tunable Ti:sapphire laser (λ_{ex} = 400 or 420 nm) pumped by the second harmonic of Nd:YAG laser, were used for the excitation. The continuous white light from the xenon lamp was used as the probe. The samples were deoxygenated by the continuous bubbling of nitrogen throughout the measurements starting from 30 minutes prior to the measurement. The optical density of solutions at excitation wavelength was maintained ca. 0.6, and the excitation power density was maintained ca. 1 mJ/cm^2.

The pump-probe technique was used to detect fast processes taking place in picosecond time-scale and also to investigate the formation of charge-separated state. The excitation source was a Ti:sapphire laser generating 100 fs pulses at ca. 800 nm, and the excitation wavelength used to conduct these studies was 420 nm. In the articles I, III, and IV, the transient absorption results were presented as decay component spectra, where the amplitudes of the components from the fitting are plotted at each wavelength.

Fluorescence decays of the samples in the nanosecond and sub-nanosecond time scales were measured using a time-correlated single photon counting (TCSPC) system (PicoQuant GmbH) consisting of PicoHarp 300 controller and PDL 800-B driver. The compounds based on red PDIs were excited with the pulsed diode laser head LDH-P-C-485 at 483 nm. The green PDIs were excited with the pulsed diode laser head LDH-P-C-650 at 648 nm. For the dibenzo[*a*,*c*]phenazine based molecules, the samples were excited with the pulsed diode laser head LDH-P-C-405B at 404 nm. Fluorescence decays were measured at the wavelength of emission maximum. The signals were detected with a micro channel plate photomultiplier tube (Hamamatsu R2809U). The time resolutions of the TCSPC measurements were 60 ps, 110 ps, and 80 ps at the excitation wavelengths 404 nm, 483 nm, and 648 nm, respectively.

4 Results and Discussion

This chapter involves a summary of the syntheses and spectroscopic results, which were introduced in the publications I–IV.

As mentioned previously in Chapter 2, during the last decade numerous bay-functionalized PDIs have been synthesized. These derivatives possess various peculiar properties, which make them attractive building blocks for the use in photoinduced donor–acceptor systems. Among all, however, the phenoxy and pyrrolidinyl substituted PDIs are of special interest. Basically, the unsubstituted PDIs are excellent *n*-semiconductors, but exhibit poor solubility due to π–π stacking when employed in complex systems. Therefore, the phenoxy groups were attached to the bay-region aiming to improve the solubility of the dye in common organic solvents while retaining the basic electron-acceptor and optical characteristics. On the other hand, the attachment of the strong electron-donating pyrrolidine groups makes the dye a good electron donor while improving the solubility at the same time. Moreover, the lowest energy electronic transition moves to longer wavelengths, which helps to harvest solar energy more efficiently. Therefore, we planned to employ these bay-functionalized PDIs in the construction of donor–acceptor systems, which can undergo directional photoinduced electron or energy transfer process. But prior to their use, we wanted to know the exact properties of the 1,7- and 1,6-regioisomers of these two bay-functionalized PDIs in view of the two reports which evidenced different behavior of the two regioisomers when *n*-octylamino and marpholino groups are attached at the bay-region.[110,111]

4.1 The Synthesis of *N*,*N*′-dioctyl-1,7(6)-dibromoperylene diimide

All the PDI based derivatives and dyads, reported in the thesis, were synthesized from *N*,*N*′-dioctyl-1,7(6)-dibromoperylene diimide **3**, which was a mixture of 1,7- and 1,6-regioisomers in a ratio ca. 3:1. The synthesis of this mixture was carried out from PTCDA **1** in two steps according to the route depicted in Scheme 4.1. At first, the dibromo-PTCDA was prepared by the bromination of PTCDA **1**, following the widely used method described by Böhm et al in 1997.[34] The reaction led to the crude product **2** which was a mixture of 1,7- and 1,6-dibromo-PTCDA along with a very small amount of 1,6,7-tribromoperylene dianhydride.[48] In this mixture, the presence of 1,7- and 1,6-regioisomers can only be detected by high-field (600 MHz) ^{1}H NMR spectroscopy in concentrated D_2SO_4. Moreover, the crude product **2** is insoluble in all the organic solvents. Therefore, it was subjected to the imidization without additional purification.

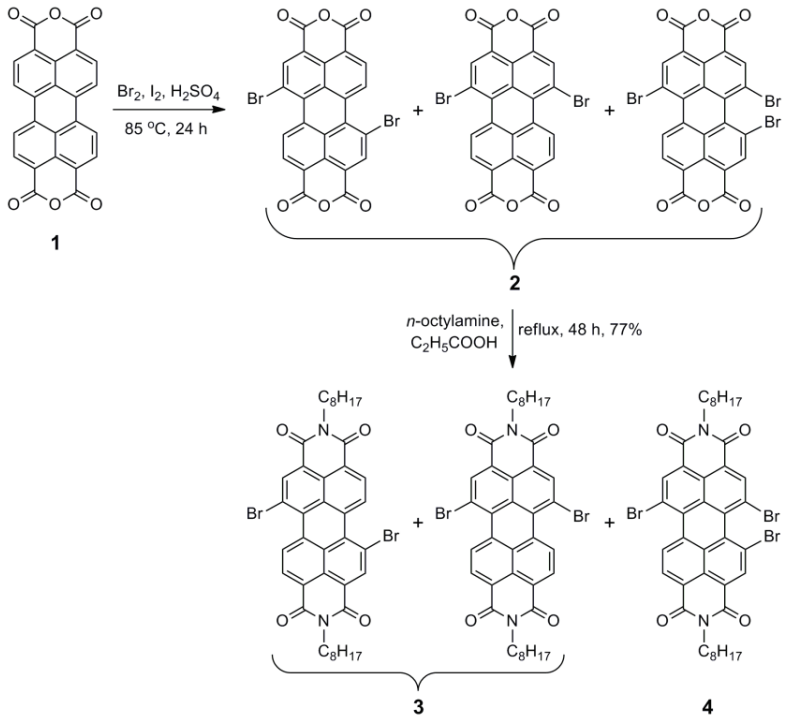

Scheme 4.1. Bromination of perylenetetracarboxy dianhydride **1** and subsequent imidization.

Imidization of the crude product **2** with *n*-octylamine in refluxing propionic acid yielded dibromo-PDI **3** as a mixture of 1,7- and 1,6-regioisomers along with a small quantity (ca. 1 %) of 1,6,7-tribromo-PDI **4**. The 1,6,7-tribromo-PDI **4** was successfully isolated from the product **3** by column chromatography (Silica-60/CH_2Cl_2). However, 1,7- and 1,6-dibromo-PDIs could not be separated chromatographically and the presence of isomers could not be detected by 300 MHz ^{1}H NMR spectroscopy. Consequently, the regioisomeric mixture was used as such for further reactions.

4.2 Chemistry of 1,7- and 1,6-Regioisomers of Diphenoxy Substituted PDI

4.2.1 Synthesis, separation, and characterization

The regioisomeric mixture **3** of dibromo-PDIs was reacted with 2,4-di-*tert*-butylphenol to afford a regioisomeric mixture of *N,N′*-dioctyl-1,7- and 1,6-di(2,4-di-*tert*-butylphenoxy)perylene diimide by the nucleophilic substitution of both bromine atoms (Scheme 4.2).

The product, after purification, was characterized by ^{1}H NMR spectroscopy (300 MHz, $CDCl_3$) and mass spectrometry. The presence of 1,7- and 1,6-regioisomers in the product was verified by ^{1}H NMR spectrum, which exhibited two sets of signals with different intensities in the aromatic region. Two well resolved doublets and singlets were observed in the region between 8.1−8.7 ppm (Figure 4.1a). In

addition, two broad doublets were overlapped at around 9.6 ppm. The integration areas of the doublets at 8.56 and 8.63 ppm revealed that 1,7-**5** and 1,6-**5** are present in the product in a ratio 70:30. These two regioisomers, 1,7-**5** and 1,6-**5**, could not be separated by conventional column chromatography. Fortunately, these two regioisomers had shown very different solubility in toluene. The minor isomer 1,6-**5** exhibited significantly better solubility (as high as 15 mg/mL) in comparison to major isomer 1,7-**5** (ca. 0.2 mg/mL). We exploited this difference to separate them from each other, successfully. The process must be repeated at least three times in order to achieve complete separation of both regioisomers. The separation process was monitored thoroughly by 300 MHz ^{1}H NMR spectroscopy.

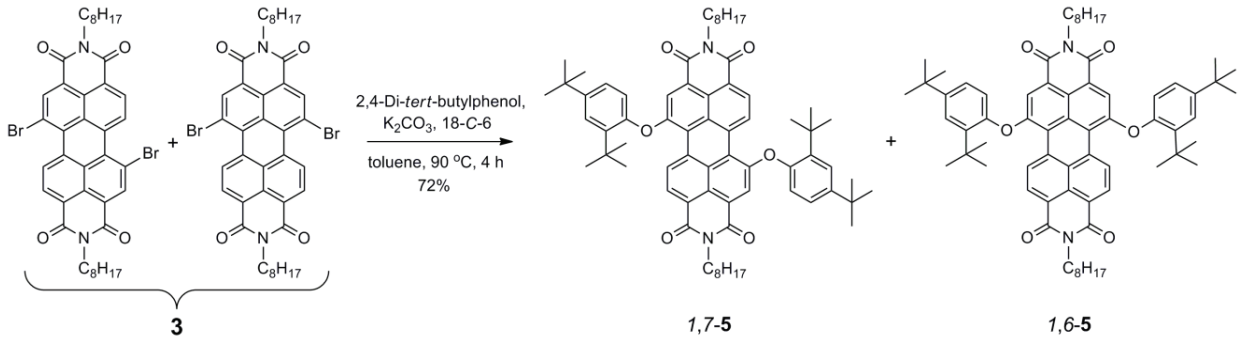

Scheme 4.2. Synthesis of compounds 1,7-**5** and 1,6-**5**.

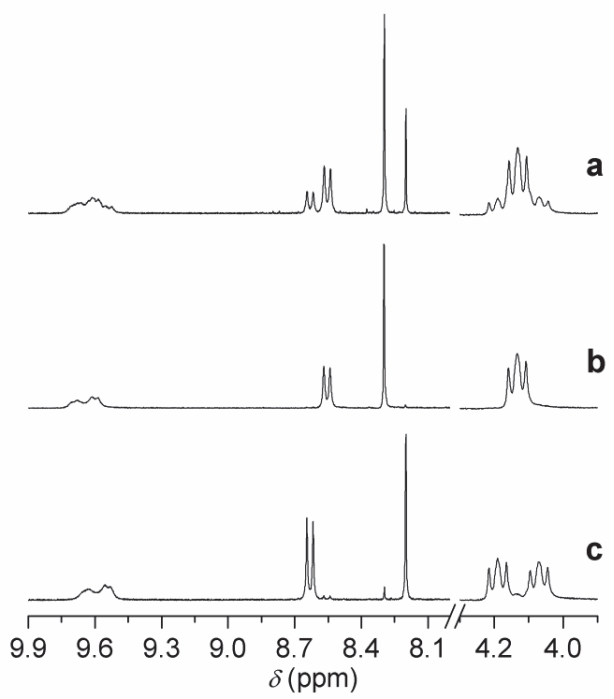

Figure 4.1. ^{1}H NMR (300 MHz, $CDCl_3$) spectra: (a) regioisomeric mixture of 1,7-**5** and 1,6-**5** (b) pure 1,7-**5** regioisomer (c) pure 1,6-**5** regioisomer.

It is to be noted that the characteristic signals of the regioisomers 1,7-**5** and 1,6-**5** in the ^{1}H NMR spectra (Figure 4.1), one singlet and two doublets of perylene core protons, exhibit significant differences in the chemical shift values (0.1 ppm for the singlets and 0.08 ppm for the doublets at 8.53−8.66 ppm). However, a convenient unequivocal assignment of the NMR spectrum to the individual regioisomers 1,7-**5** and 1,6-**5** was performed based on the signal of methylene protons next to the imide nitrogen at ca. 4.13 ppm. Due to the same chemical environment, all four methylene protons of major regioisomer 1,7-**5** appear as one triplet at 4.13 ppm (Figure 4.1b). On the other hand, for minor regioisomer 1,6-**5** two separate triplets (at 4.19 and 4.07 ppm) were observed for the same four methylene protons (Figure 4.1c). In this way, an unambiguous characterization has been made successfully on the basis of 300 MHz ^{1}H MNR spectroscopy.

4.2.2 Comparison of electrochemical and optical properties

The two regioisomers of diphenoxy substituted PDIs (1,7-**5** and 1,6-**5)**, which are mainly utilized for their good electron acceptor capability, displayed very similar redox characteristics. Both the isomers displayed the characteristic two reversible one-electron reductions at almost the same potentials (Table 4.1). For the isomer 1,7-**5**, the two reductions occurred at −0.61 V and −0.85 V (vs Ag/AgCl). Whereas for *1,6*-**5**, both first and second reductions were found to be slightly shifted to more negative values by 30 and 40 mV, respectively. As far as oxidation potential is concerned, only one irreversible oxidation peak was observed at around +1.47 V for both compounds as expected. In this way, the two regioisomers 1,7-**5** and 1,6-**5** displayed virtually the same redox capabilities.

Table 4.1. Redox potentials (*V* vs Ag/AgCl) of 1,7-5, 1,6-5, 1,7-6[a] and 1,6-6[a] obtained by DPV in benzonitrile ([a] see chapter 4.3).

Compound	E_{1ox}	E_{2ox}	E_{1red}	E_{2red}
1,7-5	+1.47	−	−0.61	−0.85
1,6-5	+1.46	−	−0.64	−0.89
1,7-6	+0.63	+0.77	−0.83	−0.99
1,6-6	+0.77	+1.28	−0.83	−0.99

The steady-state absorption spectra of both regioisomers are dominated by characteristic $\pi-\pi^*$ transitions and resemble with each other (Figure 4.2). For both regioisomers, the absorption bands attributed to S_0-S_1 electronic transition are located at around 555 nm in $CHCl_3$. However, the molar extinction coefficient was found to be lower for 1,6-**5** in comparison to 1,7-**5**. The absorption properties

of these two regioisomers are also investigated in non-polar toluene and polar benzonitrile, but no other noticeable differences were observed between the two.

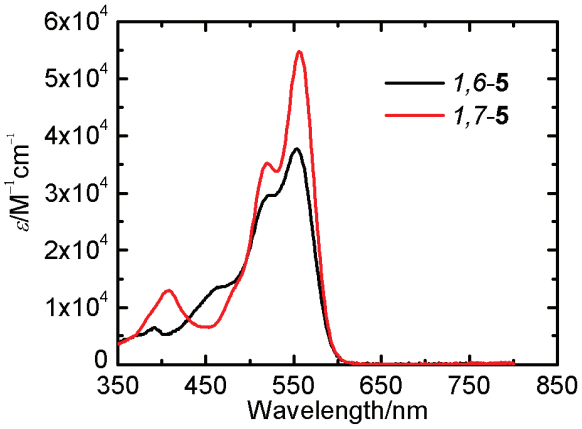

Figure 4.2. Absorption spectra of 1,6-**5** (black) and 1,7-**5** (red) in chloroform.

Further insight into the optical properties of 1,7-**5** & 1,6-**5** was gained by steady-state emission and time-correlated single photon counting (TCSPC) methods. The two regioisomers were examined in three different solvents *i.e.* toluene, chloroform, and benzonitrile. The emission spectra and fluorescence decays of these compounds in chloroform are depicted in Figure 4.3, and the data are summarized in Table 4.2.

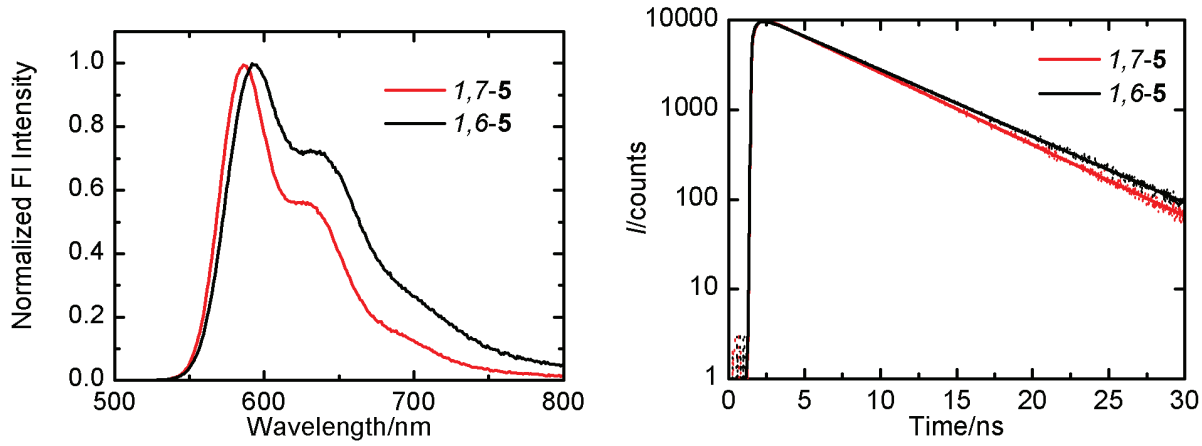

Figure 4.3. Normalized emission spectra (left, λ_{ex} = 474 nm) and fluorescence decay time profiles (right, λ_{ex} = 483 nm) of 1,7-**5** (red, λ_{mon} = 587 nm) and 1,6-**5** (black, λ_{mon} = 593 nm) in $CHCl_3$.

Both the regioisomers 1,7-**5** and 1,6-**5** exhibited approximately similar emission characteristics as well. The emission bands were approximately the mirror image of their absorption bands with Stokes shifts of ca. 35 nm. However, the emission band of 1,6-**5** (λ_{max} = 593 nm) was found to be slightly broader

and red shifted in comparison to that of 1,7-**5** (λ_{max} = 587 nm) in chloroform as shown in Figure 4.3. The emission maxima of both isomers exhibited small bathochromic shift (ca. 14−16 nm) upon moving from non-polar toluene to moderately polar chloroform (Table 4.2). Both regioisomers were found to be highly emissive, in all the investigated solvents, with fluorescence quantum yields greater than 0.92. The singlet-state lifetimes were also found approximately similar for 1,7-**5** and 1,6-**5** (Table 4.2).

Table 4.2. Optical properties of 1,7-5, 1,6-5, 1,7-6[a] and 1,6-6[a] in different solvents ([a] see chapter 4.3).

Compound	Solvent	λ_{abs}(nm)	λ_{em}(nm)	Φ_f	τ_f (ns)
1,7-5	toluene	548	573	0.97	4.91
	chloroform	556	587	0.97	5.39
	benzonitrile	553	583	0.98	4.79
1,6-5	toluene	545	577	0.96	5.52
	chloroform	554	593	0.94	5.81
	benzonitrile	550	590	0.92	5.35
1,7-6	hexane	661	703	0.54	6.08
	toluene	687	724	0.40	4.48
	chloroform	702	743	0.32	3.47
	ethanol	699	770	0.07	1.03
1,6-6	hexane	647	728	0.09	1.27
	toluene	671	735	0.07	1.26
	chloroform	688	752	0.06	1.01
	ethanol	688	778	0.02	0.51

4.3 Chemistry of 1,7- and 1,6-Regioisomers of Dipyrrolidinyl Substituted PDI

4.3.1 Synthesis, separation, and characterization

The 1,7- and 1,6-regioisomers of dipyrrolidinyl substituted PDI, 1,7-**6** and 1,6-**6**, were synthesized from the dibromo-PDI **3** by the substitution of bromine atoms with pyrrolidine groups following the well established procedure (Scheme 4.3).[39] Separation of 1,7-**6** and 1,6-**6** was performed by conventional column chromatography on Silica 100 using DCM as mobile phase. The two regioisomers were found to be of different colors; the 1,7-**6** is deep green in color, while 1,6-**6** is deep blue.

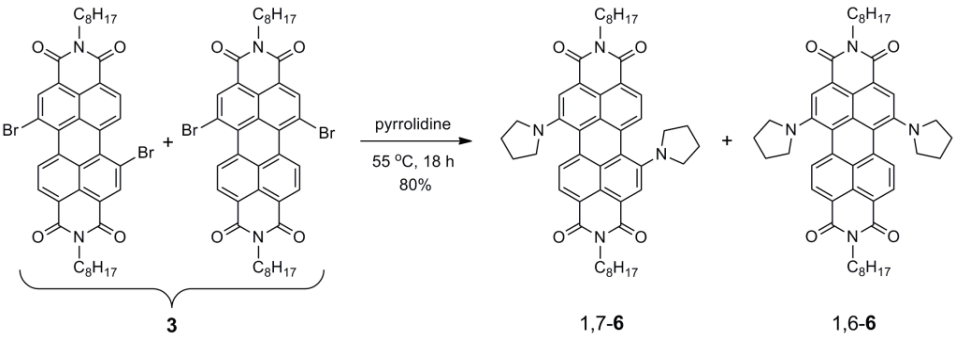

Scheme 4.3. Synthesis of compounds 1,7-**6** and 1,6-**6**.

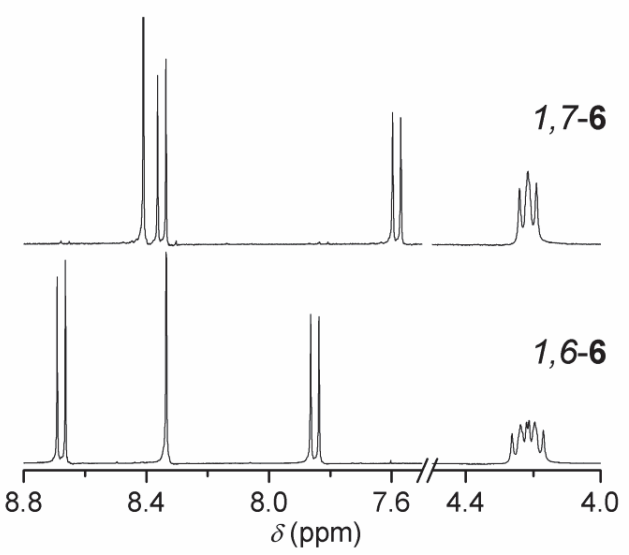

Figure 4.4. ^{1}H NMR (300 MHz, $CDCl_3$) spectra of regioisomers 1,7-**6**, and 1,6-**6**.

Both the regioisomers were characterized on the basis of 300 MHz ^{1}H NMR spectroscopy. Similar to previously mentioned 1,7- and 1,6-diphenoxy substituted PDIs, an unequivocal assignment of the ^{1}H NMR spectrum to the individual regioisomers 1,7-**6** and 1,6-**6** was based on the signal of methylene protons next to the imide nitrogen at 4.21 ppm (Figure 4.4). In the aromatic region two doublets and one singlet of the regioisomers 1,7-**6** and 1,6-**6** exhibit large differences in chemical shift values (ca. 0.35 ppm). Additionally, these aromatic signals for 1,6-**6** appear in different order (doublet, singlet, doublet) compared to that of 1,7-**6** (singlet, doublet, doublet). This different pattern of appearance of singlet and doublets makes them even more easily recognizable by 300 MHz ^{1}H NMR spectroscopy.

4.3.2 Comparison of electrochemical and optical properties

Unlike the 1,7- and 1,6-diphenoxy substituted PDIs, the two regioisomers of dipyrrolidinyl substituted PDIs (1,7-**6** and 1,6-**6**) exhibited crucial differences in their electrochemical and optical properties. The

regioisomer 1,7-**6** exhibited two oxidation peaks at moderate potentials (E_{1ox} = +0.63 V, E_{2ox} = +0.77 V). For the 1,6-regioisomer, on the other hand, the two oxidation peaks were observed at +0.77 V and +1.28 V. This difference in the oxidation potentials clearly indicates that the removal of electrons from 1,6-**6** is more difficult in comparison to 1,7-**6**. However, both the regioisomers exhibited two reversible one-electron reduction peaks at the same potentials (E_{1red} = −0.83 V, E_{2red} = −0.99 V) implying the same electron-acceptor abilities (Table 4.1).

For these two regioisomers, pronounced differences were also observed in their absorption features (Figure 4.5). In the case of 1,7-**6**, the lowest energy band is centered at 702 nm and has a small shoulder at ca. 650 nm. Whereas for the regioisomer 1,6-**6**, this band is significantly weaker and blue shifted by ca. 15 nm. In addition to the lower energy absorption at ca. 700 nm, the 1,7-regioisomer exhibits a higher energy S_0−S_2 electronic transition at 428 nm; but the corresponding band is almost absent in the case of 1,6-regioisomer. Quite surprisingly, 1,6-**6** has an additional band centered at 550 nm, which looks very similar to the lowest energy band of the diphenoxy substituted PDIs (1,7-**5** and 1,6-**5**). We presume that these differences in the absorption pattern are collectively responsible for the different colors of the two regioisomers. The lowest energy bands of both the regioisomers were found dependent on polarity of the solvent. A significant red shift was observed for both upon increase in the polarity of the surrounding medium (Table 4.2).

The emission properties of 1,7- and 1,6-dipyrrolidinyl substituted PDIs (1,7-**6** and 1,6-**6**) were investigated in four different solvents, namely hexane, toluene, chloroform and ethanol. The emission data are summarized in Table 4.2.

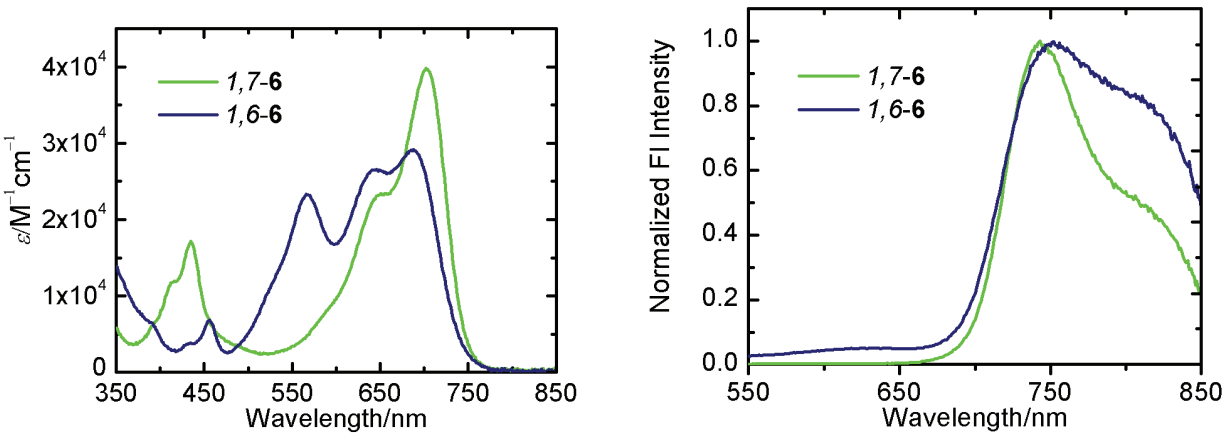

Figure 4.5. Absorption (left) and normalized emission spectra (right) of 1,7-**6** (green) and 1,6-**6** (blue) in chloroform.

The 1,7- and 1,6-derivatives displayed large differences in their emission properties as well. However, the differences were found to be more pronounced in the non-polar solvents. For example, in hexane,

the emission maximum of 1,6-**6** is bathochromically shifted by 25 nm compare to that of 1,7-**6** (Table 4.2). Whereas, in polar and weakly polar solvents (i.e. ethanol, chloroform and toluene), the emission maxima of 1,6-**6** is bathochromically shifted by ca. 10 nm relative to that of 1,7-**6**. Quite unexpectedly, large differences are observed in the fluorescence quantum yields and lifetimes of these two isomers. Both were found significantly higher for the 1,7-regioisomer compared to those for 1,6-regioisomer in all the investigated solvents (Table 4.2).

4.4 Synthesis of new derivatives of PDIs by the bay-attachment of 2-(benzyloxymethyl)-pyrrolidine

The major outcome of the aforementioned work was the exposure of the very different electrochemical and optical properties of the 1,7- and 1,6-dipyrrolidinyl-PDIs. Since the 1,7-dipyrrolidinyl-PDI has been a widely used dye for the construction of the photoactive systems, we were interested to further investigate the mutual differences in the excited-state properties of the 1,7- and 1,6-regioisomers in donor−acceptor based systems. Moreover, in the conventional 1,7-dipyrrolidinyl-PDI, the attachment of the other chromophore is possible only at the imide positions; which induces a potential drawback of keeping the two acting chromophores away from each other. It limits their applications in the donor−acceptor systems and also the performance of the synthesized systems. Within this framework, therefore, synthesis of the new derivatives with functionalized pyrrolidinyl groups was planned.

In order to synthesize such PDI derivatives, the very first task was to synthesize a suitable pyrrolidine derivative, which readily reacts with dibromo-PDI **3**. We chose *L*-proline **7** as the starting compound and transformed it to 2-(benzyloxymethyl)-pyrrolidine **11** in four straightforward steps as depicted in Scheme 4.4. Among many groups available for protecting hydroxyl groups, the selection of benzyloxy group was based on its electron donating nature and the robustness towards the harsh reaction conditions. The electron donating ability was highly desirable in order to enhance the reactivity of 2-(benzyloxymethyl)-pyrrolidine **11** as a nucleophile.

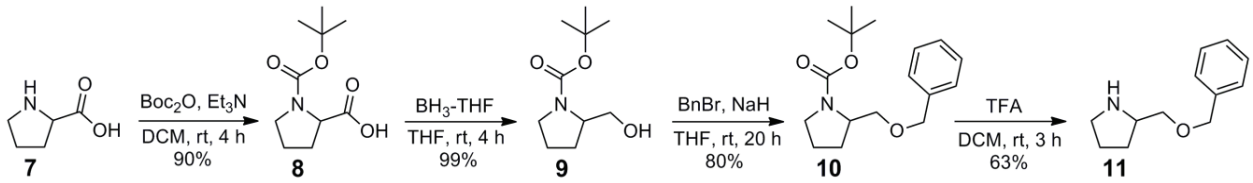

Scheme 4.4. Synthesis of 2-(benzyloxymethyl)-pyrrolidine **11** from *L*-proline **7**.

The next task was to attach 2-(benzyloxymethyl)-pyrrolidine **11** to the PDI core *via* substitution of bromine atoms of dibromo-PDI precursor **3** to obtain *N,N′*-dioctyl-1-bromo-7(6)-[2-(benzyloxymethyl)pyrrolidinyl]perylene diimide **12** and *N,N′*-dioctyl-1,7(6)-bis-[2-(benzyloxymethyl)pyrrolidinyl]perylene diimide **14** (Scheme 4.5). Taking into account that attachment of functionalized pyrrolidine to the PDI core was unprecedented, this task was considered to be the biggest challenge in the whole synthetic scheme. However, the reaction to attach a bare pyrrolidine at the bay-positions is well established, and has been routinely used to synthesize dipyrrolidinyl substituted PDI derivatives over a decade.[39] This reaction is done by heating the solution of dibromo-PDI **3** in neat pyrrolidine at 55 ^{o}C for a day. In the reaction, pyrrolidine works as both reagent and solvent. The role of pyrrolidine as a solvent, in this reaction, is feasible because it is a free flowing liquid (density = 0.852 g/mL) and easily dissolves dibromo-PDI **3**. In contrast, the functionalized pyrrolidines are either solids or dense viscous liquids which make the use of an external solvent mandatory. Consequently, in order to realize this reaction, all the crucial parameters such as solvent, mol % of 2-(benzyloxymethyl)-pyrrolidine **11**, reaction temperature, and reaction time were discovered and optimized. The most informative results are summarized in Table 4.3 and the most successful reactions are shown in Scheme 4.5.

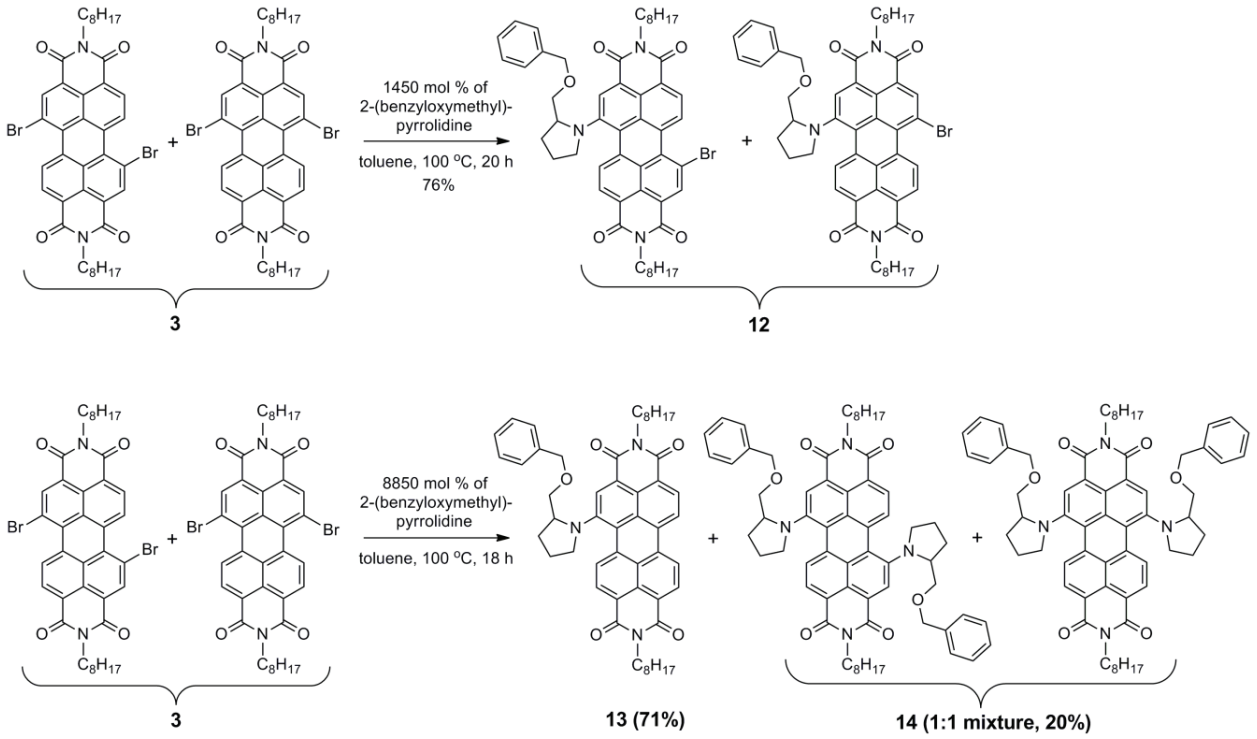

Scheme 4.5. Synthesis of 2-(benzyloxymethyl)pyrrolidinyl functionalized perylene diimides (**12**, **13,** and **14**).

Table 4.3. Coupling reaction of 2-(benzyloxymethyl)-pyrrolidine 11 and dibromo-PDI 3.

Entry	Solvent[a]	mol % of 11[b]	Temp. (°C)	Time (h)	Yield 12	Yield 13	Yield 14	Yield 3[c]
1	chloroform	840	55	24	10 %	–	–	80 %
2	toluene	840	90	24	50 %	–	–	46 %
3	toluene	1450	100	20	76 %	–	4 %	18 %
4	toluene	4000	100	21	5.7 %	72 %	10 %	–
5	toluene	8850	100	18	–	71 %	20 %	–
6	NMP	4000	100	20	4 %	43 %	8 %	–
7	NMP	8000	100	10	–	65 %	11 %	–
8	NMP	4000	100	5	50 %	23 %	10 %	–
9	NMP	1600	100	20	2 %	62 %	5 %	–
10	NMP	1600	90	20	30 %	34 %	4 %	–
11	NMP	9300	140	1	19 %	–[d]	–[d]	14 %

[a] dibromoperylene diimide (**3**) was dissolved in minimum possible volume of NMP by heating. [b] 2-(benzyloxymethyl)-pyrrolidine (**11**). [c] recovered from the reaction. [d] *N,N′*-dioctyl-1-bromo-7(6)-hydroxy-perylene diimide was the main product.

When the reaction was carried out in toluene at 100 °C with 1450 mol % of 2-(benzyloxymethyl)-pyrrolidine **11**, the mono-substituted product **12** was successfully obtained in a high yield i.e. 76 % (Table 4.3, entry 3). Therefore, these reaction conditions can be used for the efficient synthesis of **12**, which can be considered as an important synthon for the preparation of asymmetrically bay-substituted PDIs. In the next step, we further increased the mol % of **11** in order to obtain the bis-substituted product **14** in high yield. The presence of **11** in the reaction mixture in higher mol % resulted in quite surprising results. When the reaction was carried out in the presence of 4000 mol % of 2-(benzyloxymethyl)-pyrrolidine **11** (Table 4.3, entry 4), the reaction produced an unexpected mono-debrominated compound **13** as the major product in high yield (72 %). At the same time, the desired bis-subsituted product **14** was obtained as minor product in only 10 % yield. To our biggest surprise, the ^{1}H NMR analysis of the greenish-blue bis-substituted product **14** clearly revealed the presence of 1,7- and 1,6-regioisomers in ca. 1:1 ratio. This estimation was unambiguously performed based on the intensities of the characteristic signals of PDI core protons (one singlet and two doublets) in the aromatic region (Figure 4.6a).

In the idealistic case, the amount of 1,7-regioisomer in the product **14** is expected to be approximately three times higher than the corresponding 1,6-regioisomer. Simply, because of composition of starting compound dibromo-PDI **3**, which has 1,7- and 1,6-regioisomers in ratio ca. 3:1. Very similar results were obtained, when the reaction was repeated with even higher excess (8850 mol

%) of **11** (Table 4.3, entry 5). Again, the reaction yielded the unexpected mono-debrominated derivative **13** in high yield of 71 %. However, this time an improved yield (20 %) of the desired bis-substituted product **14** was obtained. This time also, the 1,7- and 1,6-regioisomers in the product **14** were found in the ratio ca. 1:1. On the other hand, when the reaction time was shortened, the mono-substituted derivative **12** was obtained as the major product in high yield.

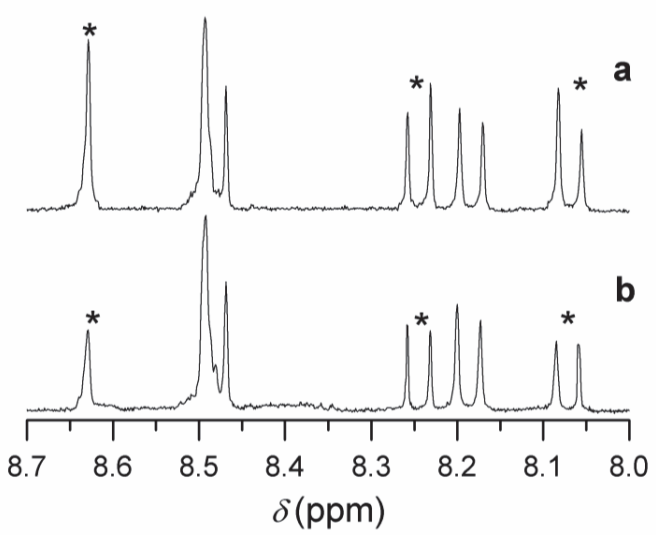

Figure 4.6. ^{1}H NMR spectra (300 MHz, $CDCl_3$, aromatic region) revealing composition of 1,7- and 1,6-regioisomers in the bis-substituted product **14** obtained from the reaction carried out (a) in toluene, and (b) in NMP. The signals corresponding to 1,7-regioisomer are marked with asterisk.

The above-mentioned results clearly indicate the difference in the chemical behavior of 1,7- and 1,6-regioisomers. Evidently, in the presence of higher mol % of 2-(benzyloxymethyl)-pyrrolidine **11**, both 1,7- and 1,6-regioisomers of dibrom-PDI **3** first undergo mono-substitution very smoothly to give *N,N′*-dioctyl-1-bromo-7(6)-[2-(benzyloxymethyl)pyrrolidinyl]perylene diimide **12** in high yield. But at this stage, the major 1,7-regioisomer undergoes debromination more efficiently to yield **13** in comparison to the corresponding 1,6-regioisomer. Therefore, the reaction produces mono-debrominated product **13** as the major product in high yield ca. 71 % and bis-substituted product **14** as the minor product, which contains approximately equal amounts of 1,7- and 1,6-isomers. These two regioisomers of bis-substituted product **14** could not be separated from each other due to their similar mobilities. Therefore, the 1:1 mixture of two regioisomers was used as such for the further reaction.

We also tried the reaction in the basic solvents to obtain a higher yield of the desired bis-substituted product **14**. In *N*-methyl-2-pyrrolidinone (NMP) also, the mono-debrominated compound **13** was obtained as major product in high yield (ca. 60 %) and the desired bis-substituted product **14** as minor product with yield of ca. 10 % (Table 4.3, entries 6 and 7). However, in this case, the 1,6-regioisomer

was obtained in even higher amount compared to the corresponding 1,7-regioisomer in the bis-substituted product **14** (Figure 4.6b). The reaction was also repeated with shorter reaction time (entry 8), lower mol % of **11** (entry 9), and also at lower and higher temperatures (entries 10 and 11), but an improved yield of bis-substituted product **14** could not be achieved.

The present study revealed that high temperature, ca. 100 ^{o}C, is essential for the efficient attachment of 2-(benzyloxymethyl)-pyrrolidine **11** to the PDI core. In addition, the choice of the solvent was also found to be highly crucial for this reaction. The yield of the mono-substituted product **12** decreased, drastically, when toluene was replaced with more basic solvent NMP (entries 3 and 9). Similarly, the yield of bis-substituted product **14** was also found higher in toluene compare to that in NMP (entries 5 and 7). This can be attributed to the higher basicity of NMP that enhances the rate of de-bromination. Furthermore, the reaction is highly sensitive to changes in mol % of 2-(benzyloxymethyl)-pyrrolidine **11** relative to dibromo-PDI **3**. In toluene, for example, in the presence of lower mol % of **11** (ca. 1500), the reaction produces mono-substituted compound **12** as the major product (entry 3). While, in the presence of higher mol % of **11**, it yields de-brominated compound **13** as the major product (entries 4 and 5).

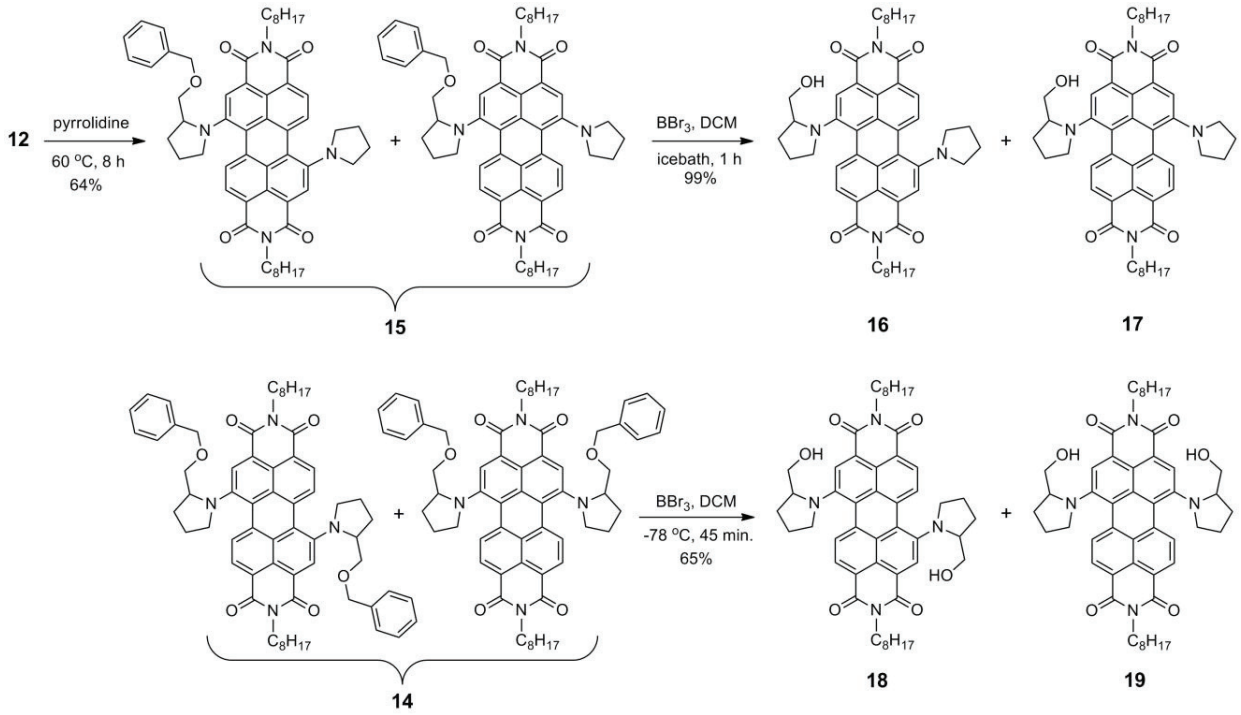

Scheme 4.6. Oxidative de-*O*-benzylation of the compounds **14** and **15** by BBr_3.

In the next step, pyrrolidine group was attached to **12** *via* substitution of the free bromine to obtain regioisomeric mixture **15** in 64 % yield (Scheme 4.6). The 1,7- and 1,6-regioisomers could not be

separated chromatographically in this case also. Finally, the protected hydroxyl groups of compounds **14** and **15** had been unmasked by de-*O*-benzylation using BBr_3 in dry DCM (Scheme 4.6). At this stage, the 1,7- (dark green in color) and the 1,6- (dark blue in color) regioisomers of the corresponding products were successfully separated either on HPTLC glass plates or by column chromatography. The separation of these regioisomers was ensured by ^{1}H NMR spectroscopy.

4.5 Synthesis and Characterization of the Single- and Double-Bridged PDI−Fullerene Dyads

As mentioned previously, we were very keen to compare the excited-state properties of the 1,7- and 1,6-regioisomers. Simultaneously, we were also interested to explore the electron-donating properties of the dipyrrolidinyl substituted PDIs in the donor−acceptor systems. Within this framework, we planned four PDI-fullerene dyads comprising covalently linked fullerene and PDI chromophores. The attachment of fullerene was carried out through the bay-region of PDI, utilizing the free hydroxyl groups of newly prepared derivatives, to achieve the close-proximity of the two acting chromophores. In view of the close-proximity of the donor and acceptor moieties, we expected these dyads to undergo efficient electron transfer.

To synthesize the dyads, the malonate fragments were first attached to the unmasked hydroxyl groups by the reaction with ethyl malonyl chloride (Scheme 4.7). Subsequently, fullerene was single-linked to the resultant PDIs **20** and **21**, and double-linked to the PDIs **22** and **23** by Bingel-Hirsch reaction in order to prepare the desired single-bridged (SB-1,7-PDI−C_{60} **24** and SB-1,6-PDI−C_{60} **25**) and double-bridged (DB-1,7-PDI−C_{60} **26** and DB-1,6-PDI−C_{60} **27**) dyads, respectively.

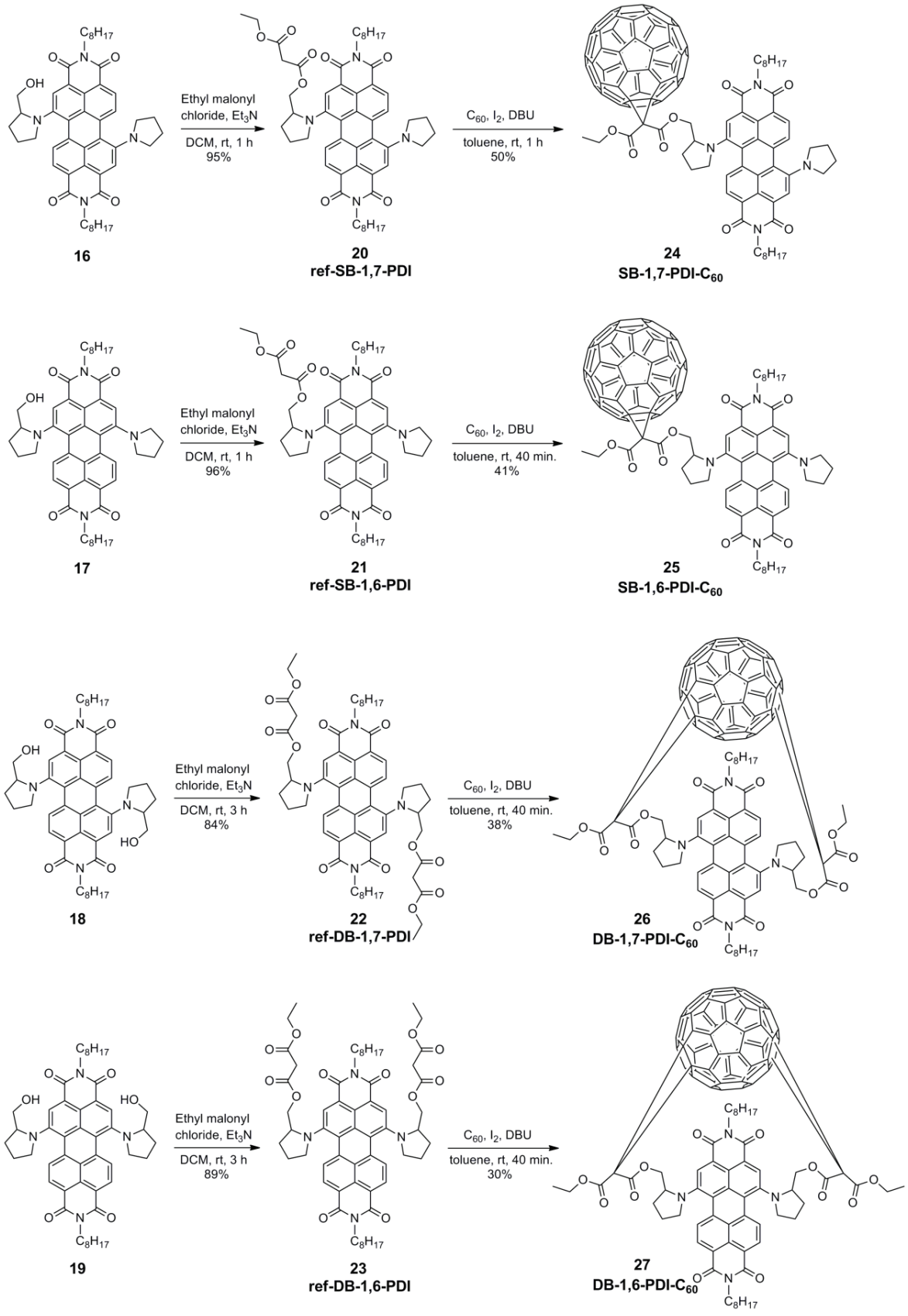

Scheme 4.7. Synthesis of the single- and double-bridged PDI−fullerene dyads.

^{1}H NMR Analysis. The aromatic regions of ^{1}H NMR spectra of the double-bridged dyads, DB-1,7-PDI−C_{60} and DB-1,6-PDI−C_{60}, were compared with the spectra of respective reference PDIs to analyze the effect of fullerene on the PDI core-protons (Figure 4.7). This knowledge was eventually used to make some preliminary estimations of the orientation of the two acting moieties with respect to each other in these double-bridged dyads. In the case of dyads, the probationary assignment of the protons to the various signals was made with the help of ^{1}H-^{1}H COSY measurements.

In both dyads, the attachment of fullerene resulted in significant shifts to the signals of nearly all PDI core-protons; which clearly revealed the close-proximity of the two chromophores. However, some interesting differences were also observed in the shifting patterns between the two dyads. In DB-1,7-PDI−C_{60}, large downfield shifts of 1.53 and 0.36 ppm were displayed by two protons (namely H^6 and H^8, respectively) due to the deshielding effect exerted by the C_{60} π-electrons. In DB-1,6-PDI−C_{60}, on the other hand, three protons, namely H^2, H^7, and H^{12}, are most affected by the C_{60} π-electrons. Among those, only one proton (H^2) displayed a downfield shift of 0.63 ppm. Whereas, the remaining two protons $H^7$and H^{12} experienced the shielding effect that resulted in large upfield shifts of 0.97 and 0.90 ppm, respectively.

These very clear differences in the shifting patterns of the PDI core-protons can be considered as indications of different orientation of C_{60} with respect to PDI in these two double-bridged dyads. This difference in orientation can also be anticipated based on the different bay-positions of PDI moieties to which the linkers are appended in the two dyads. In the case of dyad DB-1,7-PDI−C_{60}, the linkers are appended at 1 and 7 bay-positions which leads to better face-to-face orientation of the two chromophores. Whereas in the dyad DB-1,6-PDI−C_{60}, the 1 and 6 bay-positions are located on the same side of the perylene core resulting in the emplacement of fullerene more towards the imide position.

The analysis of ^{1}H NMR spectra of single-bridged dyads, namely SB-1,7-PDI−C_{60} and SB-1,6-PDI−C_{60}, was also performed in a similar manner. In these dyads also, the effect of fullerene moiety was clearly observed on the signals of PDI core-protons. However, in these single-bridged dyads, the shifts were found significantly smaller in comparison to those observed for the double-bridged dyads. These observations clearly suggest that the PDI and fullerene moieties are in close-proximity in both double-bridged and single-bridged dyads. Evidently, the two acting chromophores are closer to each other in the double-bridged dyads compared to the single-bridged dyads.

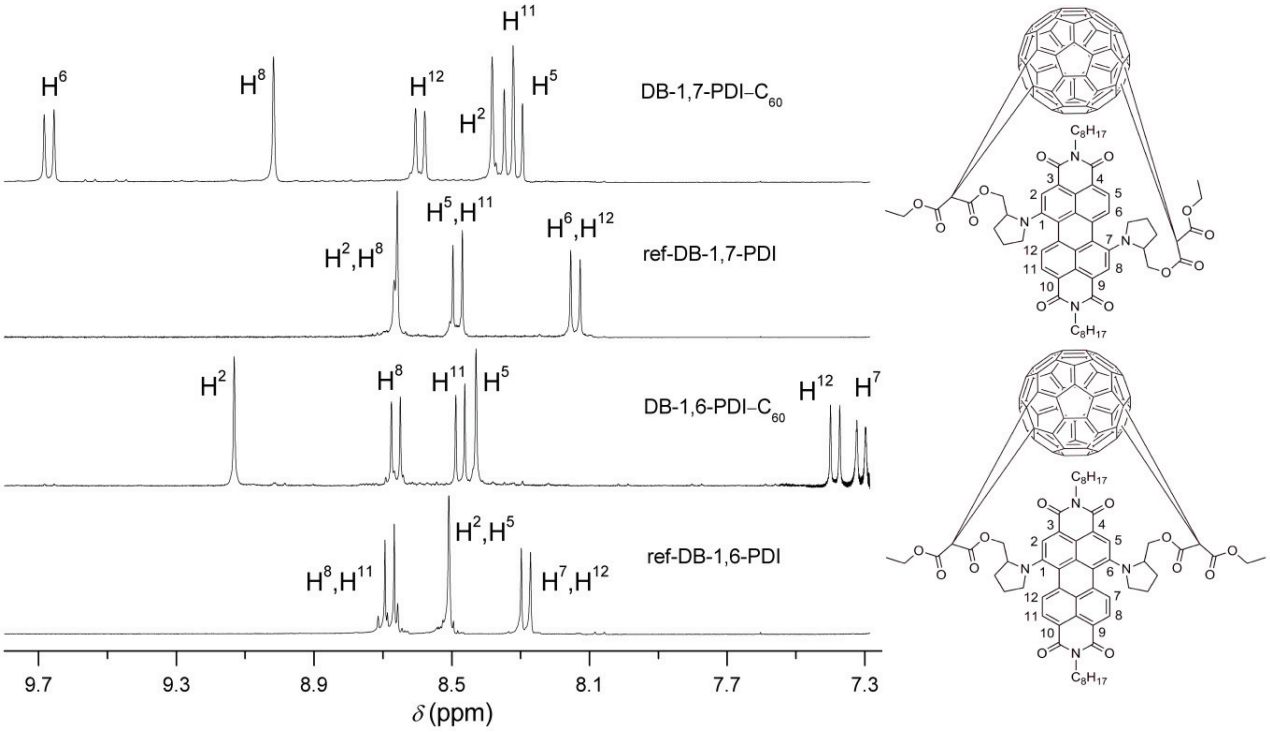

Figure 4.7. Comparison of ^{1}H NMR spectra of DB-1,7-PDI−C_{60} and DB-1,6- PDI−C_{60} with that of ref-DB-1,7-PDI and ref-DB-1,6-PDI, respectively.

4.6 Photoinduced Electron Transfer in the Single- and Double-Bridged PDI−Fullerene Dyads

Various experimental techniques including differential pulse voltammetry, steady-state absorption and emission spectroscopy, and transient absorption (picosecond pump-probe and nanosecond flash-photolysis) spectroscopy were employed to investigate and to compare the excited-state dynamics of these dyads in detail.

4.6.1 Electrochemical studies

Differential pulse voltammetric studies were performed to compare the redox characteristics of the individual entities and those of the dyads to obtain a better understanding of the ground-state interaction between the two closely linked moieties. The obtained redox potentials (*V* vs. Ag/AgCl) are summarized in Table 4.4. The DPV results led us to two noticeable observations. Firstly, the 1,7-substituted derivatives are better electron donors in comparison to their corresponding 1,6-derivatives. Consequently, in the case of single-bridged dyads, the energy of charge-separated state was found to be

lower for the dyad SB-1,7-PDI−C_{60} (1.20 eV) compared to the dyad SB-1,6-PDI−C_{60} (1.35 eV). Similarly, the double-bridged dyad DB-1,7-PDI−C_{60} (1.51 eV) also exhibited lower energy of the charge-separated state than the dyad DB-1,6-PDI−C_{60} (1.56 eV). Based on these observations, we could anticipate more efficient electron transfer for the dyads consisting of the 1,7-regioisomer as the donor in comparison to the corresponding dyads with the 1,6-regioisomer.

Table 4.4. Redox potentials (*V* vs. Ag/AgCl) of dyads and reference compounds obtained by DPV.[a]

Compound	E_{1ox}	E_{2ox}	E_{1red}	E_{2red}	E_{CS} (eV)[b]
ref-SB-1,7-PDI	+0.67	+0.82	−0.81	−0.99	−
SB-1,7-PDI−C_{60}	+0.69	+0.86	−0.51	−0.92[c]	1.20
ref-SB-C_{60}	+1.68	−	−0.50	−0.92	−
SB-1,6-PDI−C_{60}	+0.83	+1.30	−0.52	−0.93[c]	1.35
ref-SB-1,6-PDI	+0.82	+1.27	−0.81	−0.97	−
ref-DB-1,7-PDI	+0.72	+0.87	−0.79	−0.99	−
DB-1,7-PDI−C_{60}	+0.90	+1.08	−0.61	−0.86	1.51
ref-DB-C_{60}	+1.60	−	−0.58	−1.01	−
DB-1,6-PDI−C_{60}	+0.98	+1.38	−0.58	−0.89	1.56
ref-DB-1,6-PDI	+0.93	+1.34	−0.78	−0.97	−

[a] Scan rate: 0.05 V/s. [b] Energy of charge-separated state [$E_{CS} = E_{1ox}(PDI) - E_{1red}(C_{60})$].
[c] Peaks of PDI^{-}, PDI^{2-}, and C_{60}^{2-} are merged.

Secondly, in the case of the single-bridged dyads, only a negligible influence of fullerene was observed on the redox potentials of the PDI moiety, indicating almost no interaction between the two acting moieties. On the contrary, in the double-bridged dyads, a very pronounced effect of the fullerene moiety was observed on the oxidation characteristic of the PDI moiety. In the case of dyad DB-1,7-PDI−C_{60}, the first and second oxidation potentials of the PDI moiety were shifted by +180 mV and +210 mV, respectively. On the other hand, comparatively lower shifts of +50 mV and +40 mV, respectively, were observed for the oxidation potentials in the dyad DB-1,6-PDI−C_{60}. This clearly indicates a more pronounced effect of the fullerene on the PDI chromophore in the dyad DB-1,7-PDI−C_{60} compare to that in DB-1,6-PDI−C_{60}.

These observations lead to the conclusion that in the double-bridged dyads the fullerene moiety influences the closely-linked PDI chromophore in such a way that the PDI moiety does not remain as good as electron donor as of ref-PDIs. Consequently, the energy of the charge-separated state is much higher in the case of double-bridged dyads in comparison to the single-bridged dyads. Furthermore, since this effect of fullerene is more pronounced in the dyad DB-1,7-PDI−C_{60} than in DB-1,6-PDI−C_{60}, the difference in the energies of the charge-separated states of these two dyads is not as substantial as it

was observed in the case of single-bridged dyads. Therefore, a less pronounced difference can be predicted in the photodynamics of the two double-bridged dyads, DB-1,7-PDI−C_{60} and DB-1,6-PDI−C_{60}.

4.6.2 Steady-state absorption and emission studies

In both single- and double-bridged dyads, the main absorption features of the corresponding PDI moieties are mostly preserved, and consequently the dyads composed of 1,7-regioisomer are dark green in color while dyads composed of 1,6-regioisomer are dark blue (Figure 4.8). In the case of double-

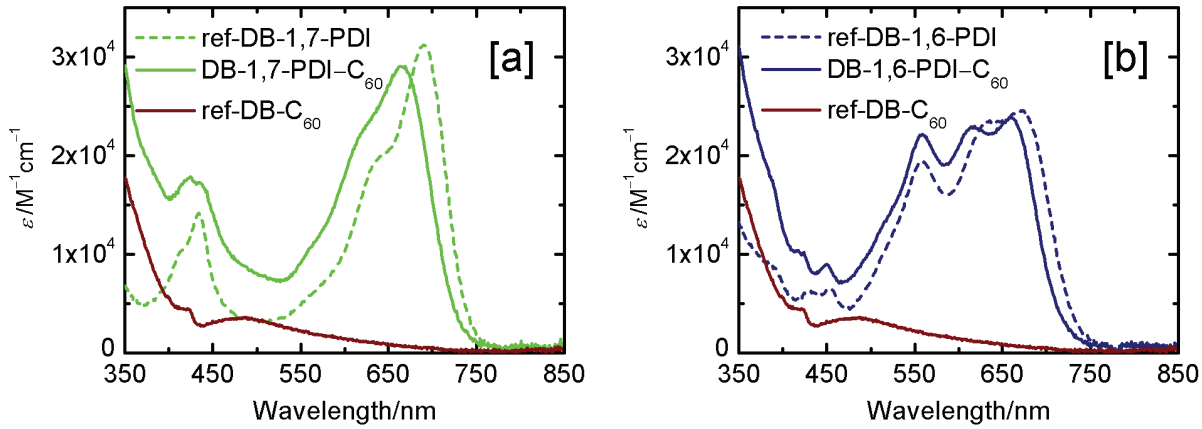

Figure 4.8. Steady-state absorption spectra in benzonitrile: [a] DB-1,7-PDI−C_{60}, ref-DB-1,7-PDI, and ref-DB-C_{60}; [b] DB-1,6-PDI−C_{60}, ref-DB-1,6-PDI, and ref-DB-C_{60}.

bridged dyads, the lowest energy band of the PDI moiety is significantly shifted to the shorter wavelengths relative to those of the reference PDIs. However, this blue shift is larger in the case of the dyad DB-1,7-PDI−C_{60} compared to the dyad DB-1,6-PDI−C_{60}. These results are in good agreement with the results obtained from the DPV studies, which also exhibited larger shifts in the oxidation potentials of the PDI moiety in the case of dyad DB-1,7-PDI−C_{60} in comparison to that of DB-1,6-PDI−C_{60}.

As far as the single-bridged dyads are concerned, the spectra of both SB-1,7-PDI−C_{60} and SB-1,6-PDI−C_{60} correspond very closely to the sum of the spectra of reference fullerene and the respective reference PDI. These results, along with DPV data, suggest that the two acting chromophores are at a certain distance from each other in the single-bridged dyads so that they don't influence either redox or absorption properties of each other.

In the subsequent steady-state fluorescence studies, the emission of the PDI moieties were found significantly quenched in all the four dyads compared to respective reference PDIs. However, more

efficiently quenched PDI emission was clearly observed in the dyads composed of 1,7-regioisomers. For example, in polar benzonitrile, highly efficient quenching (450 fold) was observed for the dyad SB-1,7-PDI−C_{60}, whilst quenching was only 70 fold for the dyad SB-1,6-PDI−C_{60}. These observations clearly indicate a more efficient photoinduced process in the dyads consisting of 1,7-regioisomer of PDI as a donor in comparison to the dyads comprising 1,6-regioisomer.

4.6.3 Picosecond and Nanosecond Transient Absorption Studies

The detailed comparative study of the photodynamics of the dyads **24**−**27** by the transient absorption techniques revealed the photoinduced electron transfer from the perylene diimide chromophore to the fullerene in all the four dyads, both in polar benzonitrile and in non-polar toluene. However, both in the single- and double-bridged molecules, the process was found to be substantially faster and more efficient in the dyads consisted of 1,7-regioisomer. The obtained time-constants for the electron transfer process in all the four dyads are summarized in the Table 4.5.

Table 4.5. Time-constants (τ) for the ET process in all the four dyads in benzonitrile and in toluene.

Compound	Solvent	$\tau_{Exciplex}$	τ_{CS}[a]	τ_{CR}[b]	τ_{T}[d]	E_{CS} (ev)[e]
SB-1,7-PDI−C_{60}	PhCN	−	2.3 ps	11 ps	−	1.20
	toluene	0.7 ps	12 ps	520 ps	−	−
SB-1,6-PDI−C_{60}	PhCN	−	2.0 ps	35 ps	−	1.35
	toluene	2.4 ps	40 ps	1−50 ns[c]	80 µs	−
DB-1,7-PDI−C_{60}	PhCN	−	6 ps	50 ps	−	1.51
	toluene	−	400 ps	1−50 ns[c]	65 µs	−
DB-1,6-PDI−C_{60}	PhCN	−	9 ps	120 ps	−	1.56
	toluene	−	500 ps	1−50 ns[c]	113 µs	−

[a] Charge-separation. [b] Charge-recombination. [c] Could not be determined accurately. [d] Triplet-state lifetime of PDI moiety measured by nanosecond flash-photolysis. [e] Energy of charge-separated state.

In the picosecond transient absorption measurements, the two components corresponding to the formation of the charge-separated state (CS) state $PDI^{\bullet+}$−$C60^{\bullet-}$ and the decay of the CS state were clearly observed for all the four dyads in polar environment (Figure 4.9). Moreover, for all the four dyads, the formation of the CS state in picosecond time-scale is followed by its decay directly to the ground-state in picosecond time-scale through charge-recombination. The existence of the CS state was unambiguously recognized by the absorption at the characteristic wavelengths of PDI radical cation at 500−600 nm and 720−800 nm, and fullerene radical anion at 1000−1100 nm which overlaps with the PDI radical cation around 1000 nm.[58,10] In the case of single-bridged dyads (Figure 4.9), the formation

of the CS state occurred approximately in 2 ps for both the dyads. Whereas, the decay of the CS state was clearly faster for the dyad SB-1,7-PDI−C_{60} (11 ps) than for the dyad SB-1,6-PDI−C_{60} (35 ps). In the double-bridged dyads, both the processes, namely formation of the CS state and its decay, were found to be faster for the dyad DB-1,7-PDI−C_{60} (6 ps and 50 ps, respectively) than for the dyad DB-1,6-PDI−C_{60} (9 ps and 120 ps, respectively).

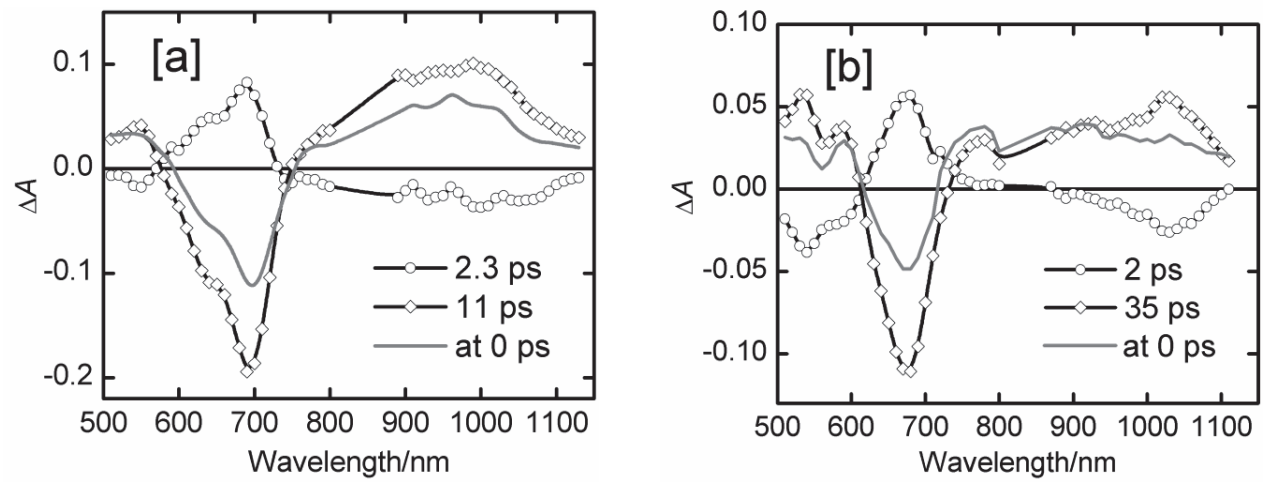

Figure 4.9. Picosecond transient absorption decay component spectra of [a] SB-1,7-PDI−C_{60} and [b] SB-1,6-PDI−C_{60} in benzonitrile.

In the non-polar environment, even more pronounced differences were evidenced in the photodynamics of the dyads. In the case of single-bridged dyads, SB-1,7-PDI−C_{60} and SB-1,6-PDI−C_{60}, we could even observe different relaxation pathways adopted by the charge-separated state. In the dyad SB-1,7-PDI−C_{60}, the formation of CS state in 12 ps is followed by its decay directly to the ground-state through charge-recombination in 520 ps. On the other hand, in the dyad SB-1,6-PDI−C_{60}, the formation of the CS state in 40 ps is followed by its decay to the PDI triplet-state in a time-scale between 1−50 ns. This PDI based triplet-state finally decays to the ground-state in 80 μs. The decay pathways adopted by the CS state of the dyads SB-1,7-PDI−C_{60} and SB-1,6-PDI−C_{60} in non-polar environment are summarized in Figure 4.10. These observations suggest that, in the dyad SB-1,7-PDI−C_{60}, the energy of the CS state is lower than that of the PDI triplet-state even in non-polar medium.

In the case of double-bridged dyads, the time-constant for the formation of the CS state was found to be 400 ps for the dyad DB-1,7-PDI−C_{60} and 500 ps for DB-1,6-PDI−C_{60}. For both the dyads, however, the CS state decays to PDI based triplet-state in a time-scale somewhere between 1−50 ns. For the dyad DB-1,7-PDI−C_{60}, the PDI (1,7-regioisomer) based triplet-state relaxed to the ground-state with a lifetime of 65 μs. Whereas for the dyad DB-1,6-PDI−C_{60}, the relaxation of PDI (1,6-regioisomer) based

triplet-state occurred in 113 μs. It is important to note that the characteristic features of the charge-separated state were found quite week in the NIR region. Thus, the electron transfer in toluene is slightly tentative in the case of double-bridged dyads. However, it has to be emphasized that no spectroscopic evidences were observed for the other possible quenching mechanisms.

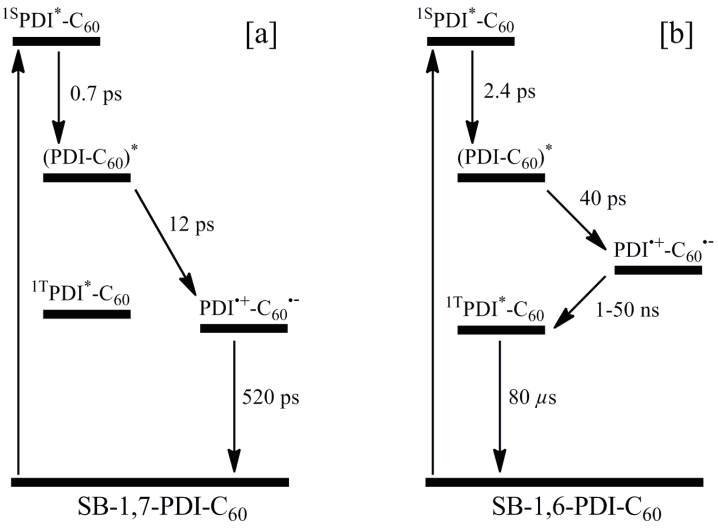

Figure 4.10. Photophysical pathways taking place in single-bridged dyads [a] SB-1,7-PDI−C_{60} and [b] SB-1,6-PDI−C_{60} in toluene.

Concluding the photochemistry study, the most important finding is the efficient electron transfer in the PDI−C_{60} dyads in both polar and non-polar media, which is observed for the first time. Another remarkable feature of SB-1,7-PDI−C_{60} dyad is the energy level of the CS state which is lower than that of the PDI triplet-state even in non-polar media, which makes the molecule a promising candidate for the solid organic photovoltaics and other optoelectronic applications.

4.7 Excited-State Interaction of Ru(II) polypyridine Complex with Red and Green Perylene Diimides

A scrutiny of the previous research reveals that mostly the PDIs with basic properties (red PDIs) have been employed in systems incorporating the metal complexes. However, the excited state behavior of the red PDI has been found to be different with different metal systems. For example, in the recently reported Pt(II) square planar structures, with PDI covalently attached to the metal center through an acetylide linkage, the ^{3}PDI excited state was successfully obtained as a result of strong spin−orbit coupling induced by Pt(II).[112] On the contrary, the strong fluorescence of the dye has been retained in the palladium complexes, despite the direct attachment of metal to the 1,7-bay positions of PDI.[113]

Similarly, other complexes of PDI−pyridine/terpyridine ligands with metals like Pt, Pd, Zn, and Fe, possess a relatively high fluorescence quantum yield and a low yield of ^{3}PDI excited state.[57,114−117] Charge transfer based interactions have also been observed in the metal-organic hybrids, comprising red PDI and either Ru-porphyrin or Ru-phthalocyanine linked through axial coordination.[76,77] Also in a recently reported PDI−[(bpy)Ru(II)Cl_2(CNbutyl)$_2$] system, charge transfer from the Ru complex to ^{1*}PDI was observed upon selective excitation of the PDI moiety.[118]

In this context, herein, we wanted to investigate the excited state interaction of the luminescent Ru(II) polypyridine complex with two different PDIs, namely the red and green PDIs. To implement this idea, a dipyrido[*a*,*c*]phenazine (dppz) moiety was first covalently attached to one of the bay-positions of PDI. The second bay-position was subsequently substituted with either 4-*tert*-butylphenoxy or pyrrolidinyl group to obtain electron-deficient and electron-rich PDI−dppz ligands, respectively. Finally, the obtained ligands were utilized to form the PDI−[Ru(bpy)$_2$(dppz)]$^{2+}$ ensembles. A comprehensive study of the excited-state photodynamics of the ensembles has been performed by means of electrochemical, and steady-state and time-resolved spectroscopic methods. Although, in all the three ensembles, the photoexcitation of either chromophore resulted in a long-lived triplet excited state of PDI (^{3}PDI) as the final excited state, the photochemical reaction leading to the triplet states were found to be essentially different for the two types of the ensembles. In the case of red PDI based ensemble, the excitation of either chromophore leads to the electron transfer from the Ru(II) complex to Ph-PDI, whereas for the green PDI based ensembles the electron transfer is observed in opposite direction and only when the Ru(II) complex is excited.

4.7.1 Synthesis and characterization of the ensembles

The PDI−[Ru(bpy)$_2$dppz]$^{2+}$ ensembles [namely 1,7-Py-PDI−Ru(II) **33**, 1,6-Py-PDI−Ru(II) **34**, and 1,7(6)-Ph-PDI−Ru(II) **37**] were synthesized from the mixture of 1,7- and 1,6-dibromo-PDI **3** according to the route summarized in the schemes 4.8 and 4.9. In the very first step, 1,10-phenanthroline-5,6-dione and 2,3-diaminophenol were condensed in ethanol at reflux to obtain 6-hydroxy-dipyrido[*a*,*c*]phenazine **28**. Subsequently, the dipyrido[*a*,*c*]phenazine (dppz) moiety was covalently linked to one of the bay-positions of dibromo-PDI **3** to obtain *N,N′*-dioctyl-1-bromo-7(6)-(dipyridophenazinoxy)perylene diimide **30** in 86 % yield. The two isomers could not be separated by column chromatography in spite of the presence of bulky dipyrido[*a*,*c*]phenazine (dppz) moiety at the bay region. Consequently, regioisomeric mixture **30** was used as such for the next step in which the free bromine atom was substituted by either pyrrolidine or 4-*tert*-butylphenoxy group.

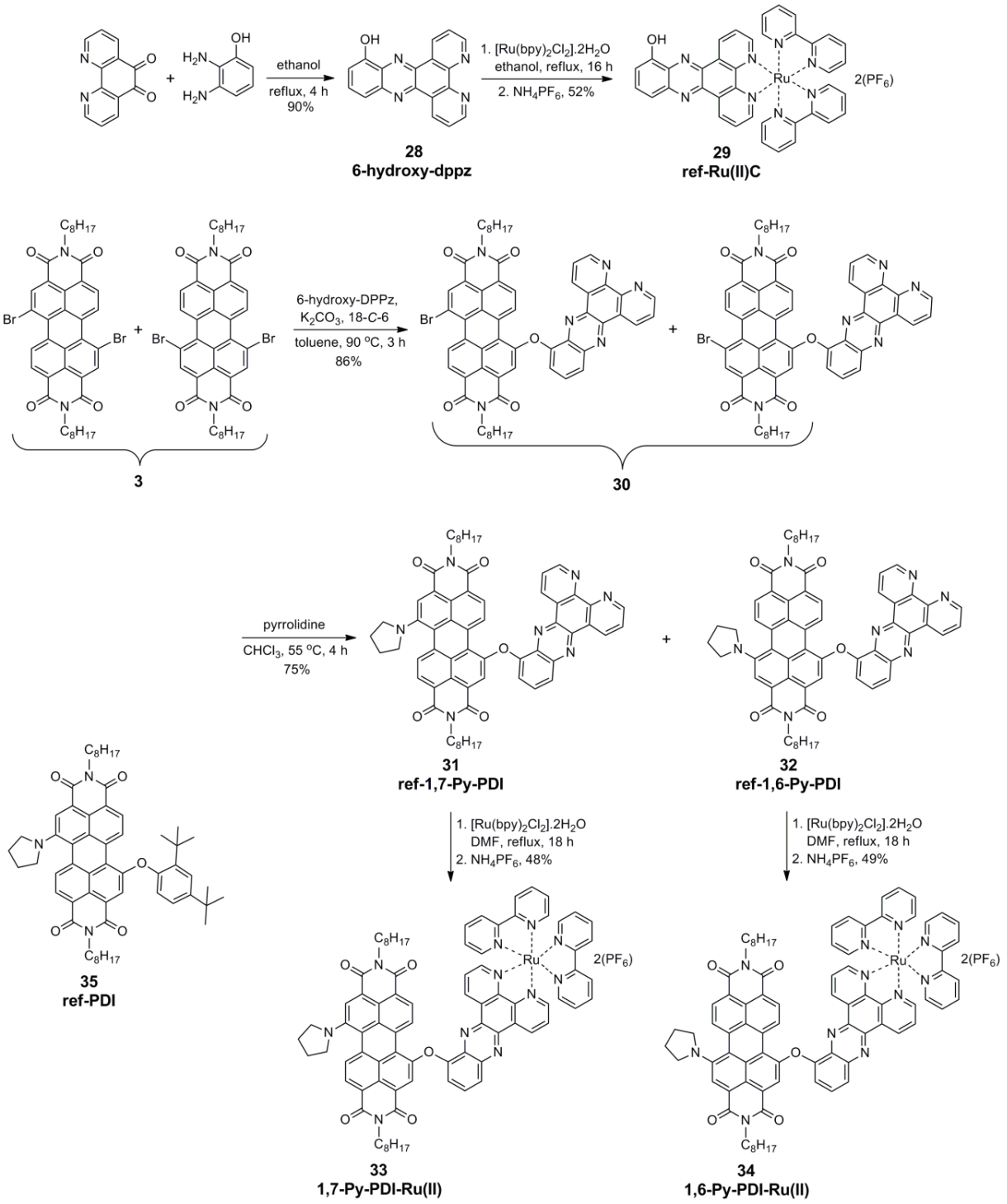

Scheme 4.8. Synthesis of 1,7-Py- and 1,6-Py-PDI−Ru(II)polypyridine dyads. The compounds **31** and **32** were utilized as reference PDIs in electrochemical and optical studies. Whereas the compound **35** (named as ref-PDI) is utilized for NMR analysis.

The 1,7- and 1,6-pyrrolidinyl derivatives (**31** and **32**) have been separated by column chromatography (silica 100/1:1 chloroform-toluene) since different redox and optical properties of those were expected.

Whereas in the case of 4-*tert*-butylphenoxy-substituted product, the resultant regioisomeric mixture **36** was used as such for the preparation of final compound keeping in mind very similar properties of 1,7- and 1,6-diphenoxy-substituted PDI. In the final step, the dyads were prepared by the reaction of the ligands with $[Ru(bpy)_2Cl_2].2H_2O$ followed by the exchange of chloride counter ions with hexafluorophosphate anions.

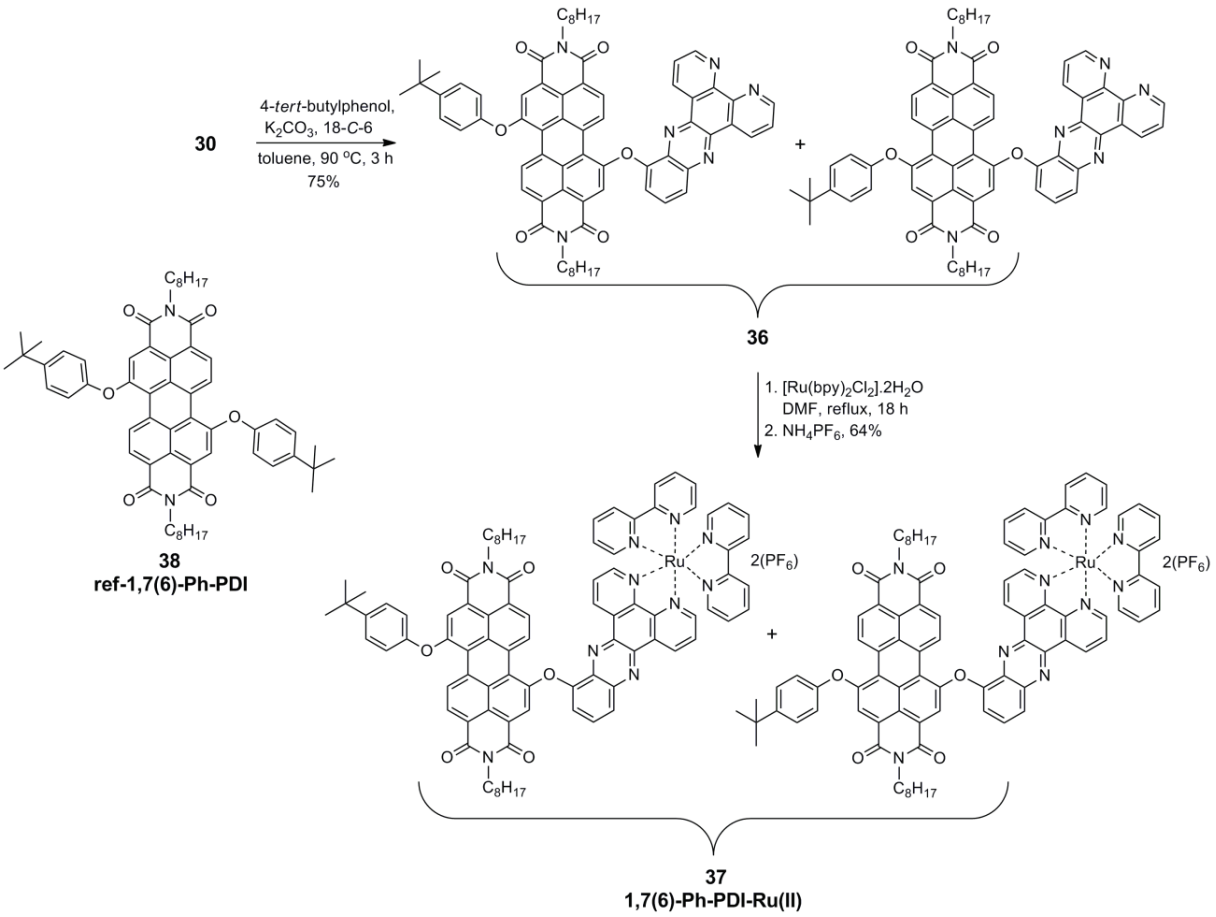

Scheme 4.9. Synthesis of 1,7(6)-Ph-PDI−Ru(II)polypyridine dyad. The compound **38** is utilized as reference PDI in the optical and electrochemical studies. It was also a regioisomeric mixture.

^{1}H NMR analysis of the ligand: Figure 4.11 represents a comparison of ^{1}H NMR spectrum of the ligand **31** with the spectra of the corresponding reference compounds, 6-hydroxy-dppz **28** and ref-PDI **35** (the structures are shown in Scheme 4.8). The assignment of the protons was made with the help of ^{1}H−^{1}H COSY measurements. Evidently, the ^{1}H NMR spectrum of the ligand displayed some characteristic features indicating that the dppz moiety is oriented towards the PDI core. In the ligand, close proximity of PDI moiety resulted in a systematic shifts to the signals of nearly all the protons of dppz moiety. For example, the protons $H^{2'}$, $H^{3'}$, and $H^{4'}$ are largely shifted to the upfield. It indicates that

these protons are closer to the perylene core and are shielded by PDI π-electrons. On the other hand, only minor shifts were observed for the other group of protons, namely $H^{9'}$, $H^{10'}$, and $H^{11'}$, which indicates that these protons are away from the perylene core. The two protons, namely $H^{6'}$, $H^{7'}$, experienced the deshielding effect and are largely shifted downfield. Similarly, the effect of the dppz π-electrons is also observed on the PDI protons. The proton H^6 is most affected and hence exhibited a downfield shift of 0.52 ppm.

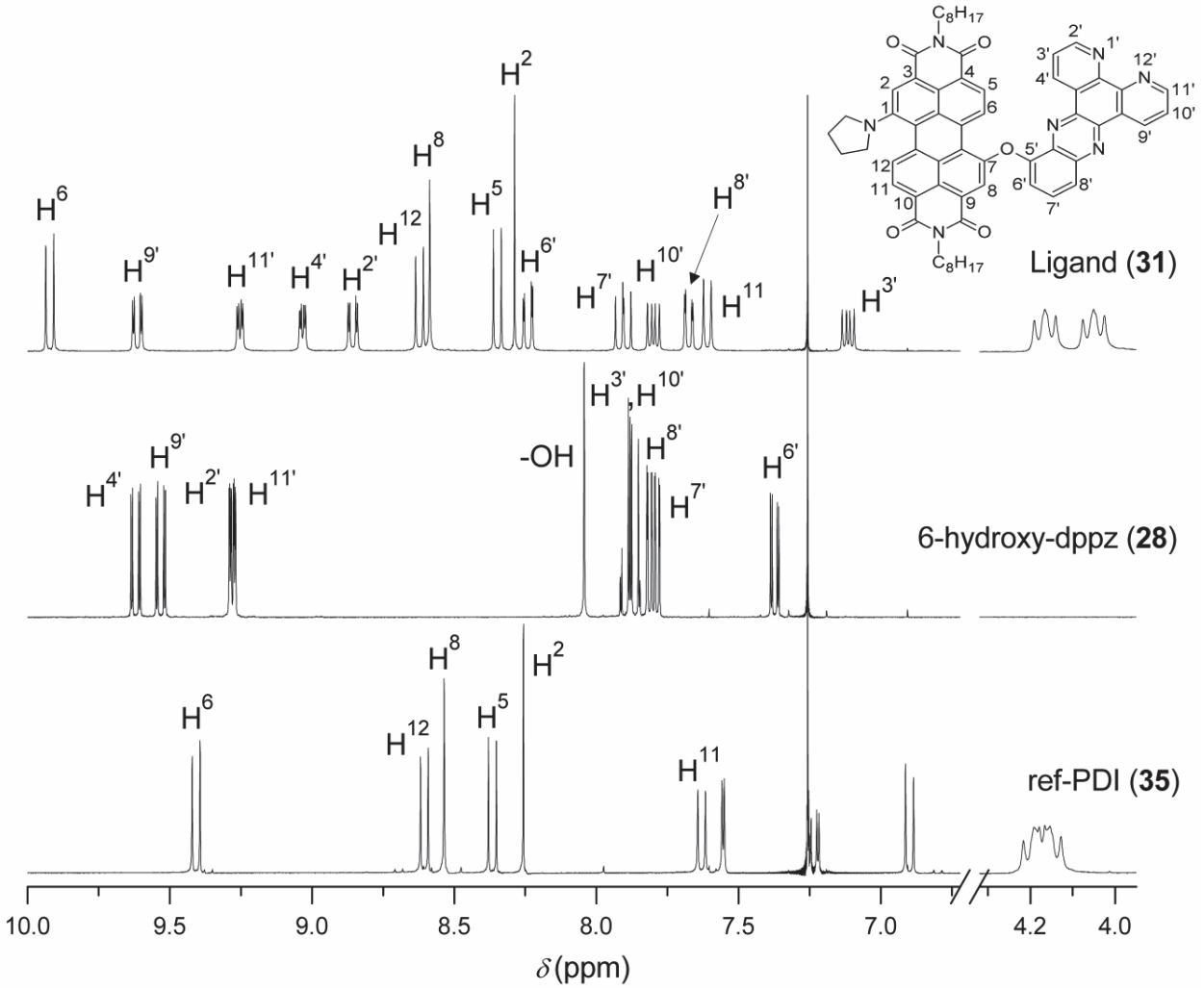

Figure 4.11. Analysis of ^{1}H NMR spectrum of the ligand **31**.

4.7.2 Observation of the photoinduced electron transfer in PDI−Ru(II) ensembles

The absorption profile of PDI−Ru(II) polypyridine ensembles exhibited characteristic features of both acting moieties (Figure 4.12). At shorter wavelengths, the absorption is dominated by MLCT transition originating from Ru(II) complex; whereas the absorption at longer wavelength is exclusively from the

PDI moiety. Therefore, the ensembles absorb in the broad range of the visible region. For all the ensembles, the PDI moiety absorbs exclusively at wavelengths higher than 500 nm. Therefore, it was possible to selectively excite the PDI chromophore.

In all the ensembles, the strong emission of the PDI moiety was found significantly quenched independent of the excitation wavelength (Table 4.6). For example, in the ensemble 1,7(6)-Ph-PDI−Ru(II), the emission of the PDI moiety was 98 % quenched (Φ_f = 0.02) in comparison to that of ref-1,7(6)-Ph-PDI (Φ_f = 0.83). In addition to the PDI emission, the emission of Ru(II) chromophore was also found strongly quenched when the Ru(II) chromophore of the ensembles was predominantly excited. These observations demonstrated that an efficient nonradiative deactivation of $^{1S}PDI^*$ dominates upon metal coordination. The possible mechanisms for the quenching may be either an electron or energy transfer between the two moieties or an efficient intersystem crossing due to the heavy atom effect exerted by the Ru metal. The possibility of the electron transfer mechanism was then evaluated based on redox properties of the compounds.

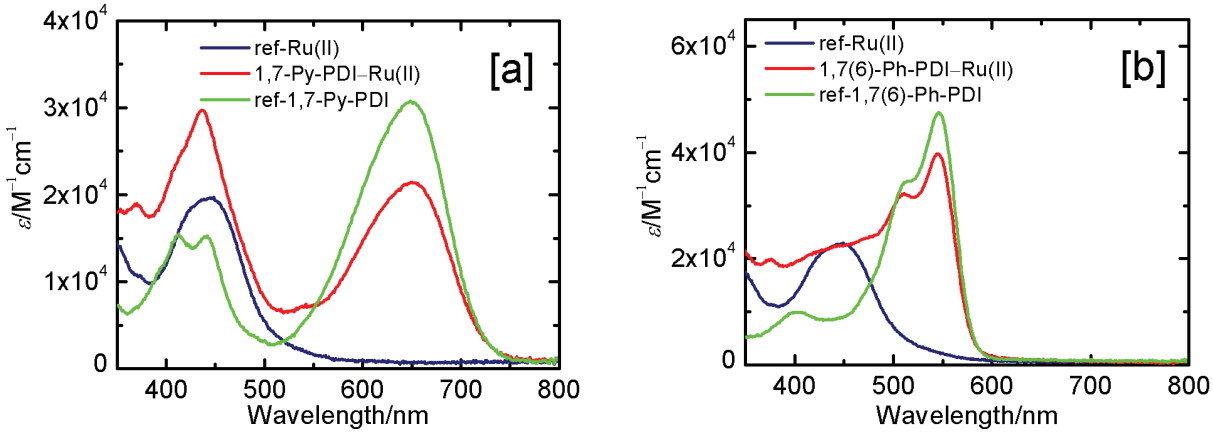

Figure 4.12. Steady-state absorption spectra of ensembles [a] 1,7-Py-PDI−Ru(II) and [b] 1,7(6)-Ph-PDI−Ru(II) along with their corresponding reference compounds in acetonitrile.

Table 4.6. Selected Photophysical data of PDI−Ru(II) polypyridine ensembles in acetonitrile.

Compound	Fl quenching[a]		Φ_f[d]	E_{S1}[e] (PDI)	E_{TI}[f] {Ru(II)}	E_{CS}[g]	τ_T[h]	k_{ET}[i]
1,7-Py-PDI−Ru(II)	97 %[b]	96 %[c]	3.3×10^{-3} (0.08)	1.8 eV	2.1 eV	1.77 eV	57 µs	$3.3\text{x}10^{11}$ s^{-1}
1,6-Py-PDI−Ru(II)	91 %[b]	89 %[c]	3.9×10^{-3} (0.07)	1.8 eV	2.1 eV	1.81 eV	35 µs	$1.4\text{x}10^{11}$ s^{-1}
1,7(6)-Ph-PDI−Ru(II)	98 %[b]	97 %[c]	2.0×10^{-2} (0.83)	2.2 eV	2.1 eV	1.97 eV	62 µs	$1.2\text{x}10^{10}$ s^{-1}

[a] Fluorescence quenching of the PDI moiety. [b] When Ru(II) chromophore was predominantly excited. [c] When PDI moiety was selectively excited. [d] Fluorescence quantum yields of the PDI moiety (Φ_f of the corresponding ref-PDIs are given in the parentheses). [e] Energy of the singlet excited state of PDI. [f] Energy of the ^{3}MLCT state of Ru(II) polypyridine chromophore. [g] Energy of the lowest charge-separated state; [$E_{CS} = E_{1ox}(D)-E_{1red}(A)$]. [h] Triplet-state lifetime of the PDI moiety measured by nanosecond flash-photolysis. [i] Rate of electron transfer, after the excitation of Ru(II) complex, obtained from pump-probe measurements.

The Ru(II) polypyridine complex exhibited a reversible one-electron oxidation at +1.37 V, which is assigned to the Ru(II)/Ru(III) redox couple. The complex also exhibited three ligand-based one-electron reductions at potentials (−0.90, −1.30, and −1.46 V) assigned to the reductions of dppz and bipyridine ligands.[119] The phenoxy substituted PDI, ref-1,7(6)-Ph-PDI, exhibited a typical voltammogram of red PDI with two reductions at low potentials (−0.61 and −0.84 V) and two oxidations at high potentials (+ 1.43 and +1.72 V). On the other hand, the pyrrolidinyl functionalized PDIs, ref-1,7-Py-PDI and ref-1,6-Py-PDI, exhibited relatively higher values for the first reduction potentials (−0.73 and −0.70 V, respectively) and significantly lower values of the first oxidation (+ 0.90 and + 0.95 V, respectively). These observations demonstrate that Ph-PDI is a good electron acceptor and the Py-PDIs are reasonably good electron donor. Based on the obtained electrochemical data, the lowest energy charge separate states were predicted as $PDI^{\bullet+}$−Ru(II)$^{\bullet-}$ for the ensembles 1,7-Py-PDI−Ru(II) and 1,6-Py-PDI−Ru(II) with the energies 1.77 and 1.81 eV, respectively, and $PDI^{\bullet-}$−Ru(III) for 1,7(6)-Ph-PDI-Ru(II) with the energy 1.97 eV relative to the energies of the ground states. It is important to notice that the direction of the charge transfer in the third ensemble is opposite to that of the first two ensembles.

The energies of the excited states were evaluated based on the absorption and emission measurements, and are presented in Table 4.6. Based on the comparison of the energies of the charge separated states and the excited states, it can be concluded that for the 1,7-Py-PDI−Ru(II) and 1,6-Py-PDI−Ru(II) ensembles the only energetically favorable ET process is possible from the triplet excited MLCT state, PDI−^{1T}Ru(II)* → $PDI^{\bullet+}$−Ru(II)$^{\bullet-}$. For the ensemble 1,7(6)-Ph-PDI−Ru(II), however, either of excited chromophores may undergo the charge transfer, PDI−^{1T}Ru(II)* → $PDI^{\bullet-}$−Ru(III) and ^{1S}PDI*−Ru(II) → $PDI^{\bullet-}$−Ru(III).

Finally, the excited state dynamics of all the ensembles was studied in both nanosecond and picosecond time-scale to shed light on the short- and long-lived products evolving from the intramolecular deactivation. In the flash-photolysis measurements, the transient absorption decays were found mono-exponential at all the monitoring wavelengths, and the long-lived triplet-state of PDI was observed as the only intermediate state regardless of the excitation wavelength (Figures 4.13[b] and 4.14[b]).

The picosecond decay component spectra of the ensemble 1,7(6)-Ph-PDI−Ru(II) are presented in Figure 4.13[a]. The time-resolved absorption right after the excitation (at 0 ps) shows typical features of the first singlet excited state of the PDI chromophore. Even though the Ru(II) complex is equally excited at 420 nm, its singlet excited state is not well seen at this time since it is less intense and does not provide characteristic features. The first resolved transition (3 ps) results in a rise of the absorption at 710 nm and minor changes in the region of the PDI ground state absorption. The following process

(86 ps) raises the bleaching of the PDI ground state absorption and reshapes the absorption in the red part of the spectrum. The longest-lived spectrum detected in the pump-probe measurements shows a gradual bleaching of the PDI ground state absorption at 540 nm and a new absorption band at 710 nm. The band at 710 nm can be attributed to the PDI radical anion and this state can be recognized as the charge separated state, $PDI^{\bullet-}$–Ru(III), with an electron transferred from Ru(II) to PDI.[78] The two-step formation of this state can be rationalized considering that two different chromophores were excited by the laser flash at 420 nm. We tend to conclude that the faster CS (3 ps) takes place starting from the PDI excited singlet state, ^{1S}PDI*–Ru(II) → $PDI^{\bullet-}$–Ru(III), and the slower (86 ps) from the triplet excited state of the Ru complex, PDI–^{1T}Ru(II)* → $PDI^{\bullet-}$–Ru(III), since the slower process increases the PDI ground state bleaching and thus its initial state should have the PDI chromophore in its ground state. This also agrees with the higher driving force of the electron transfer starting from the singlet excited state ^{1S}PDI*–Ru(II) as compared to that from the triplet state PDI–^{1T}Ru(II)* in the Marcus normal regime of the electron transfer. In this experiment the intersystem crossing, PDI–^{1S}Ru(II)* → PDI–^{1T}Ru(II)*, was not resolved because it overlaps in time with the faster step of CS and overall spectral changes associated with this reaction are weaker than for the charge transfer reaction.

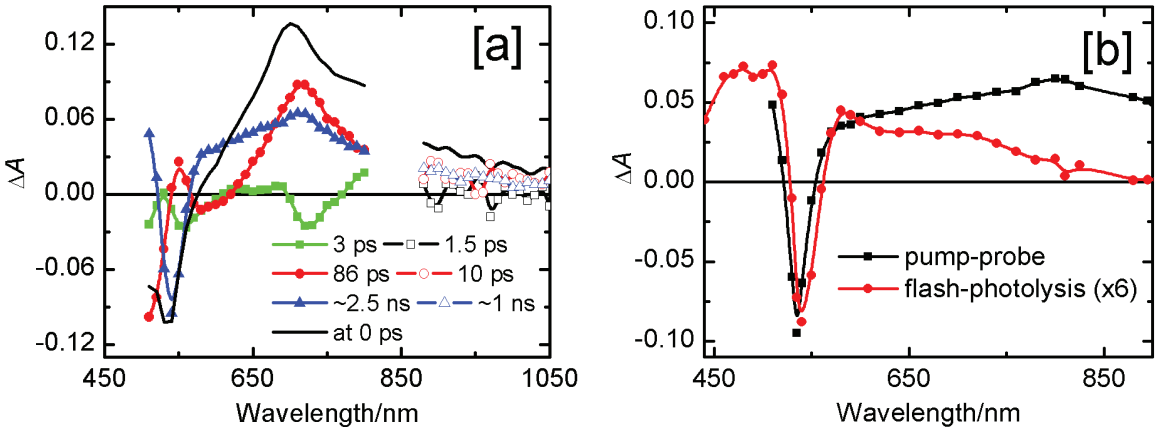

Figure 4.13. [a] Picosecond transient absorption decay component spectra of the ensemble 1,7(6)-Ph-PDI–Ru(II) obtained after the laser excitation at 420 nm in acetonitrile. [b] Comparison of the final spectrum obtained in the picosecond pump-probe measurement and the spectrum from the nanosecond flash-photolysis measurement.

The formed CS state has relatively long lifetime and its decay was not seen in the pump-probe experiments, where the maximum delay time is 1.4 ns. The time resolution of the flash photolysis instrument used is limited to 100 ns and the spectrum obtained at this delay time differs from the final spectrum detected in pump-probe (Figure 4.13[b]). In both cases the sharp negative peak at 540 nm indicates that the PDI chromophore is not in its ground state. The difference in the red part shows that at 100 ns the PDI chromophore is in the triplet state, whereas at ~1 ns the ensemble is in the CS state.

Thus, the charge recombination, $PDI^{\bullet-}$–Ru(III) → ^{1T}PDI*–Ru(II), takes place in the time interval between 1 and 100 ns. The exact value, however, cannot be determined with the instruments used for this study. The proposed reaction scheme for the ensemble 1,7(6)-Ph-PDI–Ru(II) is summarized in Figure 4.15.

The decay component spectra of the ensemble 1,7-Py-PDI–Ru(II) are shown in Figure 4.14[a]. Essentially the same spectra and very similar lifetimes were obtained for 1,6-PyPDI–Ru(II) (Figure 4.15). The first time-resolved process, 3 ps, shows a gradual increase in the bleaching of the ground state absorption of the PDI chromophore, which apparently follows the relaxation of the photoexcited Ru(II) complex. Because the intersystem crossing for the Ru(II) complex is much faster (< 2 ps), this reaction takes place starting from the triplet state, PDI–^{1T}Ru(II)*. The process can be either an energy transfer or an electron transfer. Considering that the 3 ps component shows also some increase in the absorption at 750 nm, we assume that the reaction is the charge transfer, PDI–^{1T}Ru(II)* → $PDI^{\bullet+}$–$Ru(II)^{\bullet-}$. In 53 ps, the triplet state of the PDI chromophore is formed, which then decays in a microsecond time domain as revealed by the flash-photolysis experiments (Figure 4.14[b]). In contrast

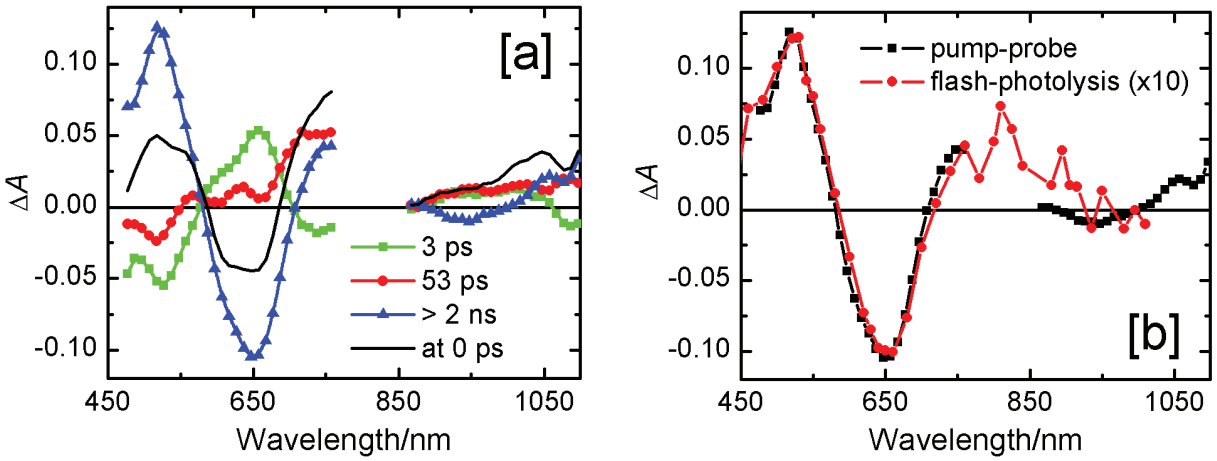

Figure 4.14. [a] Picosecond transient absorption decay component spectra of the ensemble 1,7-Py-PDI–Ru(II) obtained after the laser excitation at 420 nm in acetonitrile. [b] Comparison of the final spectrum obtained in the picosecond pump-probe measurement and the spectrum from the nanosecond flash-photolysis measurement.

to the case of 1,7(6)-Ph-PDI–Ru(II), the final transient seen in pump-probe is the same as the transient obtained in flash-photolysis (Figure 4.14[b]), *i.e.* the formation of the PDI triplet was resolved in pump-probe and the decay in flash-photolysis. The triplet state can be formed by two reactions: firstly by the charge recombination, $PDI^{\bullet+}$–$Ru(II)^{\bullet-}$ → ^{1T}PDI*–Ru(II), and secondly by the intersystem crossing of the PDI chromophore, ^{1S}PDI*–Ru(II) → ^{1T}PDI*–Ru(II). Since the singlet excited state, ^{1S}PDI*–Ru(II), is also generated by the excitation at 420 nm and the intersystem crossing was not observed for the

reference PDIs in this time scale, we have to conclude that the intersystem crossing of the PDI chromophore is strongly facilitated by the presence of Ru in the ensemble. Essentially the same results were obtained with excitation at 600 nm for 1,7-Py-PDI-Ru(II) except that ET was not observed and only the intersystem crossing was seen with a time constant of 36 ps. The proposed reaction scheme for the ensembles 1,7-Py-PDI−Ru(II) and 1,6-Py-PDI−Ru(II) is summarized in Figure 4.15 with time constants indicated for 1,6-Py-PDI−Ru(II).

The essential difference between the 1,7(6)-Ph-PDI−Ru(II) and the two other ensembles is the energetics of the PDI chromophore. Ph-PDI has a higher energy of the singlet excited state and it is a better electron acceptor. This makes the electron transfer feasible after excitation of either of the chromophores. Although we assume that the electron transfer takes place for the two other ensembles as well, but it can only start from the triplet state of the Ru(II) complex, which is relatively higher in energy. Furthermore, ET takes place in the opposite direction as compared with the ensemble 1,7(6)-Ph-PDI−Ru(II), and the CS states recombine fast with time constants of 70 ps and 53 ps for 1,6-Py-PDI−Ru(II) and 1,7-Py-PDI−Ru(II), respectively.

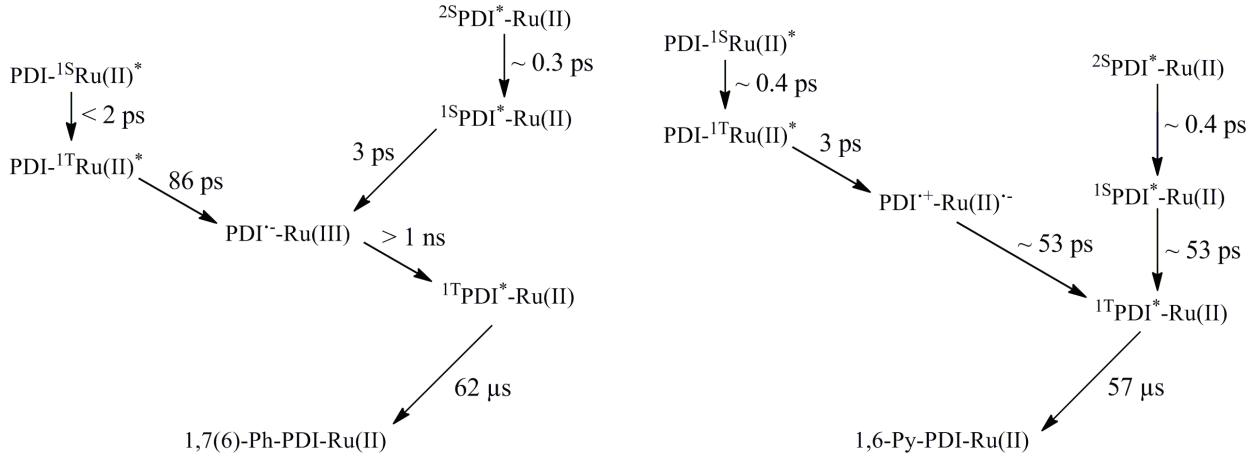

Figure 4.15. The proposed scheme depicting the photophysical processes taking place in the ensembles (Left) 1,7(6)-Ph-PDI−Ru(II) and (Right) 1,7-Py-PDI−Ru(II) and 1,6-Py-PDI−Ru(II) with time constants mentioned for 1,7-Py-PDI−Ru(II).

4.8 Photosensitization of Fullerene by Dibenzo[*a*,*c*]phenazine Molecule

Besides many favorable properties, the low molar absorption coefficient of fullerene in the visible region limits its utility in photovoltaic applications. Therefore, the main objective of this study was to attach a molecule to fullerene, which can efficiently and rapidly transfer harvested light energy to fullerene without diminishing its electron-acceptor ability. In this context, a dibenzo[*a,c*]phenazine−fullerene (DBPZ−C_{60}) dyad in which two chromophores are linked at close proximity had been synthesized and its suitability had been examined by detailed electrochemical and optical spectroscopic studies.

In the dyad, the length of the linker had been intentionally kept short to exert the close-proximity between the two acting moieties, which was necessary to ensure an efficient and rapid energy transfer from the DBPZ moiety to the fullerene. The selection of the DBPZ chromophore as antenna was mostly based on its suitable electrochemical properties. It has a very high oxidation potential, which ensures its incapability to donate electrons to the fullerene moiety. At the same time, the DBPZ moiety also has a significantly higher first reduction potential (−1.41 V, vs Ag/AgCl) compared with that of fullerene (−0.55 V). The large difference in the first reduction potentials of two electroactive chromophores {$\Delta E = E_{1red}(C_{60}) - E_{1red}(DBPZ) = 860$ mV} ensured that the two moieties will perform their well-defined roles, *i.e.* DBPZ will act as light-harvesting antenna, whereas fullerene will accept the electrons.

4.8.1 Synthesis and characterization

The DBPZ−C_{60} dyad was synthesized by the 1,3-dipolar cycloaddition reaction between 11-formyldibenzo[*a,c*]phenazine **43** and fullerene in presence of *N*-(3,5-di-*tert*-butylbenzyl)glycine **40** as shown in the Scheme 4.10. The 3,5-di-*tert*-butylbenzyl group on the pyrrolidine ring was introduced to enhance the solubility of the dyad in common organic solvents, which was essential for the characterization and detailed spectroscopic and electrochemical studies. We had also synthesized the dyad **46** using sarcosine in place of *N*-(3,5-di-*tert*-butylbenzyl)glycine **40**, but the resulting compound had very poor solubility in common organic solvents. A similar procedure was applied to synthesize ref-C_{60} **45**, using paraformaldehyde instead of 11-formyldibenzo[*a,c*]phenazine **43**. The synthesis of *N*-(3,5-di-*tert*-butylbenzyl)glycine **40** and 11-formyldibenzo[*a,c*]phenazine **43** is shown in the Scheme 4.11. The preparation of *N*-(3,5-di-*tert*-butylbenzyl)glycine **40** was carried out in two steps from 3,5-di-*tert*-butylbenzaldehyde. Whereas, 11-formyldibenzo[*a,c*]phenazine **43** was synthesized in three steps starting from 9,10-phenanthrenequinone and 3,4-diaminotoluene.

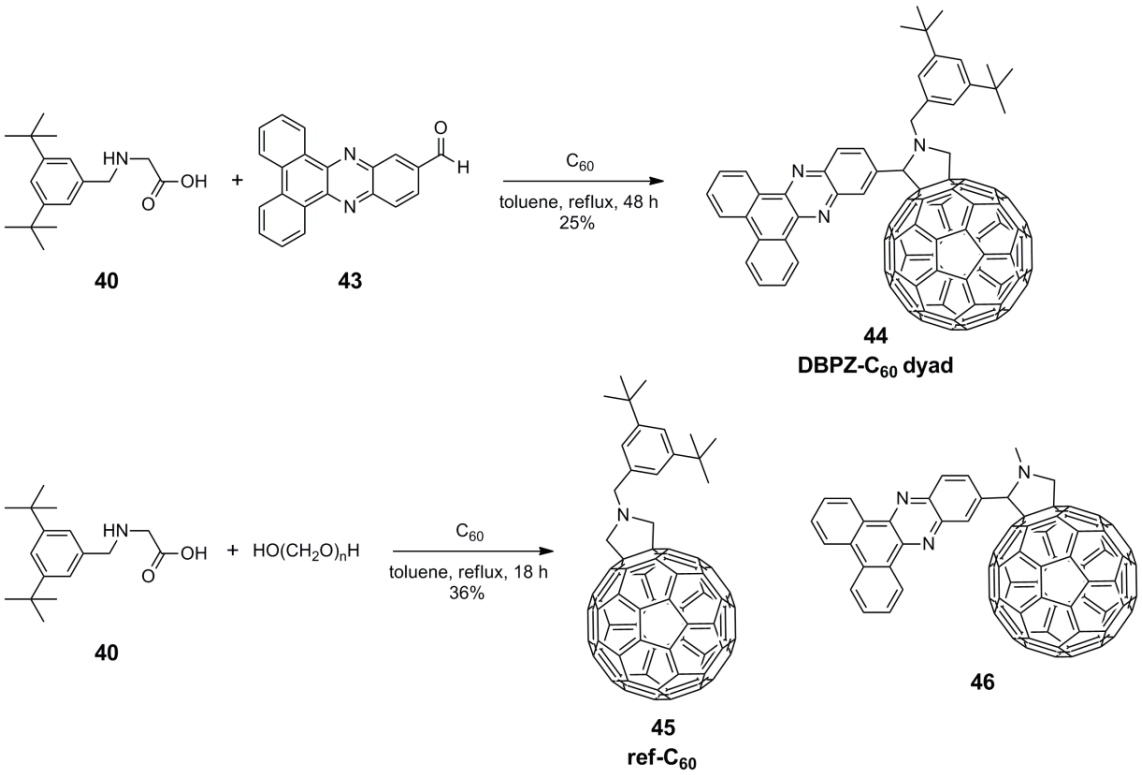

Scheme 4.10. Synthesis of the compounds DBPZ−C_{60} **44** and ref-C_{60} **45**.

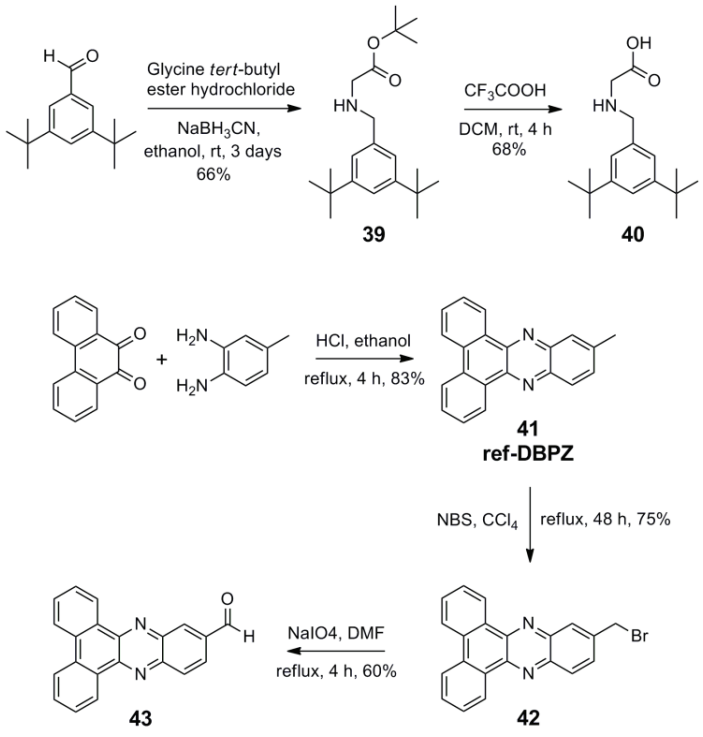

Scheme 4.11. Synthesis of *N*-(3,5-di-*tert*-butylbenzyl)glycine **40** (top) and 11-formyldibenzo[*a,c*]phenazine **43** (bottom).

4.8.2 Evidences of an efficient and fast photoinduced singlet energy transfer

The steady-state absorption spectrum of the dyad indicated a small ground state electronic interaction between DBPZ and fullerene moieties (Figure 4.16[a]). The absorption spectrum of ref-DBPZ exhibits two absorption maxima at 375 and 396 nm corresponding to $n-\pi^*$ and $\pi-\pi^*$ transitions, respectively. In the dyad, these absorption bands appear at 380 and 403 nm and are shifted to longer wavelengths by 5 and 7 nm, respectively. Subsequently, the comparison of the emission intensity of DBPZ moiety of the dyad with ref-DBPZ revealed that the emission of DBPZ moiety was efficiently quenched in the dyad. However, the quenching was relatively more efficient (98 %) in non-polar toluene compared with polar benzonitrile (89 %).

The singlet−singlet energy transfer in the dyad from DBPZ to fullerene was verified by the comparison of emission spectra of the equimolar solutions of the dyad **44** and ref-C_{60} **45**. The excitation wavelength was set to 403 nm, where DBPZ moiety absorbs predominately (the dyad has a four times higher absorbance than the ref-C_{60}) (Figure 4.16[b]). In the dyad, an almost four fold sensitized emission of the fullerene moiety was observed with respect to the ref-C_{60}. Nearly the same results were obtained in more polar chloroform and benzonitrile. Furthermore, the lifetime of the singlet-state of fullerene moiety of the dyad (1.46 ns) was almost the same as that of ref-C_{60} (1.50 ns). Thus, the results confirmed that the quenching of the DBPZ singlet excited-state is solely due to singlet−singlet energy transfer from the DBPZ moiety to the fullerene.

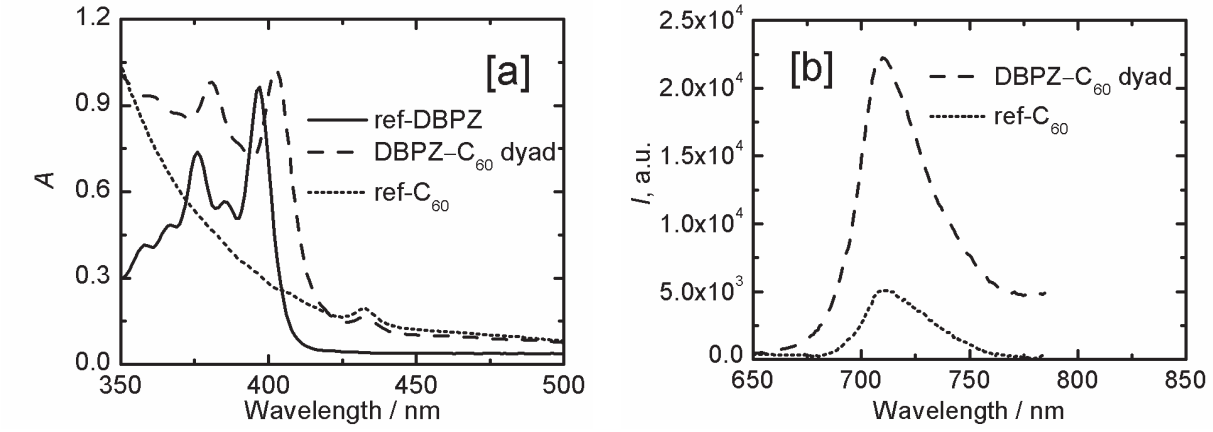

Figure 4.16. [a] Steady-state absorption spectra of the DBPZ−C_{60} dyad, ref-DBPZ, and ref-C_{60} in toluene (41 μM). [b] The sensitized emission of fullerene moiety of the dyad with respect to ref-C_{60}, obtained from excitation of equimolar solutions.

Finally, transient absorption studies were carried out in the nanosecond and picosecond time-scales to investigate the fate of excited singlet-states of DBPZ and fullerene moieties. The flash-photolysis measurements (λ_{ex} = 401 nm) of the equimolar solutions of the dyad and ref-C_{60}, exhibited the

characteristic band of the fullerene triplet-state at ca. 700 nm (Figure 4.17[a]). But in the case of the dyad, the sensitized triplet-state absorption observed for the fullerene moiety. This observation further indicated that the harvested light energy by the DBPZ antenna is transferred to the fullerene.

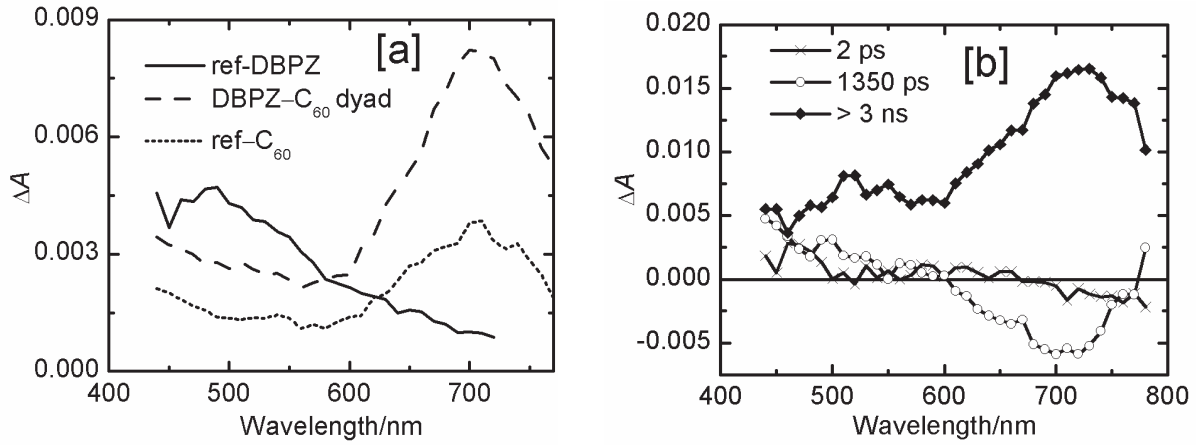

Figure 4.17. [a] Nanosecond transient absorption spectra of the DBPZ−C_{60} dyad, ref-DBPZ, and ref-C_{60} in toluene (41 μM). [b] Picosecond transient absorption decay-component spectra of DBPZ−C_{60} dyad in toluene.

The measurements with the picosecond pump-probe method (λ_{ex} = 404 nm) revealed the fast energy transfer from the singlet excited-state of DBPZ moiety to the singlet-state of fullerene in both polar and non-polar environment (Figure 4.17[b]). The energy transfer takes place in 2 ps ($k_{en} = 5.0 \times 10^{11} s^{-1}$) in toluene and in 4.7 ps ($k_{en} = 2.1 \times 10^{11} s^{-1}$) in polar benzonitrile. All these results collectively confirmed that the fast and efficient singlet energy transfer from the DBPZ moiety to the fullerene unit occurs in DBPZ−C_{60} dyad, as summarized in Figure 4.18.

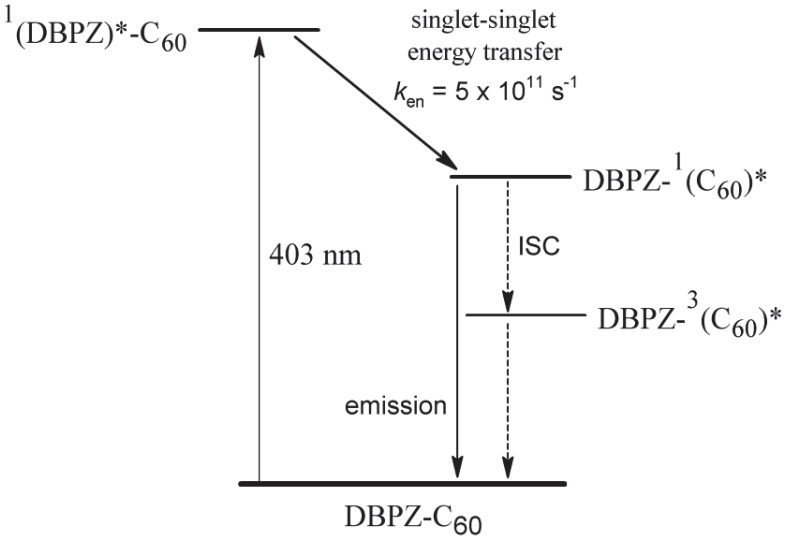

Figure 4.18. Photoinduced processes taking place in DBPZ−C_{60} dyad upon excitation of the DBPZ moiety in toluene.

5 Conclusions

1. The 1,7- and 1,6-regioisomers of diphenoxy and dipyrrolidinyl substituted PDI dyes have been synthesized, separated and characterized. The two regioisomers of diphenoxy substituted PDIs (1,7-**5** and 1,6-**5**) were separated utilizing their different solubility in toluene. On the other hand, regioisomers of dipyrrolidinyl substituted PDIs (1,7-**8** and 1,6-**8**) were separated by conventional silica gel column chromatography. Our studies have also shown that the 1,7- and 1,6-isomers of these derivatives can readily be distinguished even with 300 MHz ^{1}H NMR spectroscopy by the characteristic signals of their α-imido protons.

2. The detailed comparative examination have shown that the introduction of phenoxy groups at the 1,7- and 1,6-positions of the PDI core leads to the regioisomers that are very similar in redox and optical properties. On the contrary, the two regioisomers obtained by the substitution of pyrrolidine groups at the 1,7- and 1,6-positions exhibit profound differences in their electrochemical and optical characteristics. We found that 1,6-dipyrrolidinylperylene diimide has significantly diminished electron donor ability and inherently low emission characteristics compared to respective 1,7-regioisomer. Further extended comparative studies on the 1,7- and 1,6-regioisomers of pyrrolidinyl substituted PDIs, have also exposed differences in their chemical behavior and excited-state dynamics.

3. We have developed a synthetic methodology for the attachment of functionalized pyrrolidinyl groups to the PDI core to prepare mono- and bis-bay-functionalized derivatives of the PDI dyes. The main importance of these derivatives lies in their potential as building-blocks to construct complex light-harvesting arrays and artificial photosynthetic systems due to the presence of additional sites for the attachment of other chromophores close to the perylene core. Otherwise, in conventional dipyrrolidinyl substituted PDIs, attachment of the chromophores is possible only at the imide positions, which causes a potential drawback of keeping two acting moieties significantly far from each other. Synthesis of the PDI−C_{60} dyads, presented herein, is just one example of their utility as synthon.

4. The single-bridged PDI−C_{60} dyads exhibited efficient photoinduced electron transfer in both polar and non-polar media, which justified the strategy of the attachment of fullerene through the bay-region of PDI. In this way, our studies have also shown that the dipyrrolidinyl functionalized PDIs can perform as potential electron-donors in the D−A based systems. The single-bridged dyad SB-1,7-PDI−C_{60} demonstrated a highly efficient photoinduced electron

transfer even in non-polar medium, which makes the compound particularly attractive for the applications in solid organic photovoltaics.

5. A series of metallo-organic PDI−$[Ru(bpy)_2dppz]^{2+}$ ensembles, consisting of either red or green PDI covalently linked to Ru(II) polypyridine complex, have been synthesized and spectroscopically characterized. In all the ensembles, the long-lived PDI triplet excited state has been observed as the lowest excited state, which is generated mainly as a result of the decay of the charge-separated state. Interestingly, the direction of the electron transfer was observed to be opposite in red and green PDI based ensembles *i.e.* the red PDI acted as an electron acceptor, whereas the green PDIs acted as donors.

6. The dibenzo*[a,c]*phenazine−fullerene (DBPZ−$_{C60}$) dyad possesses an efficient and fast energy transfer from DBPZ moiety to fullerene in combination with favorable electrochemical properties. Therefore, it could also be a good candidate for the photovoltaic applications with well-defined roles of both acting chromophores; DBPZ acting as a light-harvesting antenna and fullerene acting as an electron acceptor in the photoactive layer.

6 References

1. Closs, G. L.; Miller, R. J. *Science* **1988**, *240*, 440−447.
2. Gust, D.; Moore, T. A. *Science* **1989**, *244*, 35−41.
3. Wasielewski, M. R. *Chem. Rev.* **1992**, *92*, 435−461.
4. Gust, D.; Moore, T. A.; Moore, A. L. *Acc. Chem. Res.* **1993**, *26*, 198−205.
5. Gust, D.; Moore, T. A.; Moore, A. L. *Acc. Chem. Res.* **2001**, *34*, 40−48.
6. Imahori, H.; Sakata, Y. *Adv. Mater.* **1997**, *9*, 537−546.
7. Wasielewski, M. R. *J. Org. Chem.* **2006**, *71*, 5051−5066.
8. Tomizaki, K.; Loewe, R. S.; Kirmaier, C.; Schwartz, J. K.; Retsek, J. L.; Bocian, D. F.; Holten, D.; Lindsey, J. S. *J. Org. Chem.* **2002**, *67*, 6519−6534.
9. Lemmetyinen, H.; Tkachenko, N. V.; Efimov, A.; Niemi, M. *Phys. Chem. Chem. Phys.* **2011**, *13*, 397−412.
10. El-Khouly, M. E.; Ito, O.; Smith, P. M.; D'Souza, F. *J. Photochem. Photobiol. C* **2004**, *5*, 79−104.
11. Martin, N.; Sanchez, L.; Illescas, B.; Perez, I. *Chem. Rev.* **1998**, *98*, 2527−2547.
12. Elemans, J. A. A. W.; Hameren, R.; Nolte, R. J. M.; Rowan, A. E. *Adv. Mater.* **1996**, *18*, 1251−1266.
13. Aratani, N.; Kim, D.; Osuka, A. *Acc. Chem. Res.* **2009**, *42*, 1922−1934.
14. Bottari, G.; Torre, G.; Guldi, D. M.; Torres, T. *Chem. Rev.* **2010**, *110*, 6768−6816.
15. Guldi, D. M.; Luo, C.; Prato, M.; Troisi, A.; Zerbetto, F.; Scheloske, M.; Dietel, E.; Bauer, W.; Hirsch, A. *J. Am. Chem. Soc.* **2001,** *123,* 9166−9167.
16. Paddon-Row, M. N. *Acc. Chem. Res.* **1994,** *27,* 18−25.
17. Lewis, F. D.; Letsinger, R. L.; Wasielewski, M. R. *Acc. Chem. Res.* **2001,** *34,* 159−170.
18. Guldi, D. M.; Hirsch, A.; Scheloske, M.; Dietel, E.; Troisi, A.; Zerbetto, F.; Prato, M. *Chem. Eur. J.* **2003,** *9,* 4968−4979.

19. Tsue, H.; Imahori, H.; Kaneda, T.; Tanaka, Y.; Okada, T.; Tamaki, K.; Sakata, Y. *J. Am. Chem. Soc.* **2000,** *122,* 2279−2288.

20. Vehmanen, V.; Tkachenko, N. V.; Tauber, A. Y.; Hynninen, P. H.; Lemmetyinen, H. *Chem. Phys. Lett.* **2001**, *345*, 213−218.

21. Gouloumis, A.; Rodriguez, D. G.; Vazquez, P.; Torres, T.; Liu, S.; Echegoyen, L.; Ramey, J; Hug, G. L.; Guldi, D. M. *J. Am. Chem. Soc.* **2006,** *128,* 12674−12684.

22. Huang, C.; Barlow, S.; Marder, S. R. *J. Org. Chem.* **2011**, *76*, 2386−2407.

23. Würthner, F. *Chem. Commun.* **2004**, 1564−1579.

24. Wasielewski, M. R. *Acc. Chem. Res.* **2009**, *42,* 1910−1921.

25. Kardos, M. German Patent, DE 276956, 1913.

26. Herbst, W.; Hunger, K. *Industrial Organic Pigments*, 2nd completely revised ed.; Wiley-VCH: Weinheim, **1997**.

27. Geissler, G.; Remy, H. (Hoechst AG), *Ger. Pat. Appl.*, DE 1130099, 1959 (*Chem. Abstr.*, **1962**, *57*, P11346f).

28. Kazmaier, P. M.; Hoffmann, R. *J. Am. Chem. Soc.* **1994**, *116,* 9684−9691.

29. Nakazono, S.; Imazaki, Y.; Yoo, H.; Yang, J.; Sasamori, T.; Tokitoh, N.; Cedric, T.; Kageyama, H.; Kim, D.; Shinokubo, H.; Osuka, A. *Chem. Eur. J.* **2009**, *15,* 7530−7533.

30. Nakazono, S.; Easwaramoorthi, S.; Kim, D.; Shinokubo, H.; Osuka, A. *Org. Lett. J.* **2009,** *11,* 5426−5429.

31. *High performance pigments* (Ed.: Smith, H.), Wiley-VCH Verlag, Weinheim, **2003**.

32. Langhals, H. *Heterocycles* **1995**, *40*, 477−500.

33. Wescott, L. D.; Mattern, D. L. *J. Org. Chem.* **2003**, *68,* 10058−10066.

34. Böhm, A.; Arms, H.; Henning, G.; Blaschka, P. (BASF AG) German Pat. DE 19547209 A1, **1997**.

35. Schmidt, R.; Ling, M. M.; Oh, J. H.; Winkler, M.; Könemann, M.; Bao, Z.; Würthner, F. *Adv. Mater.* **2007**, *19*, 3692−3695.

36. Ahrens, M. J.; Fuller, M. J.; Wasielewski, M. R. *Chem. Mater.* **2003**, *15*, 2684−2686.

37. Jones, B. A.; Ahrens, M. J.; Yoon, M.-H.; Facchetti, A.; Marks, T. J.; Wasielewski, M. R. *Angew. Chem. Int. Ed.* **2004**, *43*, 6363−6366.

38. Kohl, C.; Weil, T. ; Qu, J.; Müllen, K. *Chem. Eur. J.* **2004**, *10*, 5297−5310.

39. Zhao, Y.; Wasielewski, M. R. *Tetrahedron Lett.* **1999**, *40*, 7047−7050.

40. Chao, C. –C.; Leung, M. −K. *J. Org. Chem.* **2005**, *70,* 4323−4331.

41. Chen, C.; Liu, Y.; Qiu, W.; Sun, X.; Ma, Y.; Zhu, D. *Chem. Mater.* **2005**, *17*, 2208−2215.

42. Nolde, F.; Pisula, W.; Müller, S.; Kohl, C.; Müllen, K. *Chem. Mater.* **2006**, *18*, 3715−3725.

43. Avlasevich, Y.; Müller, S.; Erk, P.; Müllen, K. *Chem. Eur. J.* **2007**, *13*, 6555−6561.

44. Zhan, X.; Tan, Z. Domercq, B.; An, Z.; Zhang, X.; Barlow, S.; Li, Y.; Zhu, D.; Kippelen, B.; Marder, S. R. *J. Am. Chem. Soc.* **2007**, *129,* 7246−7247.

45. Li, Y.; Tan, L.; Wang, Z.; Qian, H.; Shi, Y.; Hu, W. *Org. Lett.* **2008**, *40*, 529−532.

46. Sivamurugan, V.; Kazlauskas, K.; Jursenas, S.; Gruodis, A.; Simokaitiene, J.; Grazulevicius, J. V.; Valiyaveettil, S. *J. Phys. Chem. B* **2010**, *114,* 1782−1789.

47. Wonneberger, H.; Ma, C. –Q.; Gatys, M. A.; Li, C.; Bäuerle, P.; Müllen, K. *J. Phys. Chem. B* **2010**, *114,* 14343−14347.

48. Würthner, F.; Stepanenko, V.; Chen, Z.; Saha-Möller, C. R.; Kocher, N.; Stalke, D. *J. Org. Chem.* **2004**, *69*, 7933−7939.

49. Rajasingh, P.; Cohen, R.; Shirman, E.; Shimon, L. J. W.; Rybtchinski, B. *J. Org. Chem.* **2007**, *72*, 5973−5979.

50. Ford, W. E.; Kamat, P. V. *J. Phys. Chem.* **1987**, *91*, 6373−6380.

51. Langhals, H.; Obermeier, A.; Floredo, Y.; Zanelli, A.; Flamigni, L. *Chem. Eur. J.* **2009**, *15*, 12733−12744.

52. Langhals, H.; Karolin, J.; Johansson, L. B.-A. *J. Chem. Soc., Faraday Trans.,* **1998**, *94,* 2919−2922.

53. Sadrai, M.; Hadel, L.; Sauers, R. R.; Husain, S.; Krogh-Jespersen, K.; Westbrook, J. D.; Bird, G. R. *J. Phys. Chem.* **1992**, *96*, 7988−7996.

54. Sadrai, M.; Bird, G. R. *Opt. Commun.* **1984**, *51*, 62−64.

55. Chen, Z.; Baumeister, U.; Tschierske, C.; Würthner, F. *Chem. Eur. J.* **2007**, *13,* 450−465.

56. Gvishi, G.; Reisfeld, R.; Burshtein, Z. *Chem. Phys. Lett.* **1993**, *213,* 338−344.

57. Würthner, F.; Sautter, A.; Schmid, D.; Weber, P. J. A. *Chem. Eur. J.* **2001**, *7,* 894−902.

58. Lukas, A. S.; Zhao, Y.; Miller, S. E.; Wasielewski, M. R. *J. Phys. Chem. B* **2002**, *106*, 1299−1306.

59. Würthner, F.; Osswald, P.; Schmidt, R.; Kaiser, T. E.; Mansikkamäki, H.; Könemann, M. *Org. Lett.* **2006**, *8*, 3765−3768.

60. Lee, K. S.; Zu, Y.; Herrmann, A.; Geerts, Y.; Müllen, K.; Bard, A. J. *J. Am. Chem. Soc.* **1999**, *121,* 3513−3520.

61. Chen, H. Z.; Ling, M. M.; Mo, X.; Shi, M. M.; Wang, M.; Bao, Z. *Chem. Mater.* **2007**, *19*, 816−824.

62. Xie, Q.; Perez-Cordero, E.; Echegoyen, L. *J. Am. Chem. Soc.* **1992**, *124,* 3978−3980.

63. Würthner, F.; Thalacker, C.; Diele, S.; Tschierske, C. *Chem. Eur. J.* **2001**, *7,* 2245−2253.

64. Rodriguez-Morgade, M. S.; Torres, T.; Atienza-Castellanos, C.; Guldi, D. M. *J. Am. Chem. Soc.* **2006**, *128,* 15145−15154.

65. Hains, A. W.; Liang, Z.; Woodhouse, M. A.; Gregg, B. A. *Chem. Rev.* **2010**, *110,* 6689−6735.

66. Rybtchinski, B.; Sinks, L. E.; Wasielewski, M. R. *J. Am. Chem. Soc.* **2004**, *126,* 12268−12269.

67. Hippius, C.; Schlosser, F.; Vysotsky, M. O.; Böhmer, V.; Würthner, F. *J. Am. Chem. Soc.* **2006**, *128,* 3870−3871.

68. Shoaee, S.; Clarke, T. M.; Huang, C.; Barlow, S.; Marder, S. R.; Heeney, M.; McCulloch, I.; Durrant, J. R. *J. Am. Chem. Soc.* **2010**, *132,* 12919−12926.

69. Kaletas, B. K.; Dobrawa, R.; Sautter, A.; Würthner, F.; Zimine, M.; Cola, L. D.; Williams, R. M. *J. Phys. Chem. A* **2004**, *108,* 1900−1909.

70. Kelley, R. F.; Shin, W. S.; Rybtchinski, B.; Sinks, L. E.; Wasielewski, M. R. *J. Am. Chem. Soc.* **2007**, *129,* 3173−3181.

71. Prathapan, S.; Yang, S. I.; Seth, J.; Miller, M. A.; Bocian, D. F.; Holten, D.; Lindsey, J. S. *J. Phys. Chem. B* **2001**, *105,* 8237−8248.

72. van der Boom, T.; Hayes, R. T.; Zhao, Y.; Bushard, P. J.; Weiss, E. A.; Wasielewski, M. R. *J. Am. Chem. Soc.* **2002**, *124,* 9582−9590.

73. O'Neil, M. P.; Niemczyk, M. P.; Svec, W. A.; Gosztola, D.; Gaines, L. G.; Wasielewski, M. R. *Science* **1992**, *257,* 63−65.

74. Odom, S. A.; Kelley, R. F.; Ohira, S.; Ensley, T. R.; Huang, C.; Padilha, L. A.; Webster, S.; Coropceanu, V.; Barlow, S.; Hagan, D. J.; Stryland, E. W.; Bredas, J.; Anderson, H. L.; Wasielewski, M. R.; Marder, S. R. *J. Phys. Chem. A* **2009**, *113,* 10826−10832.

75. Jimenez, A. J.; Spanig, F.; Rodriguez-Morgade, M. S.; Ohkubo, K.; Fukuzumi, S.; Guldi, D. M.; Torres, T. *Org. Lett.* **2007,** *9,* 2481−2484.

76. Prodi, A.; Chiorboli, C.; Scandola, F.; Lengo, E.; Alessio, E.; Dobrawa, R.; Würthner, F. *J. Am. Chem. Soc.* **2005,** *127,* 1454−1462.

77. Rodriguez-Morgade, M. S.; Torres, T.; Atienza-Castellanos, C.; Guldi, D. M. *J. Am. Chem. Soc.* **2006,** *128,* 15145−15154.

78. Ford, W. E.; Hiratsuka, H.; Kamat, P. V. *J. Phys. Chem.* **1989**, *93*, 6692−6696.

79. Shibano, Y.; Umeyama, T.; Matano, Y.; Tkachenko, N. V.; Lemmetyinen, H.; Imahori, H. *Org. Lett.* **2006**, *8*, 4425−4428.

80. Shibano, Y.; Umeyama, T.; Matano, Y.; Tkachenko, N. V.; Lemmetyinen, H.; Araki, Y.; Ito, O.; Imahori, H. *J. Phys. Chem. C.* **2007**, *111*, 6133−6142.

81. Chen, Z.; Debije, M. G.; Debaerdemaeker, T.; Osswald, P.; Würthner, F. *ChemPhysChem* **2004**, *5*, 137−140.

82. Ranke, P.; Bleyl, I.; Simmerer, J.; Haarer, D.; Bacher, A.; Schmidt, H. W. *Appl. Phys. Lett.* **1997**, *71*, 1332−1334.

83. Angadi, M. A.; Gosztola, D.; Wasielewski, M. R. *Mater. Sci. Eng. B* **1999**, *63*, 191−194.

84. Guo, X.; Zhang, D.; Zhu, D. *Adv. Mater.* **2004**, *16*, 125−130.

85. He, X.; Liu, H.; Li, Y.; Wang, S.; Li, Y.; Wang, N.; Xiao, J.; Xu, X.; Zhu, D. *Adv. Mater.* **2005**, *17*, 2811−2815.

86. Weiss, E. A.; Ahrens, M. J.; Sinks, L. E.; Gusev, A. V.; Ratner, M. A.; Wasielewski, M. R. *J. Am. Chem. Soc.* **2004**, *126*, 5577−5584.

87. Law, K. Y. *Chem. Rev.* **1993**, *93,* 449−486.

88. Li, C.; Wonneberger, H. *Adv. Mater.* **2012**, *24*, 613−636.

89. Ooyama, Y.; Harima, Y. *Eur. J. Org. Chem.* **2009**, *24*, 2903−2934.

90. Sharma, G. D.; Suresh, P.; Mikroyannidis, J. A.; Stylianakis, M. M. *J. Mater. Chem.* **2010**, *20*, 561−567.

91. Sariciftci, N. S.; Smilowitz, L.; Heegar, A. J.; Wudl, F. *Science* **1992**, *258,* 1474−1476.

92. An, Y. –Z.; Ellis, G. A.; Viado, A. L.; Rubin, Y. *J. Org. Chem.* **1995**, *60*, 6353−6361, and references cited therein.

93. Von Hauff, E.; Dyakonov, V.; Parisi, J. *Sol. Energy Mater. Sol. Cells* **2005**, *87*, 149−156.

94. Dang, M. T.; Hirsch, L.; Wantz, G. *Adv. Mater.* **2011**, *23*, 3597−3602.

95. Dennler, G.; Scharber, M. C.; Brabec, C. J. *Adv. Mater.* **2009**, *21*, 1323−1338.

96. Moule, A. J.; Meerholz, K. *Adv. Funct. Mater.* **2009**, *19*, 3028−3036.

97. Po, R.; Maggini, M.; Camaioni, N. *J. Phys. Chem. C.* **2010**, *114*, 695−706.

98. Kuciauskas, D.; Lin, S.; Seely, G. R.; Moore, A. L.; Moore, T. A.; Gust, D.; Drovetskaya, T.; Reed, C. A.; Boyd, P. D. W. *J. Phys. Chem.* **1996**, *100*, 15926−15932.

99. Bell, T. D. M.; Ghiggino, K. P.; Jolliffe, K. A.; Ranasinghe, M. G.; Langford, S. J.; Shephard, M. J.; Paddon-Row, M. N.; *J. Phys. Chem. A* **2002**, *106*, 10079−10088.

100. Von Hal, P. A.; Knol, j.; Langeveld-Voss, B. M. W.; Meskers, S. C. J.; Hummelen, J. C.; Janssen, R. A. J. *J. Phys. Chem. A* **2000**, *104*, 5974−5988.

101. Guldi, D. M.; Luo, C.; Swartz, A.; Gómez, R.; Segura, J. L.; Martín, N. *J. Phys. Chem. A* **2004**, *108*, 455−467.

102. Rodríguez, D. G.; Torres, T.; Guldi, D. M.; Rivera, J.; Herranz, M. A.; Echegoyen, L. *J. Am. Chem. Soc.* **2004**, *126*, 6301−6313.

103. Kozaki, M.; Akita, K.; Suzuki, S.; Okada, K. *Org.Lett.* **2007**, *9,* 3315−3318.

104. Chaignon, F.; Torroba, J.; Blart, E.; Borgström, M.; Hammarström, L.; Odobel, F. *New J. Chem.* **2005**, *29,* 1272−1284.

105. Pol, C. V. D.; Bryce, M. R.; Wielopolski, M.; Castellaanos, C. A.; Guldi, D. M.; Filippone, S.; Martin, N. *J. Org. Chem.* **2007**, *72*, 6662−6671.

106. Baffreau, J.; Leroy-Lhez, S.; Anh, N. V.; Williams, R. M.; Hudhomme, P. *Chem. Eur. J.* **2008**, *14*, 4974−4992.

107. Hofmann, C. C.; Lindner, S. M.; Ruppert, M.; Hirch, A.; Haque, S. A.; Thelakkat, M.; Köhler, J. *J. Phys. Chem. B* **2010**, *114*, 9148−9156.

108. Kreller, D. I.; Kamat, P. V. *J. Phys. Chem.* **1991**, *95*, 4406−4410.

109. Dawson, W. R.; Windsor, M. W. *J. Phys. Chem.* **1968**, *72*, 3251−3260.

110. Ahrens, M. J.; Tauber, M. J.; Wasielewski, M. R. *J. Org. Chem.* **2006**, *71*, 2107−2114.

111. Goretzki, G.; Davies, E. S.; Argent, S. P.; Alsindi, W. Z.; Blake, A. J.; Warren, J. E.; McMaster, J.; Champness, N. R. *J. Org. Chem.* **2008**, *73*, 8808−8814.

112. Rachford, A. A.; Goeb, S.; Castellano, F. N. *J. Am. Chem. Soc.* **2008**, *130,* 2766−2767.

113. Weissman, H.; Shirman, E.; Ben-Moshe, T.; Cohen, R.; Leitus, G.; Shimon, L. J. W.; Rybtchinski, B. *Inorg. Chem.* **2007**, *46,* 4790−4792.

114. You, C. –C.; Hippius, C.; Grüne, M.; Würthner, F. *Chem. Eur. J.* **2006**, *12,* 7510−7519.

115. Dobrawa, R.; Lysetska, M.; Ballester, P.; Grüne, M.; Würthner, F. *Macromolecules* **2005**, *38,* 1315−1325.

116. Golubkov, G.; Weissman, H.; Shirman, E.; Wolf, S. G.; Pinkas, I.; Rybtchinski, B. *Angew. Chem. Int. Ed.* **2009**, *48,* 926−930.

117. Tuccitto, N.; Delfanti, I.; Torrisi, V.; Scandola, F.; Chiorboli, C.; Stepanenko, V.; Würthner, F.; Licciardello, A. *Phys. Chem. Chem. Phys.* **2009**, *11*, 4033−4038.

118. Gunderson, V. L.; Krieg, E.; Vagnini, M. T.; Iron, M. A.; Rybtchinski, B.; Wasielewski, M. R. *J. Phy. Chem. B* **2011**, *115,* 7533.

119. Goze, C.; Leiggener, C.; Liu, S.; Sanguinet, L.; Levillain, E.; Hauser, A.; Decurtins, S. *ChemPhysChem* **2007**, *8,* 1504−1512.

Tampereen teknillinen yliopisto
PL 527
33101 Tampere

Tampere University of Technology
P.O.B. 527
FI-33101 Tampere, Finland

ISBN 978-952-15-3062-3
ISSN 1459-2045